UNIVERSITA' DEGLI STUDI DI GENOVA
Scuola di dottorato in meccanica dei fluidi e dei solidi
XXII ciclo

Ph.D Thesis
In
Geophysics

Fault Directivity and Seismic Hazard

Tutor:
Dr. Daniele Spallarossa
Dr. Giovanna Cultrera
Dr. André Herrero

Author:
Dr. Elena Spagnuolo

2007-2009

My Grandmother

Index

Introduction

In planning the design of structures in a region of potential seismic activity, a specification of the "strength" of the earthquake ground motion, or the most likelihood ground motion level, is needed.
The earthquake occurrence, and its effects, is described as a stochastic process. Thus its realization is linked to state variables defined over a a known space through a continuous function. The Ground Motion Predictive Equation (GMPE) realize this function and, despite its shortcoming as an effective design tool to control damage (Priestly, 2003), is still the most widely used representation of earthquake ground motion employed in engineering practice. As a consequence the majority of hazard estimations are based on the GMPE providing a ground motion specification as a function of a certain number of variables.

In fact in many situation there are not enough data to allow a direct empirical specification of ground motion. Only few regions, i.e. Japan, have strong-motion network and data-banks sufficient to carry out seismic hazard assessment without the benefit of regionally-derived ground motion predictive model. The central role they hold in the hazard assessment motivates the recent efforts in better synthesize all available regional informations and general knowledge about earthquakes.

GMPEs are developed on the observations. Their formulation is based on regression procedures requiring a simple mathematical formulation (details about these procedures can be found in a number of publications including Boore and Joyner, 1982; Campbell, 1985; Douglas, 2003, 2006). The model derives from general aspects of the earthquake characterization, that is the observed attenuation with distance or the magnitude scaling. Therefore the majority of these equations depend on at least three parameters: a specification of earthquake size (typically magnitude); the source-to-site geometry (typically distance) and the site classifications. The general formulation is given by:

$$lnIM = f(R) + f(M) + f(site) + \sigma \qquad \text{(I.1)}$$

Where: *IM* is the ground motion intensity measure (Baker and Cornell, 2005) quantifying the 'strength' of the earthquake ground motion; *f(M)* is a function of the magnitude scaling; *f(R)* is a function of source-site distance; *f(site)* is a function of the site response, and σ is the uncertainty quantifying the difference between a measurement point to an estimate of the expected value according to the specific model used (Cook, 1982). The explanatory variables could be affected by some degree of correlation. This correlation is generally incorporated using joint functions in the form *f(M,R)*.
The respective functional form to be used in the regression analyses are selected at the discretion of the developer.

IM is the ground motion intensity measure to be predicted and it is usually a strong ground motion parameter of engineering interest. Peak Ground Acceleration (PGA) is widely used because of its connection to the performance of a structure: in the rigid body approximation, the inertial forces promoted in a structure by the seismic actions are directly proportional to the acceleration via the mass. Thus the seismic action can be evaluated from the peak ground acceleration directly (Eurocode -EC8). Some other parameters are considered, including Peak Ground Velocity (PGV), Peak Ground Displacement (PGD) or spectral ordinates of the response spectra (PSA,PSV,PSD), directly linked to the frequency content of interest. Energy related parameters are commonly used as well, such as: Arias Intensity (AI), Root Mean Square acceleration (RMS), Power Spectral Density (PSD) in order to account for the duration of the signal or for the modulation due to the frequency content.

The representation of the ground motion through the GMPE is simple compared to the complexity of the physical process involved. If only the magnitude and distance are taken into account, the GMPEs predict isoseismal curves that are expected to be isotropic around the hypocenter and uniform if no other effects are considered (i.e. site effects). Instead, the presence of a fault plane, across which a process of failure in shear develops, make this general formulation divert from the observations on a specific case. In fact the dynamic propagation of rupture results in anisotropy effects not included in the predictions although back-analyses of

ground motions from past earthquakes have shown that such effects have a strong influence on the spatial distribution of ground motion (Strasser et al., 2009). For instance, the two standard parameters are not enough to describe the seismic source influence on the commonly used intensity measures. The uncertainty sigma provides a measure of this deficiency.

The sigma represents the quantity the predicted values depart from the data distribution. The value of sigma has a significant impact on the result of seismic hazard analysis, as discussed in Bommer and Abrhamson (2006). In particular, the "almost universal adoption of the logarithmic transform in the regression (Campbell, 1985; Douglas and Smith, 2001) means that in most cases the value of the ground motion parameter of interest will vary as an exponential function of any positive or negative increment in the value of sigma. In other words even small variations in the value of sigma may have significant impact on seismic hazard analysis results" (Strasser et al.,2009). It is customary to interpret the uncertainty sigma as incorporating an aleatory component, representing the genuine randomness of the ground motion, and an epistemic component, related to the choice of the model and regarding factors not yet included in ground motion model and therefore appearing as random factors. Klugel (2007a) have argued that the residuals of GMPEs depend on the model and "therefore cannot be interpreted as an objective inherent property of earthquakes". In agreement with this assumption a better performance of the ground motion prediction can be achieved improving the model, refining the seismic source description inside the GMPEs (e.g. NGA project, Power, 2008) and introducing new explanatory variables in the model. Better results can be obtained if the new-explanatory variables are linked by physical relations "able to capture the multidimensional effects" of the earthquake (i.e the rupture process). As long as the importance of the sigma have been recognized, a big effort has been done in this direction. The Next Generation Attenuation of Ground Motions Project (NGA project, Power, 2008) recently has come up with a new generation of predictive models accounting for other variables rather than the magnitude, distance or site characterization addressed to better synthesize all the pertinent information about the ground motion variability.

A few equations include the style of faulting as fourth variable (Abrahamson and Silva 1997; Boore et al. 1997; Sadigh et al. 1997, Campbell and Bozorgnia, 2003), although it has an almost negligible effect on the reduction of the uncertainties. Nevertheless the introduction of this new parameter is the attempt of the gradual transformation from the aleatory variability to epistemic uncertainty (e.g. Bommer, 2003).

One recent GMPEs exploiting the former achievements, is the Abrahamson and Silva (2008), a ground motion empirical model developed for the rotation-independent average horizontal component from a shallow crustal earthquakes (NGA database). A faulting – style parameter is incorporated in the source term, together with a depth to top of rupture distance: for the same magnitude and rupture distance, buried ruptures leads to larger short period ground motions than the surface ruptures. The hanging – wall effect is also included counting for the fact that at the same rupture distance stations located in the hanging wall position tends to be affected by larger ground motions peak values.

However it has been observed that ground motion experiences strong azimuthal variations that none of the aforementioned models have included in the predictions. The effect responsible of such anisotropy has been called "directivity". As the abundance of phenomenological and theoretical studies has confirmed the concreteness of the directivity effect, the ground motion strategies have moved toward models able to better synthesize such variations. Two are the directions that have been presently proposed. One is based on the observations: these models deals either with the occurrence of a macroscopic effect attributed to the directivity, or with the source-to-site geometry that is expected to drive the signal amplitude and shape. This is the case of the model proposed by Somerville et al. (1997) and subsequently by Abrahamson (2000) or Bray and Rodriguez-Marek (2004). Another direction has been performed by Spudich and Chiou (2008), whose model is mainly oriented to identify significant trends from the synthetic simulations in order to compute an analytical formulation for the directivity effect. The need of synthetics simulations resides in the fact that the data-set is not enriched in azimuthally well distributed stations and generally the empirical data set is enlarged mixing temporal and spatial characteristic of earthquakes (under the

ergodic hypothesis), so that identifying a specific trend is not trivial. Thus a guide to infer a robust parametrization on a well-defined data-set is devolved to the simulations. The large amount of synthetic seismograms gives a very detailed description of the variability that could be observed at several sites for different earthquakes. In particular, a part from site effects and propagations effects, seismic modeling allows us to capture the role of the rupture complexity on the ground motion spatial pattern (e.g., Ameri et al., 2007; Rodgers et al., 2007; Sekiguchi, 2007; Sørensen et al, 2007; Ameri et al., 2008; Causse et al., 2008; Ripperger et al., 2008; Wang et al., 2008).

Although the anisotropy effects resulting from the propagation of rupture have been generally recognized and finally incorporated in predictions, its effect has not been tested yet in an hazard context. On the contrary, all the aforementioned issues motivate an in depth analysis of its contribution on the present tools of seismic hazard assessment.

This work is mainly addressed to conduct such analysis. One guidance is provided answering to the following questions: Does directivity improve the performance of ground motion prediction in real time applications? Is directivity still effective in a PSHA framework? What deterministic hazard model can tell about directivity ?

Several are the instrument I propose to reach this goal. In Chapter 1 a brief overview on the directivity effect and its phenomenology is presented, with the main purpose to best synthesize all the pertinent informations about the phenomena and its implication in characterizing the ground motion.

In Chapter 2 the problem of real time applications is faced, where the adequately characterization of ground motion level is effective for civil defense post-earthquake response and recovery. ShakeMap (Wald et al. 2006), a recent and popular product of the U.S. Geological Survey Hazard Program, provides near-real-time maps of ground motion and shaking intensity induced by significant earthquakes. It uses the GMPEs to predict ground motion levels where no recordings are available. Clearly the more the instrumental coverage is dense, the more the ground motion description is reliable. But its effectiveness in predicting ground motion in presence of a data-gap has been not yet clarified. It is objective

of Chapter 2 to test the performance of ShakeMap with respect to the real data, starting from a region of high instrumental coverage, ending with a situation in which all the stations are removed. The directivity effect is therefore introduced in order to provide for a weak agreement with the observations.

In Chapter 3, the probabilistic seismic hazard assessment (PSHA) is examined. In PSHA the ground motion prediction capability constitute the central pillar of the formulation. Thus the uncertainty related to the ground motion prediction strongly influences the hazard evaluation. Its reduction could significantly affect the predicted hazard level. In this chapter the effectiveness of directivity on hazard formulation is tested with the development of a new approach suitable to be updated every time that new informations are collected.

In Chapter 4, the role of directivity on ground motion variability is captured in a context purified by site and propagation effects. The approach is based on the massive production of deterministic rupture scenarios on the same causative fault. Moreover this approach provides a mean to set up a synthetic data-base deputing the ground motion predictive equations when the data shortage provides no information about the seismic ground shaking potential.

Chapter 1

Directivity in the observations: a brief overview

There is no doubt that seismic records carry information about the earthquake source, such as: its dimension, the speed of rupture and other parameters of interest. The point source model is not sufficient for these purposes and one has to consider the finiteness of the source if one wishes to be able to interpret details of amplitude-variation on a seismogram.

Ben-Menahem, 1961

The asymmetry in the seismic radiation has long being recognized at low frequencies in the recordings of large earthquakes (Benioff, 1955; Kansahara, 1960). S waves and Lg waves radiated in the rupture direction are expected to be amplified respect to the same waves traveling in the other direction. This effect has been theoretically constrained by Ben-Menahem (1961), who first called this phenomenon "directivity".

Ben-Menahem explained the directivity effect by means of a finite moving source finding that the observed wave-pattern is mainly driven by the source dimension and the rupture speed.

The effect of a moving source have been extensively studied in theoretical waveform modeling, addressed to solve the finite fault radiation problem, or the Kirchoff diffraction problem. One of the most striking examples of rupture directivity in kinematic source modeling is the rectangular fault model proposed by Haskell (1964,1966). He has demonstrated the implications of an unidirectional propagation over a finite fault on the radiated spectra suggesting that it has a

smoothing effect on the waveform: weakest in the direction of rupture propagation and strongest in the opposite direction.

The directivity effect is the macroscopic expression of the propagation of rupture on the seismic causative fault. When an earthquake strokes, a fracture propagates along the fault promoting a breaking sequence of ruptured points. Each point releases the stored elastic energy partially through elastic waves propagating toward the surface. The newly S -waves front may interfere with the others released during the propagation of the rupture, leading to a modulation of the energy content both in time and amplitude.

From sixties until now the studies on directivity have been divided into two main branches even though not explicitly. The first is based on the phenomenological near-source observational evidence of a strong velocity pulse recorded at the beginning of the signal (Hall et al. 1995; Somerville et al, 1997; Cox and Ashford 2002). Since the presence of a high-energy low-frequency pulse changes significantly the structure displacement demand, directivity has suddenly attracted the civil engineering interest. Thus a big effort have been devolved in characterizing the directivity effect, detecting the pulse and improving the probabilistic hazard assessment (Tothong et al. 2007, Baker 2008; Iervolino and Cornell, 2008).

The second branch is quantitatively based on the physics of the interference process. It compares the rupture episode to an emitting source that moves along the rupture surface (Boore and Joyner,1978, Joyner, 1991; Bernard et al., 1996). From a phenomenological point of view this interpretation can be compared to the Doppler effect: the source movement generates a frequency shift in the signal as perceived by the fixed receiver. The former interpretation justifies the strong spatial heterogeneity associated to the complexity of rupture even when no velocity pulses are detected.

Directivity strongly imprints the energy content of the ground motion and plays an important role for both engineering applications and predictive purposes. In fact the

hazard assessment is generally devolved upon a ground motion model where the ground shaking is expected to attenuate isotropically with distance. This description diverges from the observations insofar as it doesn't include any source complexity. Directivity enters the ground motion prediction with the purpose of refining the source description into the predictive equations in order to break with the "oversimplified" traditional formulation. The directivity models are addressed to explain both the observed azimuthal variations and the frequency modulations of the radiated wave pattern as a function of a few rupture related parameters (namely the strike and dip angles, the rake angle, the distance from the rupture surface etc..). Nowadays two are the referential directivity models: (1) one purely related to geometrical considerations (Somerville, 1997); (2) another mostly focused on the ray theory (Spudich and Chiou, 2008). Such models are calibrated on the data set and act on the ground motion predictive equations as corrective factors.

1.1 On the directivity effect

Radiation from extended seismic sources often present an asymmetric pattern. In the direction of the rupture propagation higher amplitudes of short duration are observed. This effect was discovered by Benioff (1995) and theoretically constrained by Ben-Menahem (1961).

Suppose that the earthquake can be viewed as the macroscopic effect of a series of small earthquakes triggered by the propagating rupture wave front. The far-field elastic displacement u caused by a displacement discontinuity across an internal surface can be obtained by the integration of small area elements regarded as point sources, making the allowance for different triggering times dependent on the time the rupture propagation reaches each element. If the rupture initiates at one end of the fault and propagates along the x axis over the length L with a constant rupture velocity v_r the ground displacement can be written as:

$$u(\boldsymbol{x}, t) \propto \int_0^L \dot{f}\left[t - \Delta t(\xi)\right] d\xi \tag{1.1}$$

where f is the dislocation history over the rupture surface (the source time

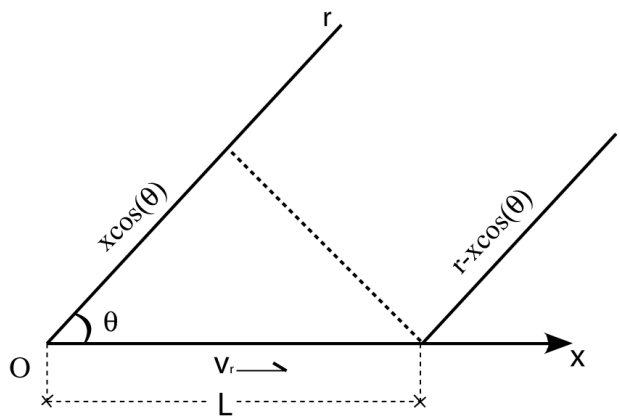

Figure 1.1 Geometrical configuration of a propagating source with constant rupture velocity vr and propagation velocity c in the x direction.

function) and Δt is a time delay due to the different travel times of waves coming from different parts of the fault. In practice, each newly ruptured segment is treated as resulting from the sum of different emitting point sources or, on the other side, as the result of one emitting source propagating allover the fault (IASPEI Software Package, Spudich and Xu, 2003).

Consider now a receiving station in the far-field, under the assumption that the wavelength (λ) can be comparable with, or less than, the fault dimension $(L^2 \ll (1/2)\lambda r)$, r is the epicentral distance). Again, making an analogy with the electromagnetic field, this is the same condition to be satisfied for the region of Fraunhofer diffraction in optics. In this region the interference within the progressively emitted body waves is possible.

The arrival time of the first emission is:

$$t_1 = \frac{r}{c} \tag{1.2}$$

The arrival time of the last emission is given by:

$$t_2 = \frac{L}{v_r} + \left(\frac{r - L\cos\theta}{c} \right) \tag{1.3}$$

where θ is the angle between the ray leaving the source and the direction of rupture propagation (figure 1.1), c is the wave propagation velocity.

The time delay Δt of a wave front emitted from one segment, relative to the emission at the first segment is given by:

$$\Delta t = t_2 - t_1 = \frac{L}{v_r} \left(1 - \frac{v_r}{c} \cos\theta \right) \tag{1.4}$$

Substituting Δt in (1.1), the displacement is given by:

$$u(\boldsymbol{x}, t) \propto \int_0^L \dot{f} \left[t - \frac{\xi}{v_r} (1 - \frac{v_r}{c} \cos\theta) \right] d\xi \tag{1.5}$$

It can be notice from (1.5) that the time history of dislocation has a dependence on the azimuth angle. Because the seismic moment must be preserved, the source time function will be narrower with high amplitude for stations located in the rupture direction, broader with smaller amplitude for stations located in the opposite direction. From (1.4) it appears also that Δt, which represents an "apparent duration" of the emission, has a dependence on the azimuth. If we take as a reference the angle for which the modulation is null (θ = 90), the duration of the emission changes by a factor Cd:

$$C_d = \frac{1}{1 - \frac{v_r}{c} \cos\theta} \tag{1.6}$$

that is is the commonly used expression for the directivity factor.

The effect can be seen in the radiation patterns of figure 1.2 computed by Hirasawa and Stauder (1965). In the same paper Hirasawa and Stauder have also discussed

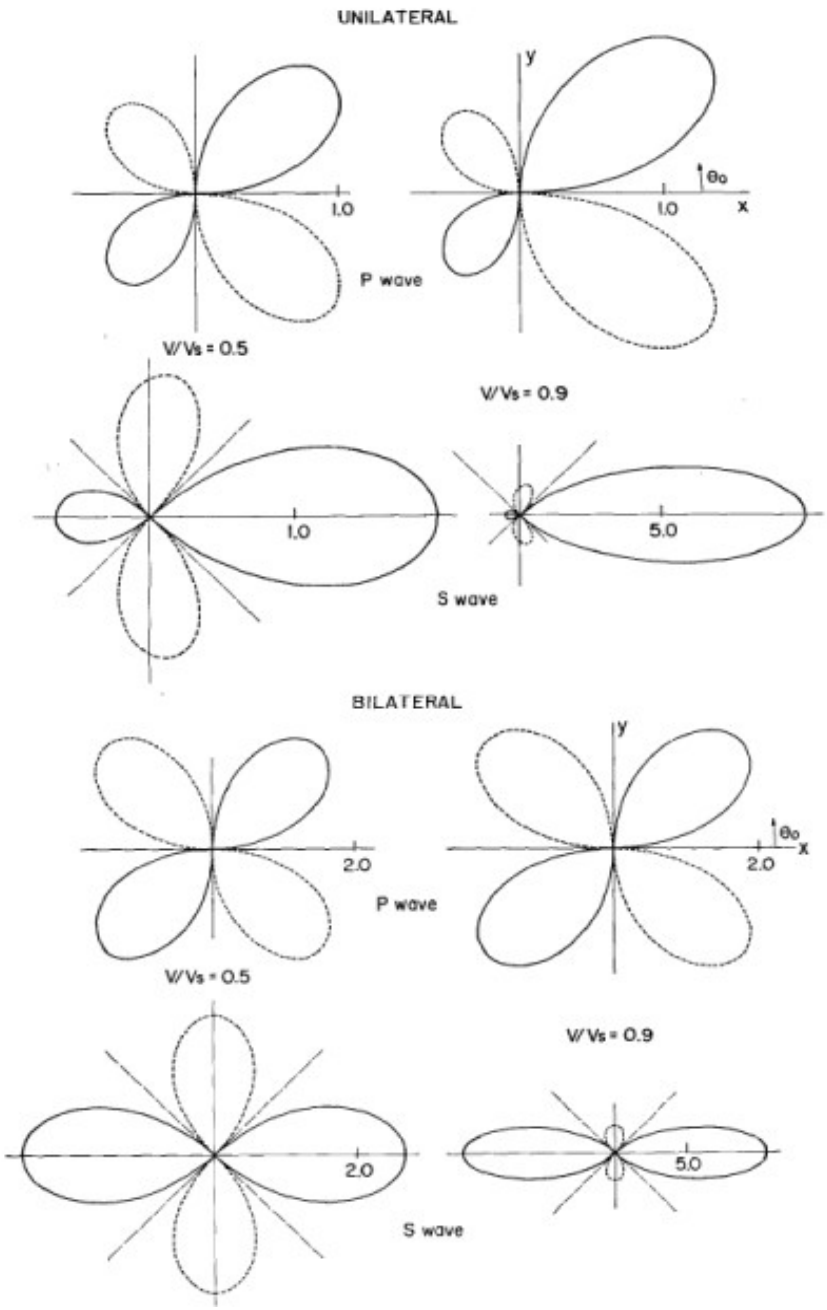

Figure 1.2: Radiation patterns of the S and P waves from sources with rupture propagation for: (a) $v_r/\beta=0.5$; (b) $v_r/\beta=0.9$ where v_r and β denote the rupture and shear wave velocities respectively. Solid lines indicates positive and dashed lines indicate negative values. Unilateral rupture on the top. Bilateral rupture on the bottom. (from Hirasawa and Stauder, 1965).

seismic body waves from fault models both in the frequency domain and in the time domain in connection with the elasticity theory of dynamic dislocations. They provide an extension of the Ben-Menahem (1961) model assuming that the rupture propagates from a point in the fault plane to positive and negative directions along its length. This is called bilateral faulting. They come out with the following the result that: "Even for the bilateral fault model, the radiation patterns of the body waves depend on the rupture velocity".

For the bilateral case is assumed that the fault in the direction of the negative x axis has the same length as on the positive side. The directivity factor can be re-written as:

$$C_d = \frac{1}{1-\frac{v_r}{c}\cos(\theta)} + \frac{1}{1+\frac{v_r}{c}\cos(\theta)} \tag{1.7}$$

The directivity effect is mainly attributed to an interference between waves radiated from different parts of the fault surface, analogously to what happen with the electromagnetic wave generation. As a consequence the contributions from each part of the fault are concentrated in the rupture direction and are dispersed in the reverse direction (figure 1.3 from Benioff, 1995).

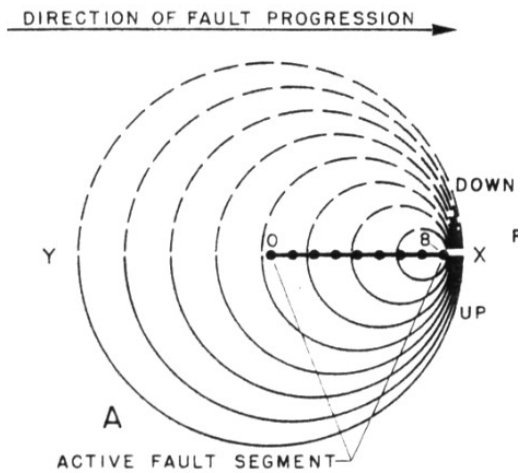

Figure 1.3: Effects of slip progression on wave amplitudes and shape (from Benioff, 1955)

In order to quantify the effect of the rupture propagation over a finite fault length we turn to the spectrum, computing the Fourier transform in the frequency domain. The displacement spectrum has a basic shape made of a plateau at low frequencies and a downward sloping envelope for high frequencies with slope proportional to ω^{-p}, where p has been extensively studied in kinematics. In fact the slope p is strongly influenced by the wave attenuation, the source radiation pattern, the finite rise time and the finite length. These factors introduce a smoothing on the waveform (Haskell, 1964). In order to see the effect of the rupture propagation over a finite fault length we take the Fourier transform of the equation (1.5). Writing the f(t) as f(ω), we get:

$$\begin{aligned} u(\boldsymbol{x},\omega) &\propto \frac{1}{L} f(\omega) \int_0^L \exp\left(i\omega \left[\frac{\xi}{v_r}(1-\frac{v_r}{c}\cos\theta) \right] \right) d\xi \\ &\propto f(\omega) \frac{sinX}{X} \exp\left[-i\omega \frac{r}{c} \right] \exp\left[i(X-\frac{\pi}{2}) \right] \end{aligned} \tag{1.8}$$

Where:

$$X = \omega \frac{L}{2} \left[\frac{1}{v_r}(1-\frac{v_r}{c}\cos\theta) \right] \tag{1.9}$$

The sinc X factor represent the finiteness of the source and it is responsible of a deviation from a purely dipole radiation pattern. Its central role in seismic sources was demonstrated by Ben-Menahem (1961) in the study of the regular sequence of holes in the amplitude spectra.

When:

$$\frac{L}{v_r}(1-\frac{v_r}{c}\cos\theta) = n\frac{2\pi}{\omega} = n\lambda$$

the displacement spectrum at the receiver will produce spectral nodes. This condition corresponds to destructive interference, and is analogous to Fraunhofer diffraction through a rectangular slit (figure 1.4 panel a).

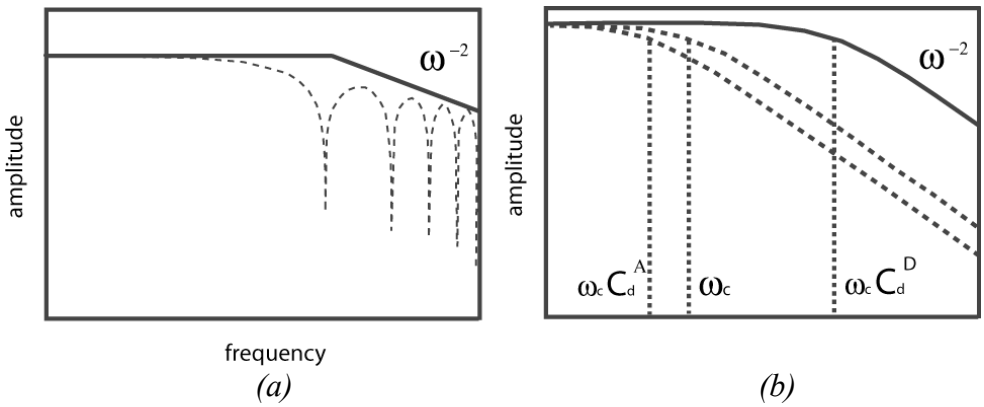

Figure 1.4: (a) the spectrum holes due to the sinc X functions. (b) Effects of the directivity on an ideal ω–square spectrum (from Convertito PhD thesis): C_d^D indicating the correction for stations located ahead the rupture propagation; C_d^A meaning the correction for stations located in the rupture propagation opposite direction. ω_c is the corner frequency

To simplify, as the S-waves from each source travel along the fault, they interfere with waves generated by the newly rupture segments, enforcing or weakening the signal amplitude. The closer the rupture velocity is to the S-waves velocity the more the waves reinforce each other.

Ben-Menahem ascribes directivity to the rupture speed and the finite source dimension; these two elements cannot be ignored whenever the dimensions of the source are of the order of the radiation-dominant wave-length.

In addition, there is a frequency shift similar to the Doppler effect in acoustics (Douglas at al. 1988), so that a monochromatic moving point source of frequency ω is observed to emit an apparent frequency:

$$\omega_a = \omega \frac{1}{v_r}\left[1 - \frac{v_r}{c}\cos\theta\right] = \frac{\omega}{C_d v_r} \tag{1.10}$$

Directivity promotes a frequency shift in the radiated spectra. The corner frequency (ω_c) is shifted by the directivity factor *Cd(θ)* for station located in the direction *θ*. The shift is toward higher frequency for station located in directive direction: more high frequency waves are observed in the rupture propagation direction (figure 1.4b).

At high frequencies, i. e. frequencies greater that the corner frequency, the amplification of the base spectral level is proportional to ω^p so that an amplification proportional to $[v_r C_d(\theta)]^p$ is expected in theory.

Generally accepted values for the Mach number (v_r/β) ranges in [0.6, 0.92]. The classical ω – square model would imply an amplification at high frequencies of Cd^2 of the acceleration spectra. For a velocity ratio of 0.9 and $\theta=0$, then $Cd=10$ and an amplification by a factor 100 is expected. However such large effects have not been reported neither quantitatively nor even qualitatively.

Another tool to evaluate the amplification is given considering the ratio D of the spectral amplitudes of seismic pulses that leave the source in opposite azimuth θ and θ +π. It can be defined a directivity function (Bullen and Bolt, 1985):

$$D(\theta)=\frac{(1+\frac{v_r}{\beta}\cos\theta)\sin\frac{\pi L\beta}{\lambda v_r}(1-\frac{v_r}{\beta}\cos\theta)}{(1-\frac{v_r}{\beta}\cos\theta)\sin\frac{\pi L\beta}{\lambda v_r}(1+\frac{v_r}{\beta}\cos\theta)} \qquad (1.11)$$

that is independent of the source time function, providing a mean to evaluate v_r and L at stations on a great circle path (e.g. Filson and McEvilly, 1967).

From equation (1.11), it follows also that seismograms from stations located at the opposite ends of the fault rupture (i.e θ=0, π), have different radiation amplitudes. In particular, the amplitude in the direction of rupture is larger than that away from the motion by a factor:

$$\frac{D(0)}{D(\pi)}=\frac{(1+\frac{v_r}{\beta})}{(1-\frac{v_r}{\beta})} \tag{1.12}$$

1.2 The detection of directivity in the observations: some attempts

The directivity effect has been theorized in order to explain the strong azimuthal heterogeneity in the ground motion recordings. The seismological expectations are thus derived from kinematic models of earthquake rupture or from the parametrization of directivity in regression. These models predict amplitude variations that, if real, should represent a first order effect in the ground motion variability. However the expected directivity effect is not systematically observed, chiefly in the high frequency range.

The directivity phenomena is well understood at low frequencies, i.e. at frequencies less or equal to the corner frequency of the earthquake. Common periods for directivity are assumed to span in the [0.5, 3.0] seconds range. Near-fault long period ground motion has been discovered in several earthquakes, i.e. 1966 M6.1 Parkfield, CA (Aki, 1968), 1971 M6.6 San Fernando earthquake (Hanks,1975), 1992 M7.2 Landers earthquake (Chen, 1995). This long period component of the strong motion was interpreted as reflecting the details of the earthquake source and ground motion propagation. Somerville et al. (1997) has pointed out that the forward directivity pulse has a dominant period of 0.6s or longer, and he has identified the fault-normal component to be more sensible to the rupture complexity.

Based on a directivity theoretical model several authors have searched for the components where the peak values are larger, attempting to fit for the rupture direction and rupture velocity. Howard et al. (2005) found that the expected maximum component of the Spectral Acceleration (SA_{max}) correlates with the orientation of a strong velocity pulse in the directivity record.

Instead, at high frequencies the characterization of the phenomenon on the data is often an issue, and a qualitative description is easier that a quantitative one. The directivity effect in the high frequency range could be masked by major effect, by way of example, the superposition of long period ground motions to regional surface waves, making it difficult to resolve events separated by less than a certain threshold, 30 seconds as in the case of 1940 M7.1 Imperial Valley earthquake (Trifunac and Brune, 1970). Clear directivity effects at high frequency are reported by several authors: Boore and Joyner (1978) showed that C_d also appears for the high frequency generated by the incoherent rupture of a moving, instantaneous source; Boatwright and Boore (1982) compared data recorded at the same site from two oppositely directed ruptures providing a striking example of the directivity effect in the acceleration recordings; Boatwright (2007) has extended the research developed by Howard at al. (2005) to small earthquakes , finding that the rupture propagation can distort the attenuation of the PGA with distance; Cultrera et al (2009) have confirmed the directivity effect observed during the Umbria-Marche seismic sequence (central Italy), availing of the synthetics simulated by an hybrid deterministic-stochastic method. However, the directivity effect as modeled in paragraph 1.1 have not been yet confirmed by the observations from a quantitative point of view. The discrepancy between the observations and the predictions has been identified in the assumption of the ω-square model (Aki, 1967; Brune 1970,1971) for the radiated spectrum. As pointed out by Joyner (1991) this classical model would imply an amplification at high frequencies of Cd^2 of the acceleration spectra. On the contrary, all the observations seem to be compatible with an amplification lesser than or equal to a *Cd* factor. Bernard et al. (1996) have demonstrated, in the case of S waves, that the directivity effect is frequency-dependent and distorts the ω-square model. Their demonstrations is related to the width of the slip pulse, that is no longer considered instantaneous: a narrow slip pulse promotes a strong dependence of the directivity effect in the direction of rupture, with a larger amplification at low frequencies controlled by Cd^2 and a smaller amplification at higher frequencies controlled by *Cd;* for broader pulses, the corner frequency is shifted toward lower values, masking the Cd^2 effect and reducing the directivity effect to *Cd* amplification of the spectral level.

1.3 The directivity corrective factors: a modification to the Ground Motion Predictive equations

Directivity enters in the ground motion predictive equations (GMPEs, see the Introduction for further details) with Campbell (1987) who modeled the peak intensity measures with a switch for directive station (θ=0°).

Bray and Rodriguez-Marek (2004) proposed a very simple parametrization to characterize the pulse-type motion resulting from forward-directivity: the empirical equation is developed on the representative pulse, its period and the number of significant pulses in the velocity time history. This approach is manly phenomenological, linked to the description of the effect rather than its causes.

However, the introduction of new parameters in ground motion predictive tools is an attempt to gradual transforming the aleatory model variability into an epistemic uncertainty (e.g. Bommer et al. 2003). As a matter of fact the high residuals hide our consciousness about the process. The effect is magnified by the ergodic assumption, allowing the replacing of temporal characteristic with spatial characteristic and used to enlarge the data-set despite the blending of specif dependencies (see Chapter 2 for further details). Once that a trend is individuated and codified into an analytical formulation, new explanatory variables can be incorporated in the ground motion predictive equation. The variance is thus hopefully decreased, because the use of a physical relation between the new parameters avoids the uncontrolled growth of the uncertainty.

The simple formalism of the GMPEs and the logarithmic dependence of the ground motion intensity measure simplify the operation. Each terms departing from the traditional formulation is incorporated by adding new functional forms.

Source parameters, and rupture process could be incorporated in the following form (see I.1):

$$lnIM = f(R) + f(M) + f(site) + f_{source} + \sigma \qquad (1.13)$$

where f_{source} is a new functional form synthesizing the finite fault contributions. This correction is usually directly derived from a dataset, or may be deduced from the theory (Convertito and Herrero, 2004; Spudich and Chiou, 2008).

The first study which considers the directivity as a function of few source parameters and the frequency, is given in the work of Somerville et al. (1997), hereafter Som97. The directivity becomes then a corrective factor to be applied to a GMPEs. A second study by Spudich and Chiou (2008), hereafter SC2008, introduces a more articulated modeling of the directivity, always as a corrective factor, embedded within the radiation pattern, to improve the ground motion predictive capability.

Somerville et al. (1997) developed a corrective factor for directivity on the Abrahamson and Silva (1997) equation (Chapter 2). The corrective factor has been formulated for strike-slip mechanisms and dip-slip faults over a data-set made of crustal earthquakes with magnitude of 6.5 or larger, and for rupture distances up to 50 km. The data-set includes all the California recordings for which the faulting mechanisms are available together with selected crustal earthquakes from other regions (e.g. the 1995 Kobe earthquake). Its analytical formulation has been calibrated on the data, applying the random effect method (Abrahamson and Youngs, 1992) to the residuals between the data-set and a reference predictive model. This strategy enables to quantify the residual dependence on the fault parameters avoiding unduly influence of events having large or poor number of recordings. It is based on two geometrical parameters: the coherence length has been simplified through the fraction of fault rupture surface lying between the hypocenter and the site; the azimuth dependence enters the formulation through the cosine function of the angle between the fault plane and the direction to the site. The corrective factor and the two geometrical parameters are related by the following equations:

$$y = \begin{cases} C1 + C2\ X\ \cos\theta & for\ strike\ slip \quad M = 6.5 \\ C1 + C2\ Y\ \cos\phi & for\ dip\ slip \quad M = 6.5 \end{cases} \tag{1.14}$$

where y is the residual of the natural logarithm of the spectral acceleration at a given period; C1 and C2 are the coefficients of the model spatial variation of average horizontal spectral acceleration; X and Y are length ratios representing the fraction of rupture surface lying between the hypocenter and the site; θ and Φ are respectively the angle measured for strike-slip faults from the epicenter to the site in the horizontal plane and the angle measured for dip-slip faults from the hypocenter to the site in the vertical plane (figure 1.5a). The smaller is the angle θ (or Φ) larger the amplitude. The larger the fraction X (or Y) of fault rupture surface (the larger the ray path difference), the larger the amplitude.

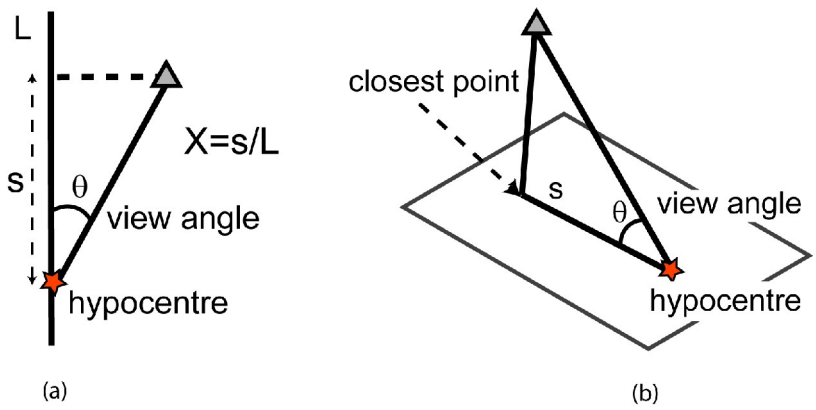

Figure 1.5: (a – from Somerville et al. 1997) Rupture and site geometry in the Som97 formulation, θ is the angle between the rupture direction and the source-site alignment;and X is the length ratio (b) the Rupture and site geometry in the SC2008 formulation. s is the linear dimension of the rupture surface toward the site in the strike direction for both Som97 and SC2008; θ is the angle between the rupture direction and the source-site alignment. SC2008 introduces also h relative to the nucleation position in respect to the exposure of the fault.

The directivity effect results in a period dependent amplification factor beginning at 0.6 seconds and increasing with period. The 0.6 threshold has been indicated as a transition between the coherent source radiation and the incoherent outline at short periods.

For strike-slip mechanism the whole area (rupture distances up to 50 km) has been taken into account; for dip-slip mechanism the corrective factor has been confined in the region between the ends of the fault (figure 1.6). This difference arises because formally, for dip-slip faults in the region off the end of the fault, the directivity variation of ground motion is less significant because in this case the directivity effect is operating up-dip (Somerville et al. 1997). Technically this region is excluded because the variation of ground motion parameters with the angle Φ is indistinguishable from its variation with the used distance definition that is the minimum distance between the site and the rupture plane (Rrup). Thus, the variations due to the directivity corrective factor are already incorporated in the predictive equation via the distance dependence.

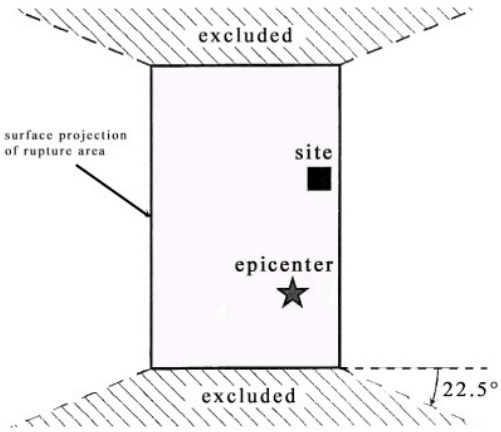

Figure1.6: Region off the end of dip-slip faults excluded from the model. From Abrahamson and Somerville (1996).

This corrective factor has the advantage to be applicable to different predictive equations since the authors enhanced the applicability of the corrective factor to other predictive models removing the bias between the data-set and the model. However, it seems not to provide a significant reduction in the uncertainties that affects the ground motion predictive equations.

Spudich and Chiou (2008) have exploited the simple formalism produced by the isochrone theory (Bernard and Madariaga, 1984; Spudich and Frazer, 1984) to developed a corrective factor for directivity over five different predictive equations (Abrhamson and Silva, 2008; Boore and Atkinson,2007; Cambell and Bergoznia, 2008; Chiou and Youngs 2008), using the same record selection criteria adopted by each author.

The isochrone ray theory has been developed to model the effect of shearing motions on a finite fault surface. It simplifies the solution of the ground motion equation reducing the double integral to a line integral along equal phase lines (isochrone). Each path of integration consists of only those points on the fault which radiate body waves arriving at the observer at a certain time (Spudich and Frazer, 1984). An isochrone velocity may be defined along the fault, being directly proportional to the isochrone spacing: in the two-dimensional case the isochrone slowness is equal to the usual seismic directivity function.

SC2008 developed the corrective factor on the basis of this statement. They consider two point sources on the fault: the hypocenter and the point on the fault closest to the site. The distance between these two points is analogous to the fraction surface of Som97 and represents the portion of fault suitable for rupture from the hypocenter toward the site. They make use of this distance to approximate the radiation pattern and calculate the S-wave polarization.

The corrective factor for directivity formulated by SC2008 depends on (figure 1.5b): the fraction of rupture surface lying between the hypocenter and the closest point to the site (S); the isochrone velocity ratio (C); the radiation pattern (R_{ri}) that

spatially modulates the ground motion amplitudes. The functional form of their corrective factor is called *IDP* for Isochrone Directivity Predictor, is the following:

$$IDP = CSR_{ri} \tag{1.15}$$

$$C = \frac{min(\tilde{c}, 2.45) - 0.8}{4 - 2.45} \tag{1.16}$$

$$S = \ln\left[min(75, max(s, h))\right] \tag{1.17}$$

where s and h represent the dimension of the rupture surface lying between the hypocenter and the point on fault closest to the site (figure 1.5b). $\tilde{c}$ is the isochrone velocity ratio.

Unlike Som97 the SC2008 corrective factor is not simply derived from the observations; the preferred directivity variables are searched over a rich data set of synthetics (URS Corporation) in order to formulate the effective functional form for a directivity model. Moreover is depends on the focal mechanism through the radiation pattern (Som97 depends only on the strike angle and it switches with the faulting style). It depends on the view angle implicitly, via the ray theory (Som97 declare the angle between the rupture direction and the site position); it depends on the velocity ratio quantifying the rupture velocity relative to the propagation speed (Som97 neglect the contribution of the velocity rupture). Thus, also the number of parameters involved in each method is not the same. Both depends on the relative position between the hypocenter and the point on the fault closer to the site but unlike Som97, which defines this relative position in the up-dip direction dimension or along the strike dimension depending on the switch over the focal mechanism, SC2008 selects the maximum component between the two. The SC2008 formulation correlates significantly with the residuals providing a relevant

reduction of the model uncertainties (up to 16% of variation respect to the no-corrected models).This reduction motivates us to incorporate this factor into probabilistic hazard analyses in-line with the SSAHC (Senior Seismic Hazard Analysis Committee) recommendations (1997).

Chapter 2

Directivity: improving the ground motion predictions in real time applications.

The large and apparently random (called aleatory from the Latin *alea* meaning dice) variability in ground motion results from using very simple models for a very complex phenomenon.

Bommer and Abrahamson (2006)

Earthquake scenarios are used heavily in emergency response planning. In Italy the Civil Protection Department are in great need of rapid and accurate informations about the earthquake, in order to properly direct rescue teams and organize the emergency response. These informations can be achieved portraying the ground motion shaking in real time (a few minutes from earthquake occurrence).

A prompt strategy for generating rapid-response ground motion maps is contouring the real data recorded at the stations. As a consequence the representation of the ground motion pattern is strongly conditional on the quality and availability of data. Nevertheless, only a few region in the world, i.e Japan or Taiwan, have an instrumental coverage as dense as needed to produce accurate shaking maps directly from the observations. Other regions, due to the paucity of the stations, would produce a contouring strongly unstable and it is necessary to bridge the instrumental gap using different strategies. One route to solve this matter has been recently proposed in 2006 by Wald et al. (U.S. Geological Survey -USGS-

Earthquake Hazard Program) through the implementation of the software package ShakeMap. ShakeMap is a technique addressed to stabilize the contouring and minimize the misrepresentation of a ground motion intensity measure augmenting the available data with predicted values over a number of phantom stations. Therefore this instrument can be regarded as an interpolation operator that uses the ground motion predictive equations (GMPEs) to "fill" the data gap. Once that the interpolation is computed, ShakeMap calibrates the interpolated surface on the available data. Near the observed strong-motion stations, the phantom stations are rejected, allowing the data to control the solution where they exist. Thus if the station network is very dense, the weight of the interpolation is weak and the ShakeMap is mainly driven by the observations. Otherwise, when the station network is lean, the selection of the proper predictive equation drives the goodness of the ground shaking estimation.

However, as pointed out in chapter 1, the GMPEs may not reproduce faithfully the ground motion close to the fault since multidimensional effects, like the directivity effect, are not accounted for. The new generation of GMPEs (e.g. Abrahamson and Silva, 2008) accounts for parameters related to the earthquake source, the site condition, and the propagation effects that, with respect to the simplest GMPE currently implemented in ShakeMap (Boore et al. 1997, Joyner and Boore, 1988), provides a more accurate description of the ground motion anisotropy. Other equations (e.g, Spudich and Chiou, 2008) account also for directivity and may improve the ShakeMaps results when a few basic seismic source parameters become available (strike, rupture laterality, etc.). Thus these equations should be implemented in ShakeMap to better constrain the ground motion variability for generating rapid-response ground motion maps once their efficacy is proved.

It has to be emphasize that a key question with respect to the application of one model respect to another is the measurement of its performance relative to the observations (the principle of the empirical control). Thus the ShakeMap gives the opportunity of directly check the quality and the applicability of the adopted strategies with respect to the modeling of real shaking. One route to test the

efficacy of the new generation predictive equations on ShakeMap, is to cut off several stations from a dense instrumental network and verify their capability of fill in the gap. Thus the test consists of: (1) computing a reference ShakeMap using a traditional GMPE over the all data available; (2) studying the degradation of the ShakeMap when the number of observations is reduced; (3) introducing a directivity term within ShakeMap modifying the GMPE with the Spudich and Chiou (2008) corrective factor; (4) quantifying the improvement of the ground shaking estimation.

In order to conduct properly the test, a dense network is needed. Thus we have investigated the 2008 Miyagi (M6.9) and the Tottori (M6.6) Japanese earthquakes which were recorded by the dense K-net (Kyoshin Network) and Kik-net (Kiban Kyoshin network) seismic networks operated by the National Research Institute for Earth Science and Disaster Prevention (NIED, 2002).

2.1 Real time ground motion estimation: Shakemap

ShakeMap is a collection of modules written in PERL, conceived in 2006 by David Wald, created to generate a rapid and automatic web-based display of the shaking level at each station on a map. It combines instrumental measurements of shaking with information from the individual station, geology (representing site amplification), earthquake location and magnitude, to estimate shaking variations throughout a geographic area. The procedure produces ground motion predictions usually on a 30 km spaced grid of phantom stations. The ground motion intensity measure is assigned to each coarse grid using a ground motion predictive equation. When a station is present its value in a boundary is preserved so that the predicted values are anchored to the observation. Thus, because the earthquake magnitude of the event could be not completely accurate at the time Shakemap is first run, the predictive curve is shifted in amplitude in oder to bring the estimations in line with the recorded data. The shifting value is called bias factor and it is computed minimizing the difference between the data value at the seismic station and the

estimated value at the same locations. The minimization is the L1 norm (absolute deviations) that has proved to be better than a least-squares method in constraining the scatter in seismic data (Wald et al., 2006).

A site correction is needed because direct interpolation may inadequately represent the true amplification. Therefore, prior to the interpolation, the observed ground motion is first reduced to a common reference "bedrock", then interpolated and finally corrected by site effects. In practice, the recorded peak ground motion amplitudes are converted into rock-site condition while the ground motion predictions are directly calculated to the phantom points to obtain a rock-site grid.

The site reduction is obtained applying frequency and amplitude-dependent amplification factors. Given the mean 30-m shear velocities (Vs30) the amplifications can be calculated for short-period (0.1-0.5 s) and mid-period (0.4-2.0 s) ranges from Borcherdt (1994, equations 7a and 7b, respectively) at four ranges of input acceleration levels (see Borcherdt, 1994, table 2). The peak acceleration (PGA) amplitude scales with short-period amplification factors while the peak ground velocity (PGV) values are corrected with the mid-period factors. Response spectral values are scaled by the short-period factors at 0.3 sec, and by the mid-period response at 1.0 and 3.0 seconds. The Vs30 are determined, when available, on geological or geotechnical based criteria. Otherwise the 30-m shear velocity is sampled from the topography relief as proposed by Wald and Allen (2007). Once the ground motion amplitudes are reduced to bedrock, shaking informations are interpolated onto a square grid uniformly sampled at spacing of 1 minute (about 1.6 km).

2.1.1 Limitations

Shakemap is simple but approximated, due to GMPE's oversimplifications. GMPEs predict a ground shaking that is more uniform than it would be expected for actual earthquake. Part of the variation with respect to the observed pattern is attributable to 2D and 3D wave propagation, path effects (such as basin edge amplifications and focusing), the other part is attributable to the rupture

complexity. When the finite fault is considered, and the the location of the epicenter is ignored, the nucleation position does not have any effect on the resulting ground motions; only the location and dimensions of the fault matter, and the same magnitude earthquakes correspond to the same ground motion shaking level. Moreover ShakeMap accounts for the finiteness of the fault by measuring the distance to the surface projection of the fault location (Joyner and Boore's distance definition). This choice may be reductive, because other effects related to the fault rupture surface may affect the ground motion peaks (i.e. hanging wall effect) and justify the observed wave anisotropy. If we were to add all these contributions to the calculations, then it would result in significantly different motions for the same magnitude earthquake or fault segment.

A first improvement can be achieved introducing the rupture parameters related on ground motion prediction in order to account for wave anisotropy or for the azimuthal variations induced by the rupture directivity.

2.2 A strategy to improve ground motion estimations

A more comprehensive description of the ground shaking can be achieved with the proper theoretical inclusion of known complex effects related to the rupture process. This improvements enter the ShakeMaps through the GMPEs. Actually the GMPE already implemented in ShakeMap are the Boore et al. (1997) and the Joyner and Boore (1988). Recently other GMPEs (Malagnini et al. 2000, Ambraseys et al. 1996, Bommer et al. 2000) have been have been implemented by Michelini et al. (2008) for applications to the Italian region in order to suite the requirement of well calibrated magnitude versus-distance equations. We focus on the Abrahamson and Silva (2008, hereafter AS2008) predictive equation that includes parameters related to the earthquake source, the site condition, and the propagation effects. This type of GMPE accounts accurately for finite fault effects and should improve the performance of ShakeMap with respect to the traditional equations already implemented in the code. This equation has also been selected by SC2008 (chapter 1) to calibrate a corrective factor for directivity. In this chapter

we have decided to use the SC2008 corrective factor rather than the som97 (chapter 1) because the former is physically based. Thus the AS2008 is proper to our purpose of incorporating a directivity term for ShakeMap applications.

In practice, in order to run this test, the PERL code have been implemented to suit the requirement of a finite fault description. Then, the AS2008 equation has been introduced inside the code. At the end, the corrective factor for directivity has been added to the base formulation. A brief overview of the AS2008 equation is given in the following paragraph. For comparison, we have also tested a relation currently used as default in southern California for all events with magnitude greater than 5.3. This equation is the Boore, Joyner and Fumal (1997, hereafter BJF1997) equation, briefly presented in the following.

Furthermore, because we have selected the Japan region to set our tests, also the regionally derived predictive equation formulated by Kanno et al (2006, hereafter Kan2006) has been considered.

2.2.1 The Abrahamson and Silva (1997) and Abrahamson and Silva (2008) ground motion predictive equation.

The Abrahamson and Silva (2008) equation (AS2008 hereinafter), is an implemented version of the 1997 equation of the same authors. This equation have been formulated on a world-wide data set including shallow crustal earthquakes. The equation is valid in a magnitude range 4.4-7.4 and for an epicentral distance of 0.1 – 200 km. The ground motion intensity measure is formulated by the following log-normal expression (the base equation):

$$lnSa(g) = f_1(M, R_{rup}) + F f_3(M) + HWf_4(M, R_x) + S f_5(PGA_{rock}) \quad (2.1)$$

where *Sa* is the spectral acceleration (g), *M* the moment magnitude, *Rrup* is the closest distance to the rupture plane (km), Rx is the horizontal distance from the edge of the fault (km), *F* is the fault type (1:reverse, 0.5: reverse/oblique, 0:otherwise), *S* is a “switch” for site class (0: rock or shallow soil, 1: deep soil),

HW a switch for hanging wall sites (1: sites over the hanging wall, 0: otherwise).

The 2008 version is improved enlarging the range of applicability of the previous equation extrapolating the model to all crustal earthquakes in California M5-M8.5 (strike-slip) and M5-8.0 (dip-slip), distance from 0 to 100 km, and spectral periods up to 10 seconds, according to the requirements of the NGA project (Power et al., 2008). The equations is calibrated on the PEER NGA database. This equations includes parameters related to: (1) the earthquake rupture, (2) site and (3) propagation effects:

1. earthquake rupture related parameters: the depth (km) to the top of seismogenic rupture (generally taken as the depth to the shallowest point on an earthquake rupture surface); the fault dip angle (0 to 90, in the Aki and Richards, 1980, convention); the average width of the fault.

2. site related parameters: the average shear-wave velocity between 0 and 30-meters depth (Vs30); the type of Vs30 in terms of being measured versus inferred (Vs30 type), the depth (km) to where shear-wave velocity is equal to 1.0 km/sec (the first occurrence if more than one depth exists).

3. propagation-effects related parameters: the shortest distance to the rupture surface; the shortest horizontal distance to the line defined by extending the fault trace (or the top edge of the rupture) to infinity in both directions. This value is used to define the hanging wall: values on the hanging wall are positive and those on the foot wall are negative.

Another implementation with respect to the 1997 version is in the managing of the horizontal components. The 1997 uses the geometric average of the maximum of the two horizontal components (which may not occur at the same time). Because the averaged horizontal component above is dependent on seismometer orientation, an orientation-independent alternative was defined by Boore et al. (2006) and used by all the NGA relationships including the AS2008. A good, brief description of this component is also given on page 7 of Campbell and Bozorgnia's (2006).

2.2.2 Boore, Joyner and Fumal (1997)

This predictive equation is used as the default relation in southern California for all events with magnitude ≥ 5.3. The relation has the form:

$$lnSa(g) = B_1 + B_2 f(M-6) + B_3 f(M-7) - B_4 f(\sqrt{R_{jb} + h}) \qquad (2.2)$$

Where, M is the magnitude, R_{jb} is the "Joyner-Boore" distance to the surface projection of the fault (km), h is determined by a simple search procedure to minimize the sum of squares of the residuals. This model assumes a shallow fault and uses only a 2D fault model with no depth term. BJF97 does not predict PSA at 3 seconds. As a first approximation we use the coefficients for PSA at 2 seconds.

2.2.2 Kanno et al. (2006)

The predictive equation of Kanno et al. (2006) has been calibrated over 91731 records from 4967 Japanese earthquakes occurred from 1968 to 1997. The data include foreign near-source data taken from earthquakes in California, Turkey and the United States, occurred in the compressional regime and in the shallow crust, matching the conditions in Japan. The relation has the form:

$$\log(Sa(cm)) = a_1 f(M) + b_1 f(R) - f(R, M) + c_1 \qquad (2.3)$$

Where R is the source distance defined as the closest distance from a fault plane to the observation site and it is the hypocentral distances in the case of earthquakes for which the fault model is not available; M is the moment magnitude. This equation incorporates correction terms for site effects and regional anomalies and a correction to model anomalous ground motions in NE Japan from intermediate and deep earthquakes occurring in the Pacific plate.

2.3 The ground motion prediction: going over ShakeMap

ShakeMap works on the Peak Ground Acceleration (PGA), on the Peak Ground

Velocity and on several Spectral Response ordinates, for reference period of 0.1 sec, 0.3 sec, 1 sec, 3 sec and on the Instrumental Intensity. We select the Pseudo Spectral Acceleration (PSA) portraying the response of a damped, single-degree-of-freedom oscillator to the recorded ground motions. We consider a reference period of 3sec, because this ground motion intensity measure reflects the pattern of the earthquake faulting geometry, with largest amplitudes in the near-source region, and in the direction of rupture (directivity). The 3 seconds PSA is also less sensitive to site effects. Even though differences between rock and soil sites appears, the overall pattern is normally simpler than the peak acceleration pattern.

Part of our analysis is conducted on "reasoning" on the ShakeMap procedure, in order to evaluate its predictive capabilities in presence of a data gap and to control its performance in managing a forced impoverishment of the instrumental coverage. A strategy to run this test consists in comparing the ShakeMap results with a reference map computed using all the data available in a zone of good azimuthal coverage. We have selected the Japan region, having both the Kik-net network and the K-net network. The K-net network is composed with about 1000 broadband strong-motion seismographs, with a dynamic range up to acceleration of 40 cm/s^2. The Kik-net strong motion net, is composed of about 800 high-sensitive seismographs deployed national-wide and installed both at top of the borehole and down the borehole to more that 100m depth.

The reference map should constitute a representation purified of possible artificial effects introduced by the ShakeMap procedure. This requirement is driven by the fact that ShakeMap combines established informations at randomly located stations and those used for the interpolated grid to achieve the best agreement with the observations. Therefore both the bias and the site corrections operated by ShakeMap depend on the number of the data available within a selected distance. Thus a comparison with two maps derived from a different instrumental coverage would results in a complex pattern that only reflects the disagreement between data-derived and empirically derived contouring maps.

The best solution would be computing a reference map interpolating merely the

data set, if the data set is as dense as needed to guarantee an adequate resolution. That means that the grid spacing should be able to sample the wavelength corresponding to the maximum frequency of interest in order to suitably describe the long period waves anisotropy in presence of a station gap. Moreover the grid spacing should be almost the same to allow a comparison between the ShakeMap results and the data derived interpolation.

The instrumental coverage of the Japanese net (about 1 station every 30 km) provides a space sampling that encounters both the aforementioned conditions on several parts of the region of interest. It makes us confident on the result of the comparison even when a simple graphical interpolator is used except for zones where the data gap is wide spread.

In computing the reference map we adopt the same procedure used by ShakeMap to refine the grid spacing in 1.6km. We use an adjustable-tension continuous curvature surface gridding algorithm that fits the constraining data exactly (Smith and Wessel, 1990). The interior and boundary tension factor, *surface_tension*; is set to 0.9. The tool is available within the Generic Mapping Tools (GMT, Wessel and Smith, 1991). Moreover, we also account for another operation computed by ShakeMap that is the GMT *blockmean* routine. This routine reads arbitrarily located (latitude, longitude) points and writes out a mean position and value for every block in the define grid region. Thus:

"despite fitting the data in the derivation of the continuous surface, the grid of values sampled from this surface we produce does not include the exact location of the data, unless by close coincidence. For this reason, the exported fine grid we produce is insufficient for recovering the exact values of the data at the original station locations". (ShakeMap Manual - DRAFT: Version 1.0 6/19/06 – Wald et al. 2006) .

This comment gives warning about the problem of retracing the original recorded values on a map. Thus point to point comparison may be understandably altered by the interpolation effects.

We apply the proposed strategy to two Japanese events, in order to detect weak points of the ShakeMap procedure and assessing the improvements introduced by considering new multidimensional effects.

2.4 The graphical representation of the results

The proposed analysis avails mainly of graphical tools to make a comparison between the real data (the reference map) and the predictions made by ShakeMap. Thus, we anticipate here the description of the figures that will be used henceforth in order to help the reading of the results. Here we refer to the 2008 Iwate-Myiagi earthquake as an example, but the same figures are also computed for the 2000 Tottori-ken earthquake. Each figures has a caption indicating the earthquake they refer to. A detailed description of their meaning is given in each related respective section.

Figure 2.1-a, portrays a map of the recorded PSA (3s) distribution (contoured in %g) for the magnitude 7.0 Miyagi – Iwate Nairiku earthquake. This figure results from the GMT interpolation of the data and illustrates the nature of the ground motion shaking. This map represents an example of our reference map to which all the analysis will be referred to.

Typically, for moderate-to-large events, the PSA pattern reflects the earthquake fault geometry, with largest amplitudes in the near-source region and in the direction of rupture directivity. A detailed analysis of the ground shaking of the earthquake is postponed to the following sections (paragraph 2.5 and 2.6). Here is to show that for a moderate-sized event with an abundance of ground-motion recordings, the information generated by ShakeMap (figure 2.1-b) and the reference map are similar except in zone when the data are sparse. The comparison between this two maps shows that the use of accurate finite fault related predictive equations has very limited effects because near fault effects are well constrained observationally. The effect of the ground motion predictive equation is evident in presence of a data-gap (i.e. at the south edge of the fault).

Figure 2.1-b is generated applying the site correction. Thus, the contours that connected remote stations have a more complex shape with respect to the simple interpolation of the reference map. This effect is evident within the valleys and the surrounding mountains. When the site effect is removed (figure 2.1-c) the overall pattern in the source proximity doesn't change significantly. Thus, it is more a reflection of the rupture process.

For events which occurred in a sparsely instrumented region the ShakeMap result is conditional on the accuracy of the GMPE in characterizing the near-fault ground motion. In order to test the ShakeMap performance when no informations about the shaking are available, a new run is made with all the recordings cut off (figure 2.1-d). In this case, the site correction obtained from the topography preserve the elongated shape toward the south-eastern part of the map, while in the source proximity of the fault higher values are predicted along the surface exposure. The hanging wall effect is taken into account: it enlarges the isoseismal in the NW direction. This anisotropy is a consequence of the parametrization of the AS2008 having introduced parameters strongly related to the rupture surface. When the site correction is removed, the effect of the AS2008 outcrops clearly (figure 2.1-e). For a visive comparison the results achieved using Kan2006 (figure 2.1-f) and BJF1997 (figure 2.1-g) are also portrayed. Neither the AS2008 or the other two GMPE are able to explain the high values obtained toward the south and at the SW edge of the fault. This observation encourages the introduction of a directivity term. However, the fact that the site correction for topography was to explain the elongation of the isoseismal toward the south, make us suspicious of possible first order site effects.

Another instrument suitable to explain these results is given by the visualization of the data distribution around the median predicted value (figure 2.2). These figures show the distribution of the real data (red triangles) as a function of Rrup, that is the minimum distance between the site and the rupture surface. The black circles illustrates the AS2008 median prediction in panel a,b and c. This curve separates into two distinct trends because of the use of switching operators into the

functional form of the GMPE. A major effect is due to the hanging-wall (HW) switcher. The black circles of panel d and e are referred respectively to the BJF1996 and Kan2006 equation. The BJF1996 shows a marked separation of the curve even though no switcher are present. This effect is due to the fact that the BJF1996 equation depends on the Joyner-and-Boore distance while we have chosen to plot the predicted values versus Rrup to be consistent with the other graphs. The (gray squares) shows the ShakeMap final prediction on the interpolated phantom stations. This type of visualization help to better understand the procedure of ShakeMap because it illustrates clearly the three operations it makes to reach its final result.

1. Panel (a): using the AS2008 predictive equation ShakeMap assigns to each point on the phantom grid a model of attenuation with distance. Then when a station is found within a certain distance range, its value is taken and the predicted one is rejected. Then, a site correction is applied to give the final distribution represented with gray squares in figure.

2. Panel (b): the dispersion of the gray squares is now different because all the stations are cut off. The site correction, topographically derived is still considered.

3. Panel (c): both the data and the site correction are removed. The gray squares match closely the predictive curve.

Panel (d) and (e) show respectively the distribution of the data with respect to the BJF1997 equation and Kan2006 equation. The log log trend of the AS2008 predictive equation (black circles) has a complicated dependence on distance due to the introduction of rupture related parameters. This result can be regarded as an attempt to capture the ground motion variability. In general the ground motion variability is clearly underestimated. New multidimensional effects may be included to better characterize the ground motion in the near source.

Figure (2.2-f) show the distribution of the PSA of the reference map resulting from

the interpolation of the real data via GMT (azure squares). The distribution of the interpolated values (panel f) is similar to the interpolation of ShakeMap (panel a). This figure is to show that the initial comparison is reliable and give us an idea of the real dispersion versus the dispersion reproduced by ShakeMap.

In order to visualize a comparison between the predictions and the real data relative to the source location, it is useful to trace on a map a quantitative indicator comparing two values with one another. We use the difference (dPGA in %g - figure 2.3) rather that the relative difference because the latter weights the small variations of small values as it weights strong variations of larger PSA values. In the hazard practice instead, the small variations are usually considered less important. As a consequence, the relative difference could result in a misleading representation. The zero value represent the best agreement between the prediction and the observations. The polar palette ranges in the [-5 %g, 5 %g]. Outside this range the map saturates highlighting the more significant variations. Red color corresponds to zones where the prediction overestimates the real data. Blue color corresponds to zones where the prediction underestimates the real data.

Figure 2.3 shows the comparison of different ShakeMap with respect to the reference map (GMT interpolation of the real data):

1. Panel (a): differences obtained running ShakeMap without data (thus representing the mere effect of the GMPE), using the AS2008 equation and the site correction for topography. (figure 2.1d – figure 2.1a)

2. Panel (b): differences obtained running ShakeMap without data using the AS2008 equation. Site corrections for topography are not included (figure 2.1e- figure 2.1a)

3. Panel (c): differences obtained running ShakeMap without data using the Kan2006 equation. Site corrections for topography are not included. (figure 2.1f – figure 2.1a)

4. Panel (d): differences obtained running ShakeMap without data using the BJF1997 equation. Site corrections for topography are not included. (figure 2.1g – figure 2.1a)

These comparisons shows that strong variations are obtained in presence of a data gap (blue spot at the SW edge of the fault). In these zones ShakeMap attributes to the phantom grid a value predicted by the GMPE. Conversely, the GMT interpolation of the real data in this zones is strongly conditional on the distance from the first available observation and on the adopted interpolation strategy. Thus the difference resides mainly in the choice of the interpolation strategy and we consider these zones not reliable for further comparisons. Fortunately the dense instrumental coverage preserve us of having a large number of such "non informative" areas.

It has to be notice that the selection of one model with respect to another changes significantly the prediction in the near-fault region. BJF1997 (figure 2.3-d) produce a strong overestimation of the observation in the region backward the fault as can be also appreciated in figure 2.1-g. On the contrary Kan2006 (figure 2.3c) predicts better the observations in the northern part of the fault.

ShakeMap shifts the predictive curve multiplying the amplitude for the bias correction to realize the minimum variance condition. Thus a better performance should be achieved when all the stations are considered. As a consequence one may expect that the use of a minimum number of stations (at least 6 within 70 km are required to activate the bias correction) would have improved the comparisons of figure 2.3. Figure 2.4 shows the effect of the bias correction calculated with 9 stations located at various distance from the source. Stations have been chosen randomly among the K-net and Kik-net network. The introduction of a minimum number of stations does not preserve from significant departures from the real distribution, because the location, the distance and the quality of the recorded data rather that the number of stations itself, are of importance. In this case the introduction of several stations results in a lowering of the ground motion prediction and, as a consequence ShakeMap underestimates the real pattern.

Clearly a certain minimum number of stations improves the performance. However, as can be seen in figure 2.2 (all panels), the main problem seems to be related more to the different trend between the real data distribution and the predictive curve rather than to a scaling property.

Other interesting results come from the comparison between the real data distribution and the predicted values along geographical sections (figure 2.5). This analysis give us the opportunity of examine in detail the nature and the possible causes of the scattering along specific azimuthal directions. Moreover it allows a direct comparison with the predictive curve and the real data distribution. We have selected the parallel fault (left panels) and the transversal fault (right panels) directions. For each panel, map on the bottom shows the latitude and longitude stations grouped by color, each color representing a quadrant section of the geographical map. The color-coded stations are thus reported in the amplitude versus distance graph on top, where the real data distribution, inside a region along the geographical section, are in red and blue symbols, and the ShakeMap predicted values in gray squares.

1. Panel (a): No site correction is applied. All the data are considered.

2. Panel (b): No correction is applied. No data are considered.

3. Panel (c): No correction is applied. No data are considered. The directivity term of is included with the SC2008 corrective factor.

2.5 The Iwate – Miyagi Nairiku (M=7.0) 2008 earthquake application

The 2008 Iwate-Miyagi Nairiku (M7.0) earthquake occurred northwest Japan on June 14 at 8:43 (JT). It is a shallow inland crustal earthquake, a reverse fault event, whose fault plane strike to the southwest and dips to the northwest according to moment tensor solution, aftershock distribution and surface fault break. This event have displayed a strong directivity toward the South.

2.5 The Iwate – Miyagi Nairiku (M=7.0) 2008 earthquake application

According to the model of Cirella (personal communication) the following rupture parameters are assumed: a 44.38x19.02 km fault dimension, a 209° strike angle, 40° dip angle and 105° rake angle. The instrumental coverage is made of 81 stations of the K-net network and the 65 stations of the Kik-net network. Figure 2.6 shows an enlargement of the fault over which the slip areal distribution is portrayed and the slip direction is traced with arrows. The slip distribution and the slip direction are obtained from the inversion of strong motion data (Cirella personal comunication).

The observed PSA at 3.0 seconds displays a strong directivity toward the south (figure 2.1-a) with high peak (15%g) recorded along the surface exposure of the fault, strong peak values (20%g) at the north edge of the fault, and slight values (8%) toward the south. The white pattern shows a distinct area of very low PSA(3.0s) values located on the north/north-eastern part of the Iwate prefecture, and corresponding to the relative high mountains region (the Kitakami Mountains).

The analysis of figure 2.3a-b-c, portraying the differences between the predicted values and the reference map, shows a strong variation along the fault exposure, marked in the NE direction, in the hanging wall zone and at the south-western edge of the fault. Looking at the maps obtained with the AS2008 (panel a and b) is noticeable that the site correction (panel a) has a dramatic effect in the northeast edge of the fault and partially reduce the extension of the blue spot in correspondence of the three stations located in front of the SE edge of the fault. The blue spot on the SW edge of the fault is due to the sparse station coverage, thus it is not representative in our analysis.

All the difference maps show a marked underestimation (in blue) in the S and SW part of the map, appearing in an extensive area of the map. A strong overestimation (in red) is achieved along a belt on the N -NE part of the map. This “split” is traceable in the log-log amplitude versus distance plot (figure 2.2). The data are clearly divided into two parts respect to the predictive curve. This effect is reduced when the prediction is computed with the use of Kan2006 equation (figure 2.2e).

One of the causes of this marked division could be ascribed to the choice of AS2008. The observed dispersion of the data with respect to the median could be a consequence of the fact that the predictive equation is not region specific. In order to exclude this hypothesis we have tested the regionally derived Kan2006 predictive equation (figure 2.2e and figure 2.3c). The use of this equation provides a different interpretation of the ground motion in the near source where the real data toward NE is better reproduced. However the splitting into two zones is still marked and the choice of the predictive equation seems nearly irrelevant in explaining the red belt surrounding the fault at NE.

We have also investigated on the nature of the AS008 regression with respect to the data distribution for specific sections (figure 2.5), approximatively the parallel fault and the transversal fault direction. The outliers correspond to the station MYG005 (blu) and MYG004 (red) located at the SW edge of the fault and at approximatively 12 km est from the fault respectively. The parallel section (along strike NE section left column) shows several outliers in the southern part of the fault while the predictive equation in northern part has a slope that diverges from the median trend. The predictive equation seems shifted by a constant factor toward SE even though the slope of the data distribution seems to fit the median trend; this shift could be interpreted as the effect of an erroneous evaluation of the position of the fault. However it has to be pointed out that the position of the patch of slip (figure 2.1) strongly imprints the radiated energy at low frequencies. Thus, in order to account for this effect the position of the patch of slip should be taken into account in computing the GMPEs. This result may be acquired favoring the use of the distance from the most energetic zone rather than the Joyner and Boore distance definition. As a matter of fact, the main slip patch on the Iwate-Miyagi fault is offset toward the southern part with respect to the position of the nucleation and the strong amplifications in the south may be justified by the slip patch position (figure 2.1).

2.5.1 On the need of deterministic factors in the ground motion predictive models

Due to the evident separation of the maps in two distinct zones (a strong overestimation in the NE direction and in the hanging wall zone; a strong underestimation in the S-SW part if the map) we investigate if this behavior could be ascribed to a directivity effect. However, the corrective factor of SC2008 (figure 2.7b) obtained for the specific rupture settings, has an unimportant effect on reducing the misfit, either in amplitude or in spatial distribution between the prediction and the real data (figure 2.7c and figure 2.5c). The directivity effect as modeled by SC2008 appears as a second order effects and it results masked by major specific regional features.

First order effects maybe ascribed to the propagation. As a matter of fact, the earthquake occurred in a zone of concentrated deformation along the Ou Mountain Range so that the causative fault is entrapped between two different high mountains regions completely distinct in nature and separated by the Kitakami plateau area. On the western part of the map, a tectonically uplifted zone is present, named the Dewa Hills. The complexity of the tectonic surroundings have motivated several authors to study the regional-scale seismic tomography in and around the focal area. Wang et al. (2008) have determined high resolution 3D seismic images of the crust using a large number of P and S wave arrival times with data from routinely operated stations. Okada et al. (2009) used more dense data from not only the routine operated stations but also some dense temporary stations. Their results show two distinct low velocity belts where the velocity gradient partially correlates with the pattern retrieved in our analysis. However, propagation effects constitute a multidimensional physical effect, strongly related to the site specific characteristic, that the GMPEs do not actually include. Some effort has been done in the work of Panza et al. (2003) dealing with the reflection of seismic waves. It has to be notice that the introduction of propagation effects is an attempt to introduce deterministic characteristic into the GMPE. The same attempt motivates the introduction of the corrective factors for directivity.

The example of the Myiagi-Iwate earthquake demonstrate the need of introducing multidimensional effects inside the ground motion predictive equations. Otherwise the predicted ground motion variability tends to underestimate the observed variability and the application of a GMPE to a specific case, i.e. ShakeMap applications, when only a few real informations are available to anchor the result, only partially represents the effective ground shaking.

2.6 The 2000 Tottori-ken Seibu (M=6.6) earthquake application

The Tottori earthquake (M6.6) occurred at 13:30 (JST) on October 6, 2000, in the western part of Tottori prefecture, Honshu, Japan. It is a strike slip, pure left lateral event. It was the the first large event to occur after the completion of several large instrumental networks in Japan, including Hi-net (High Sensitivity Seismograph Network), KiK-net, K-net, and GEONET (GPS Earth Observation Network).

The inferred fault had a length of 40 km, a width of 20 km, a strike angle of 150°, a rake angle of 0° and a dip angle of nearly 90° degree (Piatanesi et al. 2007). The slip has two main patches reaching a maximum value of 1m (figure 2.8).

The observed PSA at t= 3.0s have displayed a strong directivity toward the north (figure 2.9a) with high peak (15%g) recorded at the edge of the surface exposure of the fault. The ShakeMap predictions are in good agreement with the reference map thanks to the dense distribution of the station around the fault. The Vs30 retrieved using the slope of the topography is uniform (600- 660 km/s) for the entire region except along the shore zone where the Vs30 ranges between 240-300 km/s (Global Vs30 Map server – U.S. Geological Survey web site). The effect of this low velocity zone is evident when all the stations are removed (figure 2.9d). In this case high values are predicted along the fault exposure in correspondence of the low velocity area. When also the site correction is removed (figure 2.9e) the AS2008 equation elongates the isosesmal around the fault with higher PSA values in the hypocentral proximity. Instead, the observed ground motion presents a drop

shaped elongation toward NE with smaller PSA values in the region at the south of the hypocenter. It has to be notice that earthquake stroke in a sedimentary basins surrounded by the mountains of the western Tottori prefecture and nearby the Daisen volcano which not only may have influenced the nucleation and rupture process (Zhao et al. 2004) but also the wave propagation.

The trend of the AS2008 equation is roughly in line with the mean distribution of the real data (figure 2.10a). Within 10 km site effects remains of first order. So that even if the stations are removed the prediction matches the real distribution (figure 2.10b). For greater distances the data distributes uniformly around the predicted curve showing a great variability for distance greater than 100km. The prediction obtained using a simple GMT interpolation (figure 2.10f, azure squares) provides a greater variability with respect to the ShakeMap predictions. The difference here is evident and is strongly driven by the use of an attenuation model to connect remote stations.

Figure (2.11a,b) shows that the predictive equation underestimates the real data around the epicentral location and toward the N direction where highest PSA (3 sec) are observed. A significant overestimation appears in the fault parallel direction at the edge of the fault surface exposure.

2.6.1 Introducing the directivity term

Figure (2.13b) shows the pattern expected for the directivity correction to the AS2008 equation. Because the hypocenter is located close to the center of the fault, the directivity pattern shows a bilateral rupture, with lobes elongated in the strike direction (red) predicting an amplification of the AS2008, and a wing-shaped zone spreading in the transversal zone (blu) where a de-amplification appears.

The incorporation of such directivity term tends to worsen the agreement with the real data (figure 2.13c). In fact, it amplifies further the disagreement (red spot on the map) in the rupture direction. This consideration is clarified in figure 2.12c where a direct comparison between the prediction and the real data is given along

the parallel and the transversal section.

However low frequencies are mainly driven by the earthquake faulting geometry. The ground motion intensity at one station reflects the radiated energy from different parts of the fault. Strong intensities are expected to be recorded in correspondence of the position of the patch of slip. Thus, we advance the hypothesis that the corrective factor should be centered where the patch of slip is located. This solution provides a way to account for the distance from the most energetic zone. The model of Piatanesi et al. (2007) retrieve a slip distribution balanced round the hypocenter. Other studies (Semmane et al. 2005, Iwata and Sekiguchi, 2001) predict a shallow patch of slip located in a few kilometers south (about 8 km) from the hypocenter. The corrective factor computed with this relocation provides the differential pattern of figure 2.14b where a significant improvement is achieved in the misfit between the real data and the prediction in the southern part of the fault. The northern pattern, and the ground motion underestimation along the fault exposure continue to be not well resolved.

2.7 Discussion

The ground motion predictive equation (GMPE) is the result of a regression over a collected empirical data set. It represents a statistical mean behavior that characterizes the ground motion variability as a function of several parameters (at least the size and the source-to-site distance). This mean function generally is adequate to capture a macroscopic trend, that is, the ground motion attenuation with distance. As a consequence, in ShakeMap applications, when the prediction is supported by a dense instrumental network, it is effective to “fill in” the station gap. Major problem outcrops when the data are not available. In fact, the mean trend only partially capture the ground motion variability due to rupture related parameters, especially in the near source distance range where the wave amplitudes are sensitive to restricted areas of the fault and therefore are sensitive to specific characteristic of the rupture process. Moreover, we have pointed out that significant contributions to the ground motion variability of a specific event are attributable to the waves propagation representing in some cases a first order

effect. This observations have been clarified with the use of figure 2.3 and 2.11 comparing the ground motion real variability to the predicted one. It has to be noted that the introduction of rupture related parameters have significantly improved the predictions, though it has still a small impact with respect to the real variability. This is the case of our attempt to introduce the directivity term that seem still to be embedded in the overall variability. The impression is that other multidimensional effects are needed to better constrain the results.

It has to be also pointed out that the formulation of the GMPE is still affected by several problems related to the paucity of the data. In fact it is common practice to enlarge the data-set exploiting the underlying stationarity of events with time, that allows us to replace temporal characteristic of earthquake occurrence by spatial characteristic (ergodic hypothesis). This assumption worse the agreement with regionally specific features as a consequence of the fact that data are collected from different area of the world. Therefore specific trends that maybe help to derive physical based relation between the parameters and the observed ground motion are often masked by the overall variability. The new relations that has been introduced to explain the variability are therefore damped down in favor of a more generic statistical behavior.

In that sense, the big effort that has been done to capture the statistical ground motion variability has an apparency more pertinent to a probabilistic context (i.e. Probabilistic Seismic Hazard Assesment – chapter 3) rather that to an application on a specif earthquake scenario. In this case, more accurate and regionally derived GMPE are needed to better represent the rapid shaking response where the data are extremely sparse.

The same problems affects the calibration of a physical relation, in our case the SC2008 directivity model. The SC2008 is set up with a supporting simulation techniques, and then it is calibrated over the same data set of AS2008. The results achieved in this chapter shows that the correction that it promotes on the GMPE is not suitable to explain the ground motion variability in the near source neither in amplitude, nor in the pattern. If we exclude the hypothesis that first order

propagation effects could mask the directivity effect as modeled by SC2008, the other chance is that the directivity model is not representative of the directivity effect in the single case application. Maybe other features , i.e. the slip position or the rupture velocity, are more suitable to explain the physical process for the specific case, and have to be favored in the computation of a directivity model especially now that our knowledge about the source is sufficiently advanced.

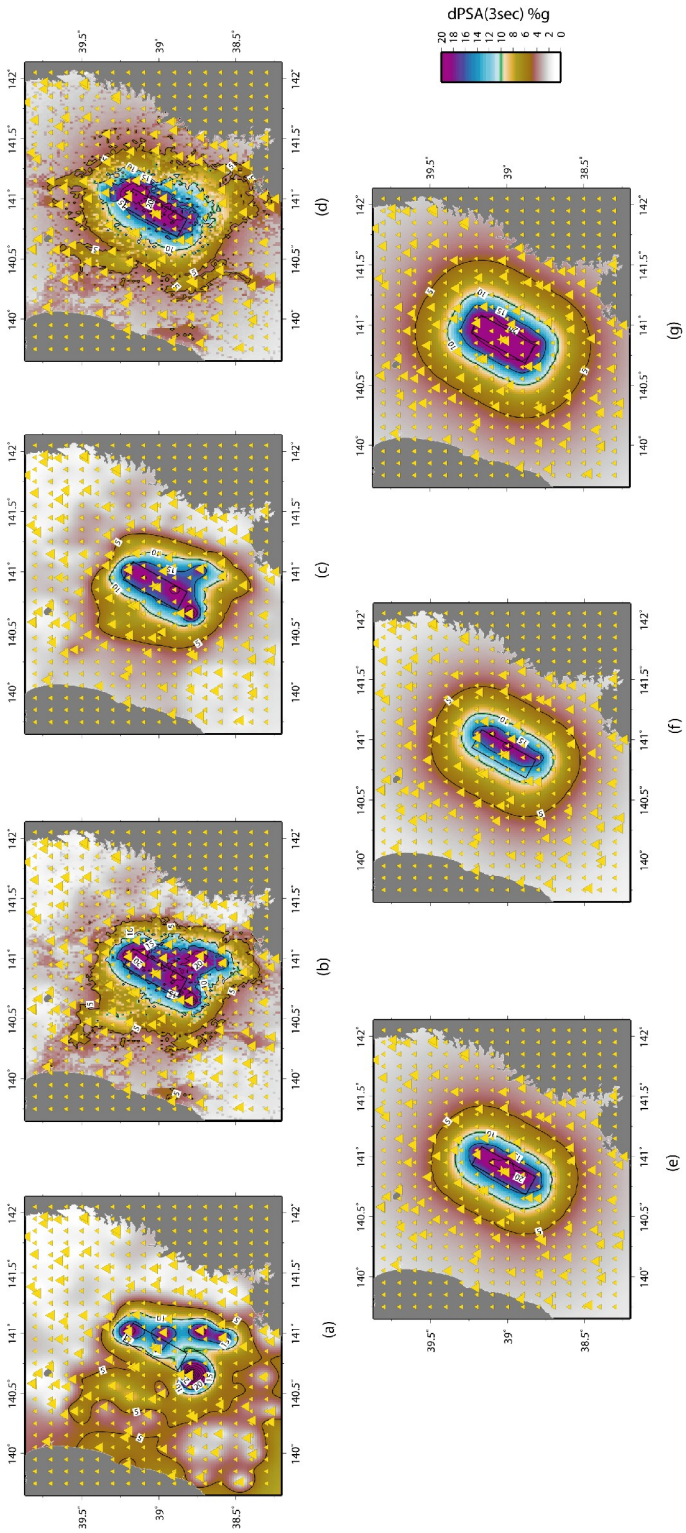

Figure 2.1: The 2008 Iwate - Miyagi Nairiku (M=7.0) earthquake. PSA (3 sec), given in %g. Big triangles are the recording stations; small triangles are the phantom stations.
(a) the reference map computed through a graphical interpolation of the real data ;
ShakeMap results using AS2008: (b) with stations, with site correction; (c) with stations, NO site correction; (d) NO stations, with site correction; (e) NO stations, NO site correction;
ShakeMap results using: (f) Kan2006, NO stations, NO site correction; (g) BJF1997, NO stations, NO site correction.

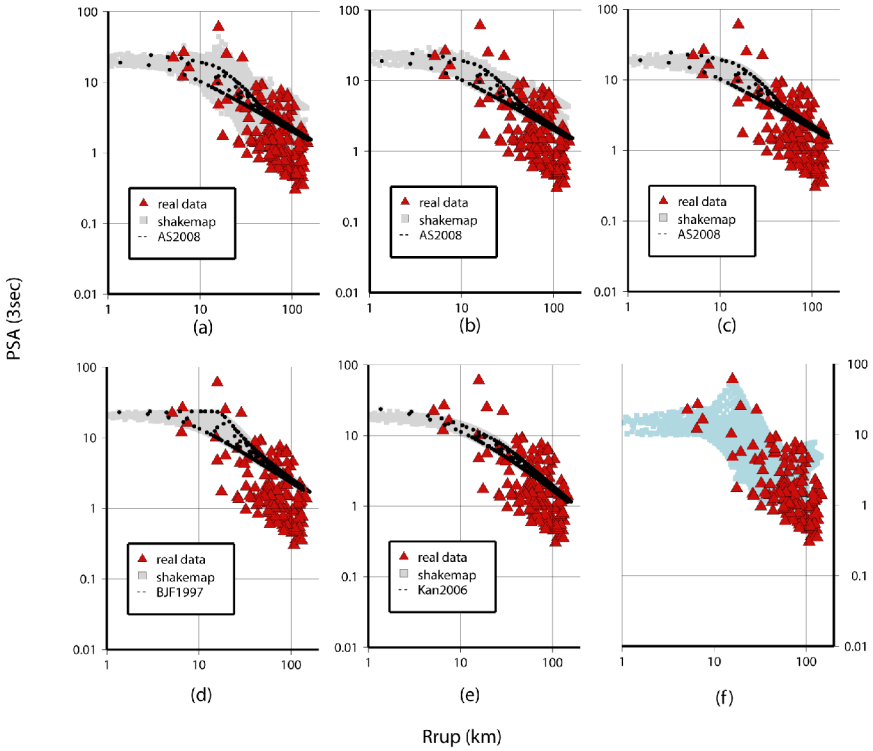

Figure 2.2: The 2008 Iwate - Miyagi Nairiku (M=7.0) earthquake, PSA (3 sec) peak values versus the Rrup distance.
GRAY SQUARES: ShakeMap final prediction on the interpolated phantom stations; RED TRIANGLES: real data ; BLACK CIRCLES: the predictive equation.
(a) with the data, with site correction, using AS2008; (b) NO data, with site correction, using AS2008; (c) NO data, NO site correction, using the AS2008; (d) NO data, NO site correction, using BJF1997; (e) NO data, NO site correction, using Kan2006;
(f) azure squares represent the real data interpolation via GMT (each point is a value of the reference map)

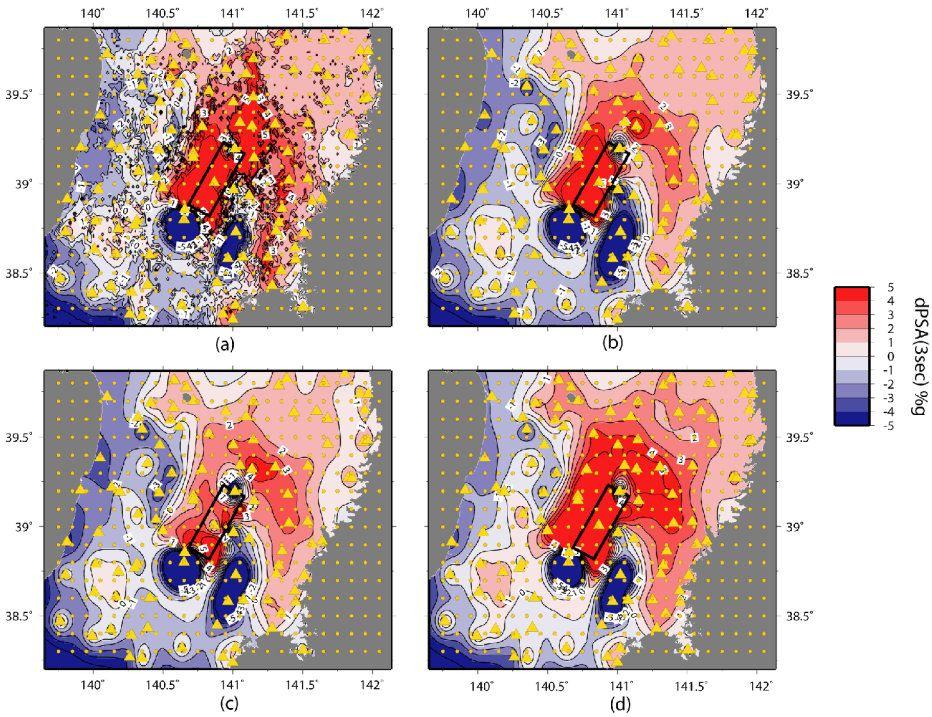

Figure 2.3: The 2008 Iwate - Miyagi Nairiku (M=7.0) earthquake; comparison of different ShakeMap with respect to the reference map (GMT interpolation of the real data): (a) NO data, using the AS2008 equation, with site correction; (b) NO data, using the AS2008 equation, NO site correction;(c):NO data, using the Kan2006 equation, NO site correction;(d) NO data, using the BJF1997 equation, NO site correction.

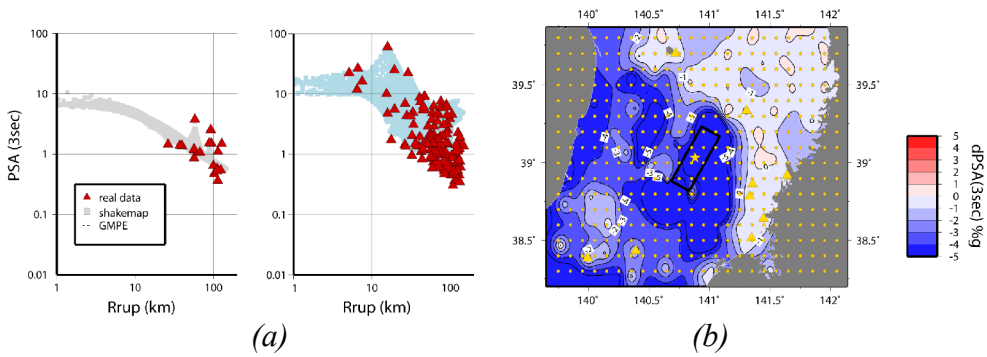

Figure 2.4: The ShakeMap ground motion prediction made with 9 stations. The effect of the bias is the reduction of the predictive equation amplitude to fit the available data. (a) the real data distribution (red triangles); on the left the ShakeMap prediction (gray squares); on the right the real data interpolation (azure squares). (b) the difference map (dPSA - %g) made between the ShakeMap prediction resulting with 9 stations and the real data distribution.

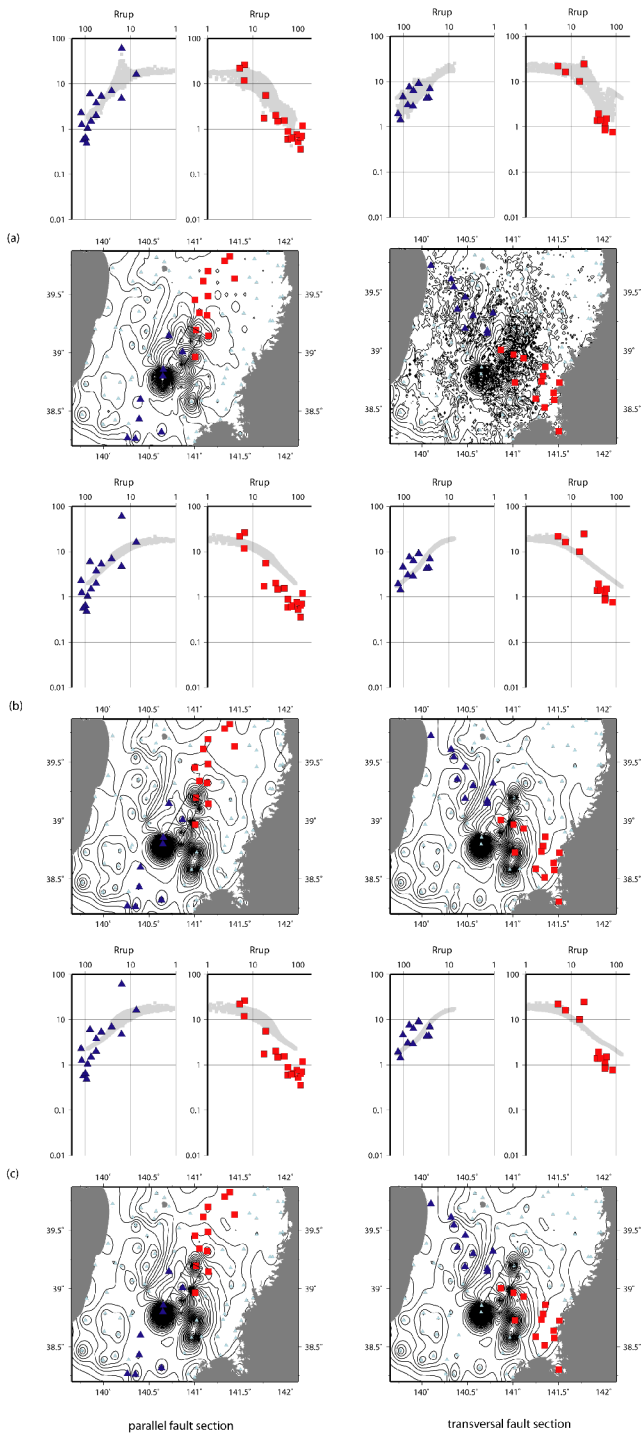

Figure 2.5:The 2008 Iwate - Miyagi Nairiku (M=7.0) earthquake real data distribution along geographical sections: the fault parallel direction (left panel); the transversal direction (right panel). Blue and red symbols divide the data into two sub-sections with respect to the hypocentral position. Gray squares represent the ShakeMap interpolation: (a) All the data are considered; No site correction is applied.(b) No data are considered, No site correction is applied. (c):No data are considered, No correction is applied. The directivity term is included with the SC2008 corrective factor.

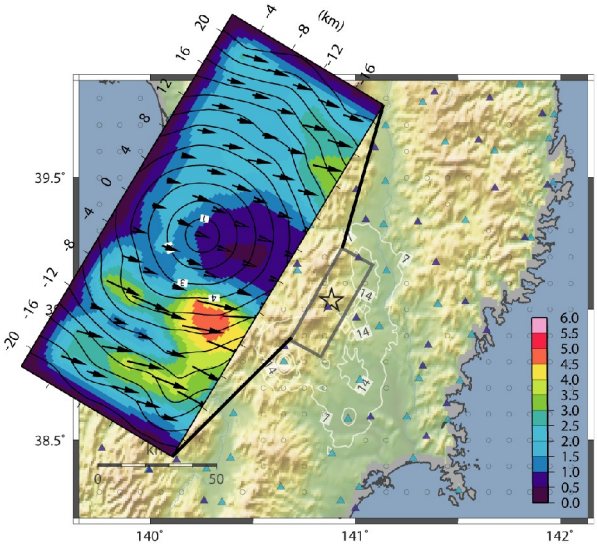

Figure 2.6: The 2008 Iwate – Miyagi Nairiku (M7.0) earthquake. The enlargement on the left shows the slip distribution (colored palette) and the slip direction with black arrow (Cirella personal communication). The black rectangle on the map shows the fault projection on surface. The white contouring represents the PSA 3 sec ShakeMap final product. The star represents the hypocenter.

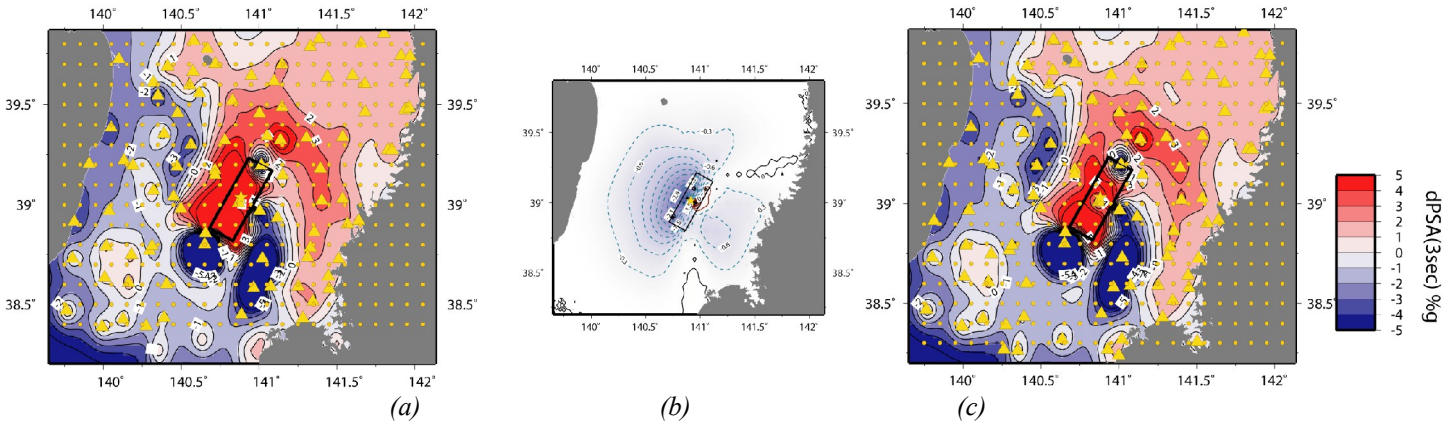

Figure 2.7: The comparison with the ShakeMap predictions with AS2008 and the AS2008 corrected for directivity. (a) Difference map when no stations and no site correction are condisidered; (b) the directivity corrective factor of Spudich and Chiou 2008- blue dashed lines represent a deamplification of the AS2008, red solid lines represents an amplification; (c) as panel a but with the directivity corrective factor in panel b.The star represents the hypocenter.

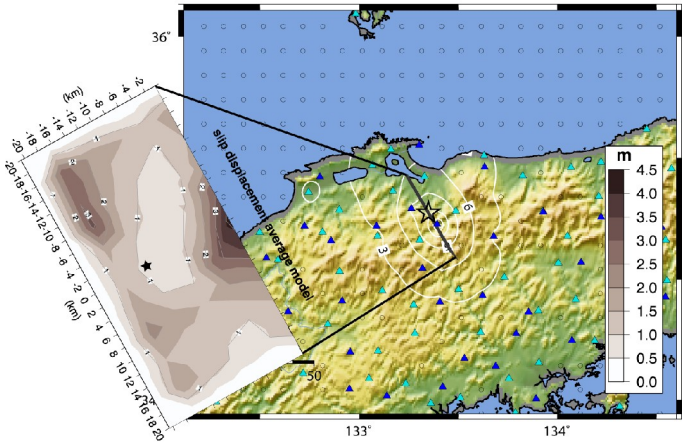

Figure 2.8: The 2000 Tottori-ken Seibu (M6.6) earthquake. The enlargement on the left shows the slip distribution (gray palette – Piatanesi et al. 2009). The black segment on the map represents the fault projection on surface (this is a pure left lateral strike slip event). The white contouring represents the PSA 3 sec ShakeMap final product. The star represents the hypocenter.

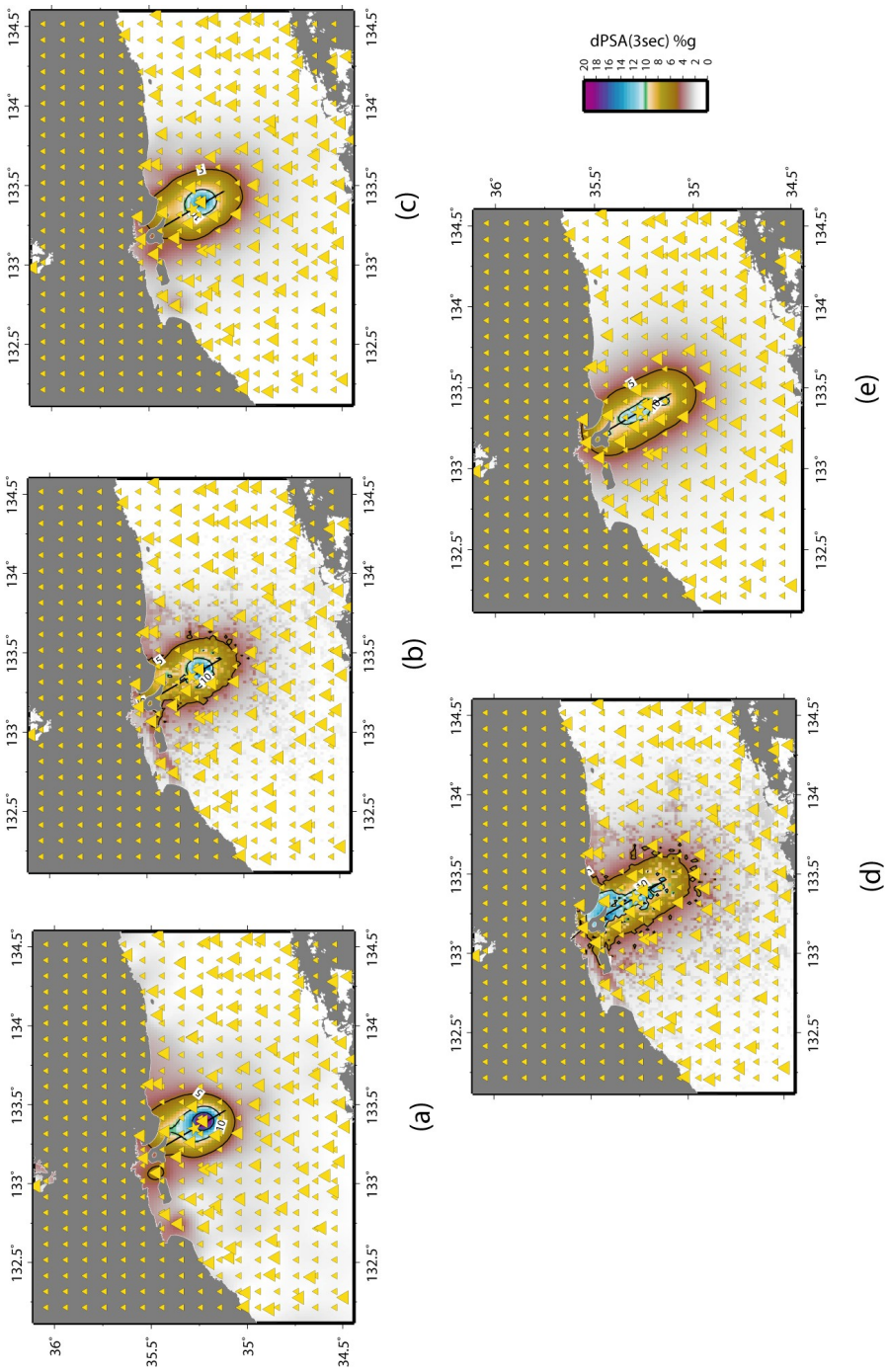

Figure 2.1: The 2000 Tottori- ken Seibu (M=6.6) earthquake. PSA (3 sec), given in %g. Big triangles are the recording stations; small triangles are the phantom stations.
(a) the reference map computed through a graphical interpolation of the real data ;
ShakeMap results using AS2008: (b) with stations, with site correction; (c) with stations, NO site correction; (d) NO stations, with site correction; (e) NO stations, NO site correction.

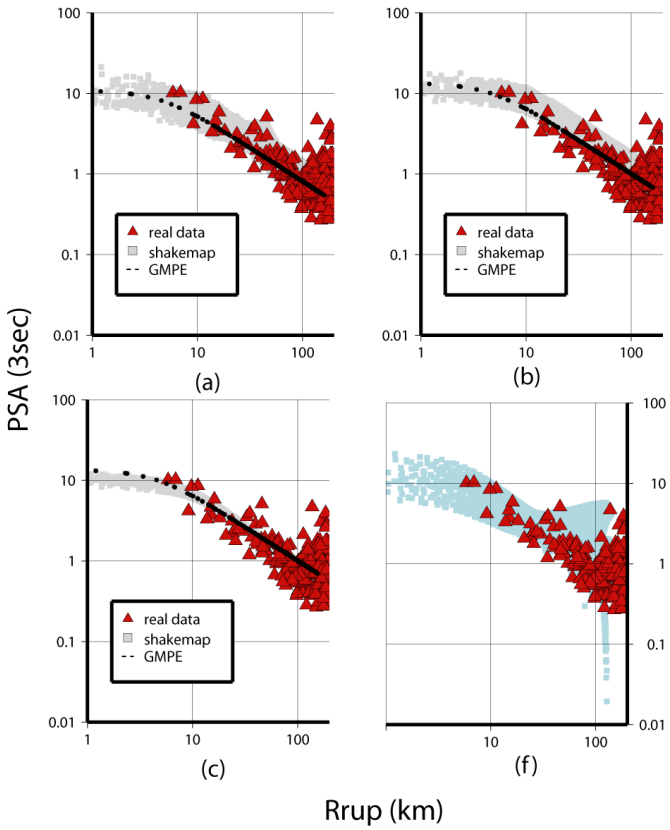

Figure 2.10: The 2000 Tottori-ken Seibu (M=6.6) earthquake, PSA (3 sec) peak values versus the Rrup distance. GRAY SQUARES: ShakeMap final prediction on the interpolated phantom stations; RED TRIANGLES: real data; BLACK CIRCLES: the predictive equation.(a) with the data, with site correction, using AS2008; (b) NO data, with site correction, using AS2008; (c) NO data, NO site correction, using the AS2008; (f) azure squares represent the real data interpolation via GMT (each point is a value of the reference map)

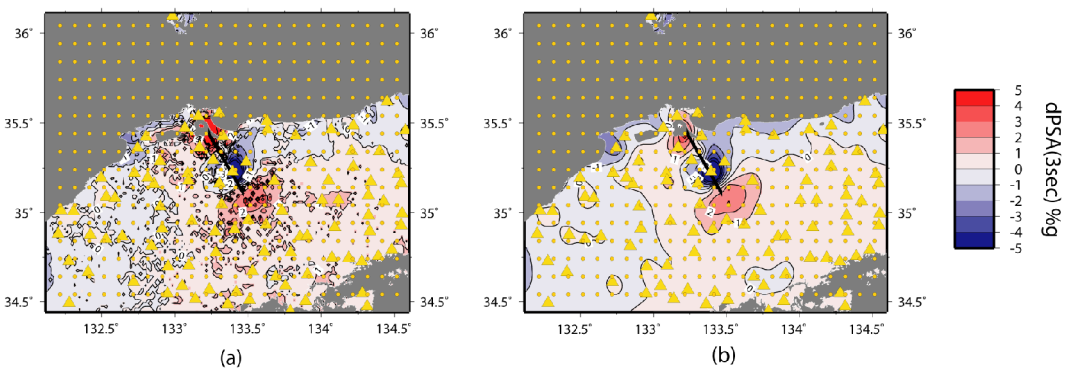

Figure 2.11: The 2000Tottori-ken Seibu (M=6.6) earthquake; comparison of different ShakeMap with respect to the reference map (GMT interpolation of the real data):(a) NO data, using the AS2008 equation, with site correction; (b) NO data, using the AS2008 equation, NO site correction.

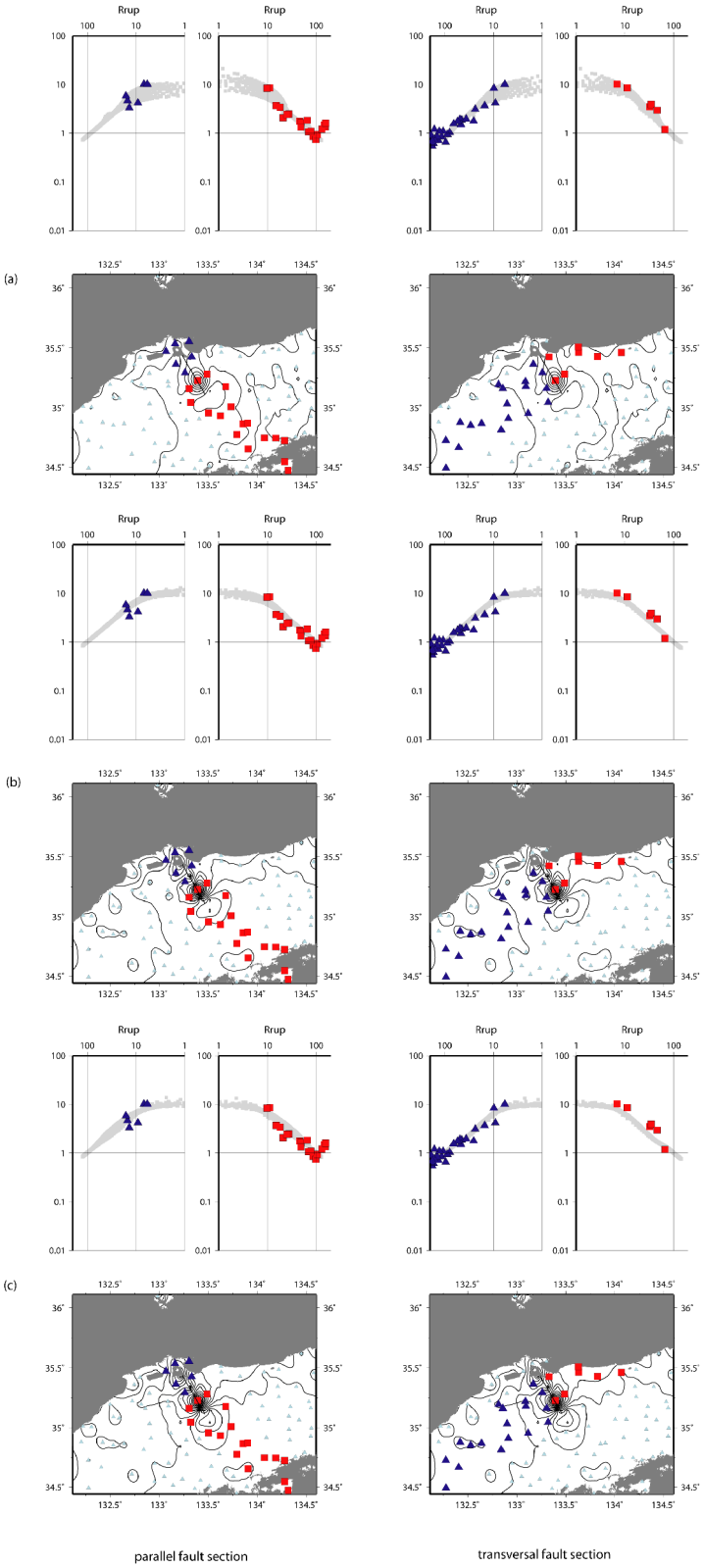

Figure 2.12:The 2000 Tottori-ken Seibu (M6.6) earthquake real data distribution along geographical sections: the fault parallel direction (left panel); the transversal direction (right panel). Blue and red symbols divide the data into two sub-sections with respect to the hypocentral position. Gray squares represent the ShakeMap interpolation: (a) All the data are considered; No site correction is applied.(b) No data are considered, No site correction is applied. (c):No data are considered, No correction is applied. The directivity term is included with the SC2008 corrective factor.

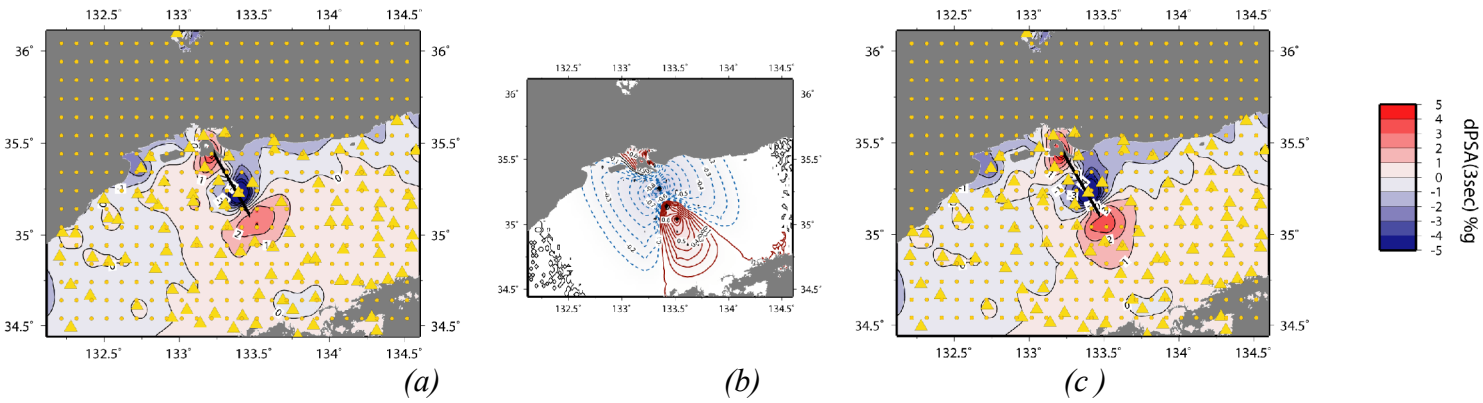

Figure 2.13: The comparison with the ShakeMap predictions with AS2008 and the AS2008 corrected for directivity. (a) Difference map when no stations and no site correction are considered; (b) the directivity corrective factor of Spudich and Chiou 2008- blue dashed lines represent a deamplification of the AS2008, red solid lines represents an amplification; (c) as panel a but with the directivity corrective factor in panel b. The star represents the hypocenter.

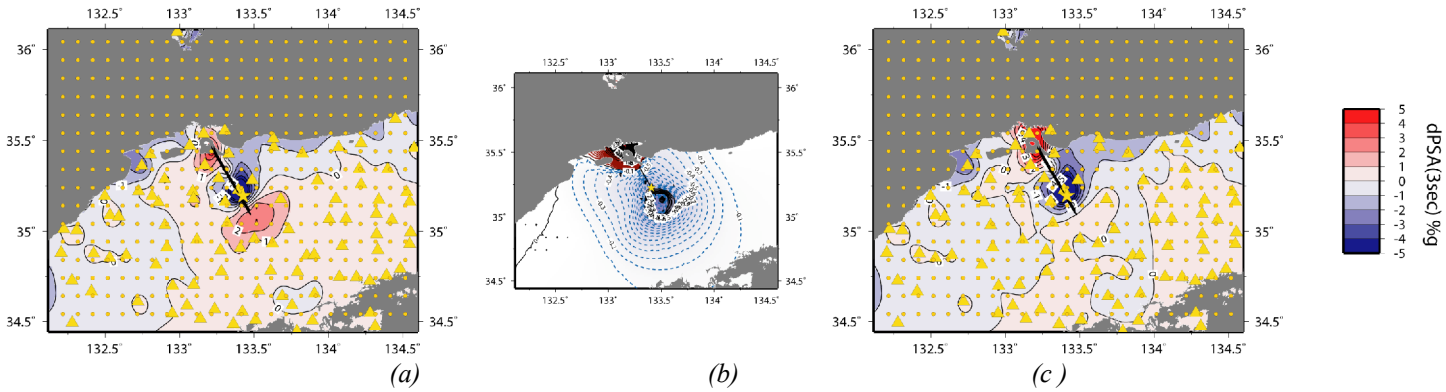

Figure 2.14: As figure 2.13 but the corrective factor is centered near the zone where the slip-patch is located.

Chapter 3

Is Directivity Still effective in a PSHA framework?

It also time to acknowledge the great progress made by deterministic analysis methods and to incorporate these methods into a probabilistic framework for a meaningful risk analysis.

Klugel (2007a)

The hazard assessment provides quantitative evaluation of the nature of ground shaking at specified location that could be induced by future earthquakes. Such evaluation serves to inform engineering decisions concerning the location and the design of structure. In particular in the planning of structure design a specification of the ground motion value exceedance at a site in a time window is needed.

The most wildly used long-term hazard assessment model is the Probabilistic Seismic Hazard Analysis (PSHA), that uses the complementary cumulative distribution function to compute the probability of exceedance of a ground motion intensity measure. The PSHA conventional formulation (Cornell, 1968; McGuire, 1976,1995) depends on the integral of a number of explanatory variables, at least magnitude and source-to-site distance, and on a continuous function linking the ground motion intensity measure (IM) with the whole parametric space. This continuous function is provided by the Ground Motion Predictive Equations (GMPEs) resulting from a regression analysis of the real data distribution. The real values depart from the prediction of a certain quantity sigma representing the

unexplained part of the ground motion (chapter 2). The value of sigma has significant impact on the results of seismic hazard analysis as discussed in Bommer and Abrahamson (2006), Reiter (1990) and McGuire (2004). Figure 3.1 shows the impact of sigma on seismic hazard curves for PGA generated with the equation of Boore et al. (1997) using the original sigma value (0.23) and other additional values of the standard deviation selected exclusively to test the impact of the standard deviation on seismic hazard results. From figure 3.1 we also gather that longer is the time of interest, larger is the influence of sigma on the hazard assessment.

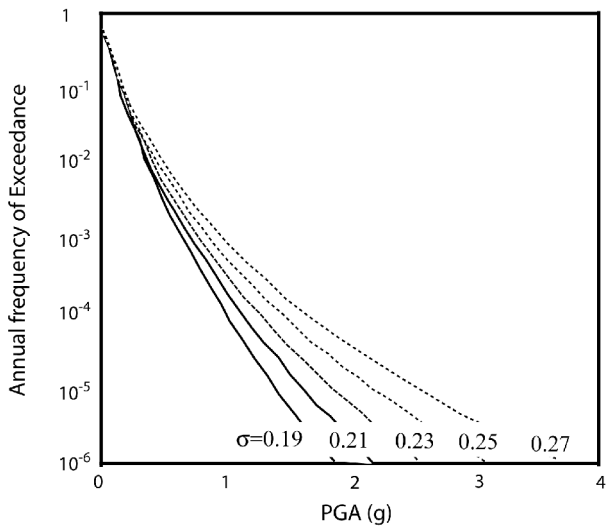

Figure 3.1:Impact of the aleatory variability of ground motion (σ) on seismic hazard results. The graph shows hazard curves for PGA generated with the equation of Boore et al. (1997) using the original (0.23) and modified values for the standard deviation of log10(PGA) for a fictitious site affected by two source zones(Bommer and Abrahamson 2006).

Thus, a way to steady the PSHA predictions is to reduce the sigma value improving the performance of the GMPEs. A first step is to refine the seismic source description inside the GMPEs (Strasser, 2009) incorporating explanatory variables not yet included in the computation.

The introduction of a specific parameter of the seismic source in the probabilistic

hazard estimation is often done in a prevalently deterministic way, with a set of parameters which describe the fault geometry. By way of example Convertito et al. (2006) use a characteristic earthquake scenario inside a probabilistic framework, defining the two first moments of the GMPEs from a large number of deterministic simulations. Frankel (2007) propose a mixed approach where the median value of GMPEs is modified on the basis of a deterministic computation and a recurrence rate is associated at each scenario. Another approach have been developed by Convertito and Herrero (2004) proposing a method to include, in the traditional equation of the PSHA, the influence of the focal mechanism. It is based on the introduction of a corrective factor, obtained from theoretical considerations, on the GMPEs. Contrary to the aforementioned approaches, the distribution of parameters (dip and strike angle) is continuous and described with a joint probability density function (pdf).

The idea of describing the distribution of the parameters associated to the seismic source by a pdf is not new. Abrahamson (2000) introduces four articulated distances rather than the simplest Joyner and Boore one, defined as the distance between the site and the fault projection on surface. In order to allow the integration over these four parameters, he increases the dimensionality of the PSHA formulation adding one integral for each new distance definition involved. The distances vary on a continuous parametric space with a statistical distribution described by the pdf. Other approaches (Tothong et al., 2007; Iervolino and Cornell, 2008, Somerville 2003) uses the occurrence rate of a source effect (e.g. a velocity pulse) rather than the statistical distribution of the explanatory variables. These methods slightly diverge from traditional seismological approaches in the fact that the description is made on the effects rather than on the underlying physical process. Their formulation is motivated by the need of accounting (probabilistically) for the effects that appear in the near – source, that are not systematically observed and thus, not predictable in advance. Among these effects there is the directivity that modulates the energy released during the earthquake causing even strong variations with respect to the traditional predictions (Chapter 1

in this thesis). The directivity effect has been extensively studied and modeled at least in the long period range and its contribution to the ground motion have been included in the GMPE through the corrective factors of SC2008 and Som97 presented in Chapter 1. The introduction of a physical relation guarantees a minimal range of predictability of the phenomena once that the explanatory variables that describe the process are constrained in a certain range. However, the directivity effect have been not yet included or tested in a PSHA framework.

It has also to be marked, as pointed out in Chapter 1, that the introduction of new explanatory variables and a relation linking them should lead to a reduction of the variance and a better performance of the hazard prediction. The objective of this chapter is to demonstrate the effectiveness of the directivity model both for the fault source and the areal source. To achieve this goal the traditional hazard formulation is improved, following the formulation of Abrahamason (2000) and Convertito and Herrero (2004), to enable a correct treatment of the multivariate statistical model.

3.1 The traditional hazard formulation

The probabilistic hazard computation is based upon the theorem of the total probabilities stating that "the prior probability of A is equal to the prior expected value of the posterior probability of A". That is, for any random variable *B:*

$$P(A)=E[P(A/B)] \tag{3.1}$$

where P(A|B) is the conditional probability of A given B. When the data set is made of a set of discrete random variables the theorem translate in the preposition that, if n mutually excluding events $B_1,B_2,...,B_n$ are considered, then the probability of an event A is given by the sum over the n-dimensional events B:

$$P(A)=\sum_N P[A/B_n]P(B_n) \tag{3.2}$$

If the event A corresponds to the exceeding of a certain threshold the equation 3.2 becomes:

$$P(A>a)=\sum_{N} P[A>a/B_n]P(B_n) \tag{3.3}$$

For a continuous space, the lower and the upper sums tend to the integral of the conditional probability of exceedance, and finally we arrive to:

$$P(A>a)=\int_{N} P[A>a/b]P(b)db \tag{3.4}$$

The theorem of the total probability is used to compute the probability of ground motion parameters to exceed a certain threshold. The event *b* corresponds to all the variables explaining the ground motion variability (e.g. earthquake size, source-to-site distance). The distribution of the ground motion intensity measure is provided by the use of theoretical/empirical models. *f(b)* quantifies the chance of the variable to occur and taking part to the ground motion level.

The traditional approach (Cornell, 1968) incorporates the influence of all potential sources of earthquakes and the average activity rates (α) assigned to them. Thus the probability of having an exceedance event is given by:

$$E(IM \geq IM_0)=\alpha \int_R \int_M f_R(r) f_M(m) P_{IM}[IM(m,r) \geq IM_0/m,r]dmdr \tag{3.5}$$

where *E* represents the frequency of exceedance of an intensity measure (*IM),* for a given threshold (IM_0). P_{IM} denotes the standard normal complementary cumulative distribution function (CCDF) which is based on the usual assumption that the ground motion intensity measure is a log-normal aleatory variable conditioned by the occurrence of the magnitude-distance couple (m,r). The probability of occurrence of each term of the couple comes into the integral through the probability density functions (pdf) f_M and f_R..

The temporal occurrence in PSHA is frequently described as an homogeneous

stationary Poisson process: the earthquakes can be treated as independent variables uniformly distributed in time occurring with no memory of time, size or location respect to the preceding events. Therefore the probability of having N events in the time t is given by:

$$P(N,t)=\frac{(\lambda t)^N \exp(-\lambda t)}{N!}$$

where λ is the mean frequency of occurrence. In a PSHA framework, the annual mean frequency of occurrence is $E(IM>IM_0)$ and the probability of having at least one event in a time t is given by:

$$P(IM \geqslant IM_{0,} t)=1-P(N=0,t)=1-e^{-E(IM \geqslant IM_0)t} \tag{3.6}$$

Therefore, it follows from equation (3.5) that the basic seismic hazard identity (3.6) could be rewritten as:

$$P(IM \geq IM_{0,} t)=1-\exp\left[\alpha t \int\int P_{IM}[IM(m,r) \geq IM_0 / m,r]\, f_R(r)\, f_M(m)\, dr\, dm\right] \tag{3.7}$$

where the output of the integration (3.7) is a single estimated hazard curve as a function of IM which represents the exceeding probability of the selected range of values for a time period. However the result of the PSHA can be expressed also with a map: for a given time period, the map shows the exceedance values achieved with the same probability.

3.1.1 Basic ingredients

PSHA traditional approach is based on the main assumption that the seismicity is uniformly distributed inside each seismic zone. Therefore the probability density function for magnitude is generally based on a recurrence relationship. This relation indicates the chance of an earthquake of given size to occur during a

specified period of time. The most widely used is the Gutenberg-Richter law (1954) which express the cumulative number of earthquakes exceeding a given magnitude. The Gutenberg-Richter is defined over an infinite range of magnitudes. Nevertheless, in the PSHA application, the definition of a bounded range is necessary. In the practice of the PSHA the standard Gutenberg-Richter is substituted by a truncated version (McGuire and Arabasaz, 1990). Thus, the earthquake occurrence, expressed in terms of mean annual rate of exceedance, leads to the following probability density function:

$$f_M(M) = \frac{d}{dm} F_M(M) = \frac{\beta\, e^{-\beta(m - m_{min})}}{1 - e^{-\beta(m_{max} - m_{min})}} \tag{3.8}$$

Where F_M is the cumulative distribution function for the magnitude m, m_{min} is the minimum magnitude, m_{max} is the the maximum magnitude, β depends on the slope (b) of the Gutenberg-Richter recurrence law through a relation given by:

$$\beta = b\ ln10$$

Another basic ingredient is the calculation of the probability density function for distance. The definition of the distance pdf is strongly related to the definition of the seismic source. A commonly accepted model is based on assuming that earthquakes occur spatially "at random" within a seismic area or within a finite fault, every single point on the source have the same probability of nucleating a seismic episode (hypothesis of homogeneous seismicity). Thus, [*f(r) dr*] represents the portion of the seismic area at a distance r from the site. When the source is approximated by a segment or a point its distribution is retrieved through analytical expressions (figure 3.2a,b). When the source is areal it is calculated with numerical methods (figure 3.2c). The procedure generally adopted consists in dividing the irregular source zone into a large number of discrete elements of equal or unequal area (CRISIS: Ordaz, 2001; EQRISK: McGuire, 1975). Then, the expression may be obtained computing the values of *r* that correspond to the center of each element. The conditional probability of exceedance of a certain ground motion

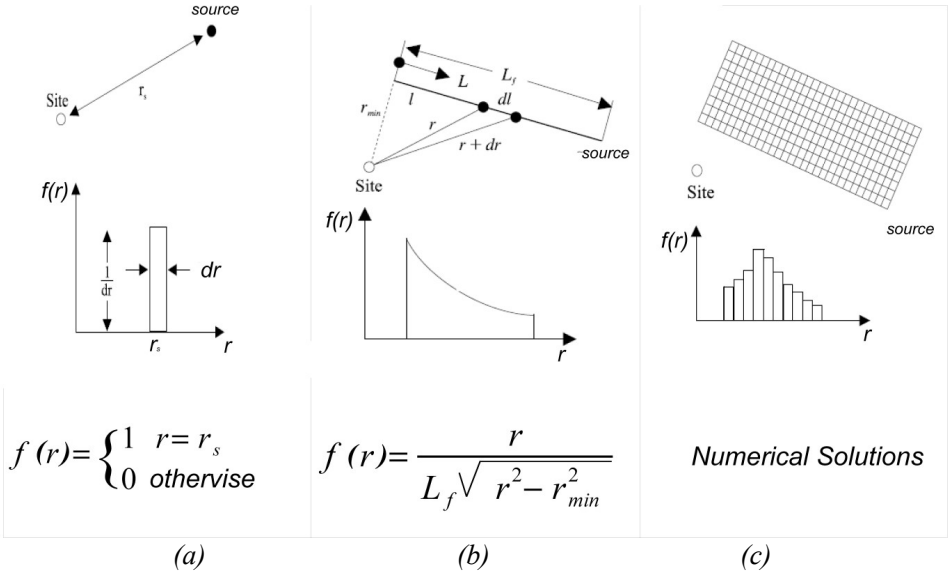

Figure 3.2: Examples of the distance distribution f(r): (a) the point source; (b) the line source; (c) the finite fault model.

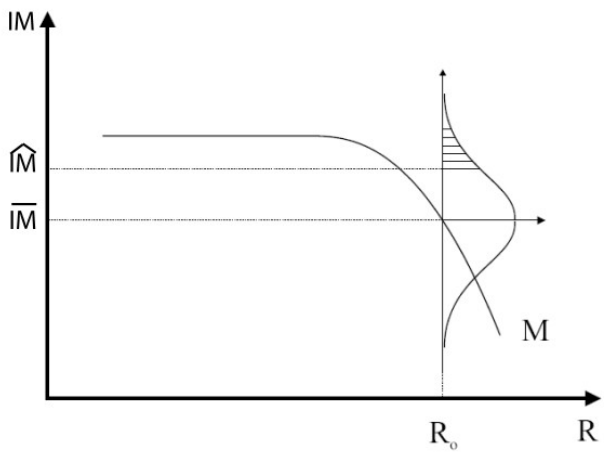

Figure 3.3:The log normal distribution of the PGA. Here IM is a ground motion intensity measure, $\widehat{IM}$ is a fixed ground motion level , $\overline{IM}$ is the predicted ground motion value. R_0 is the fixed distance, M is the fixed magnitude.

level is given by (figure 3.3):

$$P[IM \geq I\hat{M}_0 / m, r] = \frac{1}{\sqrt{2\pi}\sigma} \int_{I\hat{M}}^{\infty} e^{\frac{-(IM - I\bar{M})^2}{2\sigma^2}} dIM \tag{3.9}$$

under the assumption that the ground motion intensity measure (IM) is log-normally distributed. In this case the probability of exceedance is related to the difference between the variable IM and the mean value of the log - normal distribution $I\bar{M}$. This mean value is obtained using a ground motion predictive equation (GMPE – see Chapter 2) linking the IM to the explanatory variables. $I\hat{M}$ is the fixed ground motion level to exceed.

3.1.2 One major limitation of the traditional formulation

Eq (3.5) illustrates that for the calculation of the probability of exceedance of a certain ground motion intensity measure, the knowledge of the joint probability distribution of all random variables involved is required. Nevertheless the ground motion variability depends implicitly on other variables not included as explanatory variables in the ground motion model and responsible of the deviation between the empirical predictions and the observations. For instance, the rupture process is not included in the GMPE formulation and, as pointed out in Chapter 2, that means that several scenarios, i.e different choices of the nucleation point, would correspond to the same M-R couple. Thus the likelihood of having an occurrence is increased. In the PSHA practice that means that the conditional probability of exceedance is systematically overestimated.

A better performance would surely be acquired accounting for a few more parameters, linked to the IM by a physical relation and suitable to better constrain the ground motion variability.

3.2 The hazard model implementation

As pointed out in the previous section, the introduction of new parameters in the GMPEs formulation should better explain the ground motion variability, reducing the residual between the prediction and the observation and leading to a better definition of the conditional probability of exceedance. Because the GMPE represents the core of the (3.5), the introduction of a new explanatory variable in the GMPE implies a recasting of the PSHA formulation.

A new dimension, i.e. a new parameter (x) could be introduced in the traditional hazard formulation adding one integral over the parametric space *X*, a weighting pdf_x, expressing the behavior of the variable in the parametric space, and a corrective function to the predictive equation. Formally the introduction of the new variable X affects the kernel of the integral changing the computation of the joint probability of having an exceedance event. Equation 3.5 becomes :

$$E(IM \geq IM_0) = \alpha \int_R \int_M \int_x f_R(r) f_M(m) f_x(x) \\ P_{IM}[IM(m\ \ r) * corr(x) \geq IM_0 / m\ \ r\ \ x] dm\, dr\, dx \tag{3.11}$$

The parameter X may correspond to numerous and diverse characteristic of the seismic source as focal mechanism, source geometry, rupture kinematics, source function parameterization, relative position of the observer with respect to the fault (footwall / hangingwall amplification, near field effects, directivity modifiers). The equation (3.11) may be completed with an increase number of integrals as the dimensionality of the parameter space grows. In addition to the increasing cost of the computation, it is necessary to pay attention to the relation between the selected parameters, because many of them are dependent on each other (e.g .source dimension and magnitude). Thus, in some cases it is more efficient to group the parameters, linked by a physical model able to capture the multidimensional effect (e.g. the radiation pattern, faulting style, etc.). For instance, Convertito and Herrero

(2004) have described the focal mechanism through the faulting style, implying a dependency between the dip angle and the rake of the fault. In this work we use directivity modifier in order to account for specific characteristic of the seismic source rupture (Chapter 1).

The incorporation of Som97, and SC2008 as well, requires on top of the distance and magnitude the addition of three parameters describing the focal mechanism (strike Φ, dip δ, rake λ), one parameter related to the velocity rupture normalized by the shear wave velocity (v_r/β) and finally the laterality representing the position of the hypocenter relative to the fault. This quantity ranges between [-1, 1] and 0 is the condition of perfect bilaterality. For the focal mechanism we have adopted the convention of Aki and Richards (1980): ($0<\Phi<2\pi,\ 0<\delta<\pi/2,\ -\pi<\lambda<\pi$).

The definition of the bounds of the v_r parameter is mainly subjective. In this study. for instance, we do not allow supershear velocity, i.e. the ratio v_r/β cannot be greater than 1. The effect of those velocities on the seismic radiation is still a matter of debate (e.g. Bizarri and Spudich, 2008), especially in a kinematic context. Thus the higher limit is set to the one of the Rayleigh's wave (0.92β), the lower bound is arbitrary fixed at 0.6β. The main problem relies in the fact that datasets are not rich in events having a variety of rupture velocities. Spudich and Chiou (2008) have reported a weak correlation between the velocity ratio and the residuals. Thus, we have tested the effectiveness of the velocity ratio on our formulation finding a weak contribution to the hazard estimations. As a consequence we have decided to neglect its variability from now on, setting its value at 0.8 that is, on average, a good approximation for most earthquakes.

The bound definition for each parameter is not sufficient. A description of each associated pdf is needed in order to compute a relative probability of occurrence. In general, when no a priori informations are available, the variate is taken uniformly varying in the parametric space. In this case the pdf is uniform and every value has the same chance to occur. As mentioned before, this could be the case of the v_r.

In this theoretical study we decide to adopt *ad hoc* probability density functions in order to test the effectiveness of the corrective factor under controlled conditions. However the proposed formulation enables a site-specific updating once the probability density functions of the involved parameters becomes better known.

If all the parameters needed to incorporate directivity in PSHA are substituted in place of X , the equation (3.11) becomes:

$$E(IM \geq IM_0) = \alpha \int_R \int_M \int_\phi \int_{v_R} \int_\Delta \int_\Lambda \int_\Xi f_R(r) f_M(m) f_\phi(\phi) f_{v_r}(v_R) f_{\Lambda,\Delta}(\lambda\ \delta) f_\delta(\delta) f_{(\Xi)}(\xi) * P_{IM}[IM(m, r, \phi, v_R, \delta, \lambda, \xi) \geq IM_0 / m, r, \phi, v_R, \delta, \lambda, \xi] * dm\, dr\, d\phi\, d\lambda\, d\delta\, dv_r \tag{3.12}$$

where Φ is the strike angle, V_r is the rupture velocity, δ the dip angle, λ the rake angle, ξ is the laterality.

Eq. (3.12) has been implemented in a fortran 77 code using the standard procedure for integrating function by quadrature. This involves the partitioning of the parameters ranges into a finite number of subintervals, the evaluation the integrand at a selected point within each interval, and the summation of weighted products of the integral and the subinterval width. The code is addressed to be updated every time new informations about the rupture process are available, simply adding one more discrete summation over the parametric space. We handle the source-to-site system characterization conceiving two different strategies: the first consists in collapsing the entire finite fault system to a representative point; the latter consider the finite fault in its entirety. The first approach is supported by two different reasons: (1) this formulation is easier to handle, for example in monitoring the results; (2) it is easily applicable whereby the finite fault is unknown, that is the case of hazard assessment derived from spatially-smoothed historic seismicity or when a seismic zone, rather than a seismic fault, is considered . The second approach is intended to test the effectiveness of directivity when a finite fault is

known in deterministic terms.

3.3 Collapsing the entire system to a point

A first strategy consists in collapsing the entire finite fault system to a representative point.

Here we conceive a moving source on a prescribed direction. Because we are using a probabilistic approach all the involved arbitrary variables are free to move inside a certain range. The fault centroid is taken as representative point, fixed in space, while the hypocenter position is kept free to move all over (figure 3.4). Thus the directivity relative parameters are free to move inside a certain range. The relative

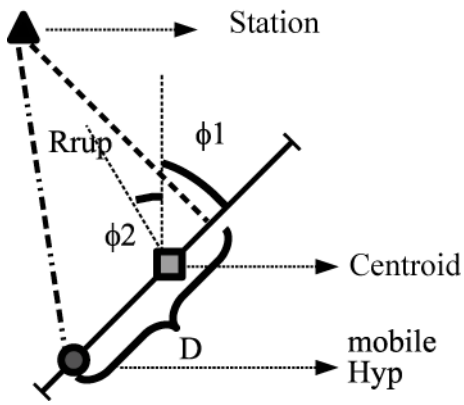

Figure 3.4: Schematic representation of the simplified source-site system model. The centroid is taken as the more representative point of the source, fixed in space, while the hypocenter moves exploring the geometric space.

position between the hypocenter and the centroid defines a segment length and sets a direction in space to be used as an input in the analytical formulation of the directivity corrective factors.

Φ1 is the strike angle, Φ2 is the angle between the propagation of rupture and the source-to-site direction. D represents the fault surface suitable to rupture toward the station. It is the portion of surface as viewed under the angle Φ2. Rrup is the minimum distance between the station and the segment centered on the centroid. Rrup is essential in computing the corrective factor of SC2008. Moreover Rrup

enters the base formulation of the AS2008 ground motion predictive equation on which the correction of SC2008 is calibrated. Instead Som97 uses Abrahamson and Silva (1997) (see chapter 2 for a detailed description of the Abrahamson and Silva, 1997,and 2008 equation).

Our starting point is the comparison between the test model proposed by Spudich and Chiou (2008) for a strike-slip finite fault (61x28km^2, M=7) and the relative centroid model approximation. We compare the surface representation of the

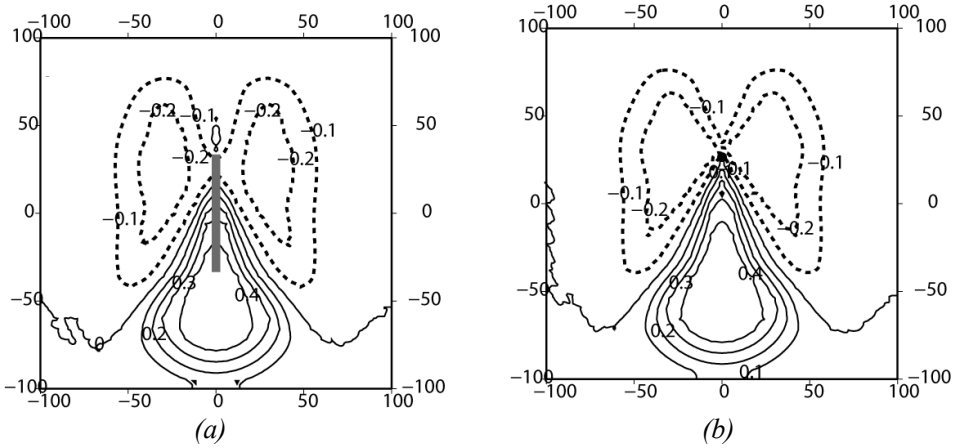

Figure 3.5: Surface projection of the directivity corrective factor for SA at 5sec.. Comparison between the test case reported in Spudich and Chiou 2008 for a strike slip fault 67 km length and 15 km width (panel -a-) and the point approximation developed in this study (panel -b-). The corrective values are almost the same except for points very close to the hypocenter where finite fault dimension collapse in one single point. Dashed lines represent negative values. Solide lines represents positive increment.

corrective factor for spectral acceleration at 5 seconds (figure 3.5). The comparison shows a good agreement over the entire map except for point very close to the hypocenter where the rupture dimension collapses to a single point.

3.3.1 Test on a strike-slip fault

A first test investigates on the directivity effect due to a rupture propagating toward the south on a strike-slip fault. We refer to the example proposed in the work of

Spudich and Chiou (2008) of a M=7 strike-slip event. We make use of the point approximation in order to assess the influence of the directivity factor in a probabilistic framework, where the faulting style and the magnitude are fixed and the hypocentral position and the strike angle are varied in their respective ranges. Thus, in a probabilistic framework, a statistical transposition of the information on the hypocenter location and the striking direction is needed. To this purpose we select *ad hoc* density distributions for this purpose: a narrow Gaussian for the hypocenter position centered on the northern part of the fault (figure 3.6a) and a zero centered Gaussian for the strike angle variable (figure 3.6b).

For first we develop a reference hazard map portraying the spectral acceleration ordinate (5 sec) at a probability of exceedance of 10% in 50 years. Preparation of this map follows the traditional strategy derived from fault-specific sources simplified in the following by mean of the centroid approximation. Then, a second map is computed, portraying the same features as the reference one, but derived via the implemented strategy. To stand out the variations caused by the corrective factor for directivity we set up the relative percentage difference between the two maps.

The achieved pattern (figure 3.6) shows clearly the increment of the hazard assessment in solid lines and the decrease in dashed lines. The variation pattern follows the layout promoted by the corrective factor: positive contributions to the PSHA are detectable in the region ahead the rupture propagation; in contrast a negative contribution appears in a wing shaped region transversal to the rupture propagation. The increment is up to 50% in the propagation direction using the SC2008 corrective factor (on top), while in the rupture transversal direction the decrease is up to 20%. The size of the lobes depends partially on the width of the Gaussian distribution of the strike-angle, and thus it is related to the uncertainty on the strike-angle parameter. On the other side, the Som97 corrective factor (on bottom) provides an increment greater than 100% in the propagation direction and a decrease of up to 70% in the opposite direction. The two patterns differ mainly in the regions of low directivity effects near the epicenter where the SC2008

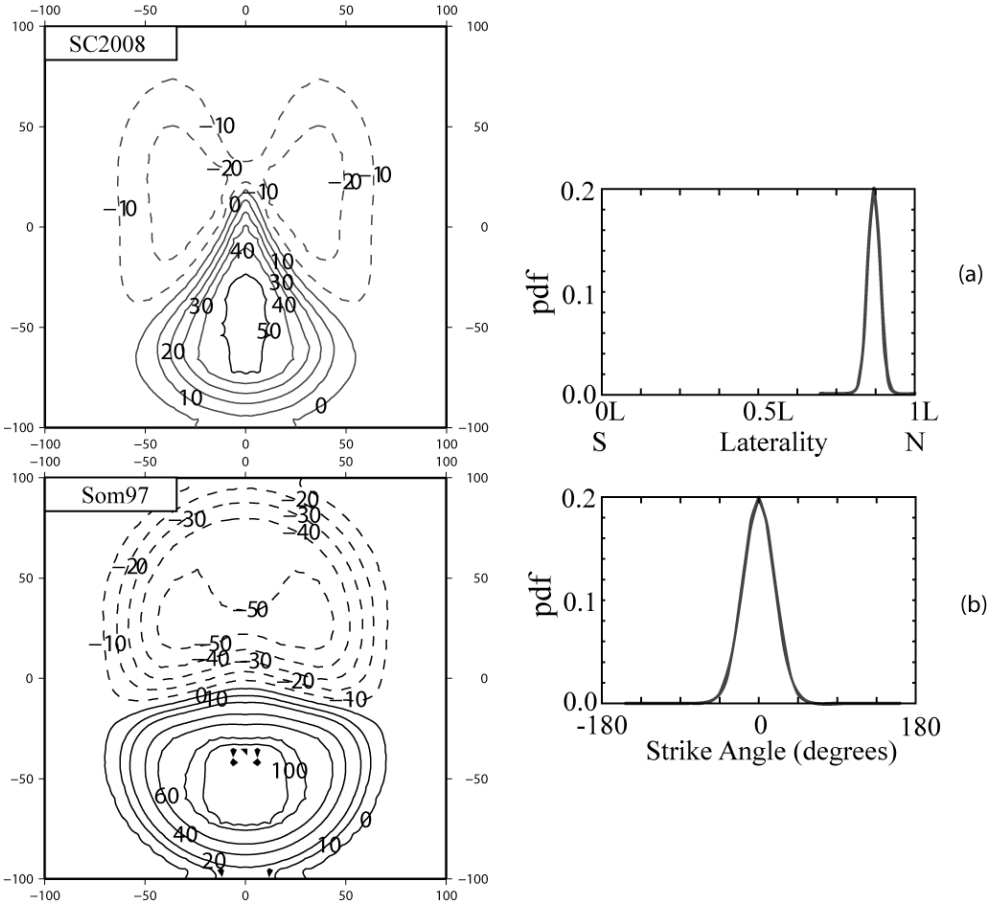

Figure 3.6: Centroid approximation. Maps show the relative percentage difference between hazard maps (SA 5s, probability of exceedance 10% in 50 years) corrected for directivity and hazard maps obtained with a null corrective factor. On the top left the SC2008, on the bottom left Som97. Dashed lines represent negative values. Solid lines represents a positive increment. (a) Laterality Gaussian distribution centered on the north part of the fault. (b) Narrow strike-angle Gaussian distribution centered on zero (b).

corrective factor predicts much narrower zones of amplification in the forward (south) direction and a small deamplification in the backward (north) direction. This difference is attributable to the effect of the radiation pattern that is taken into account explicitly only in SC2008 corrective factor.

Supposing now we have no informations about the hypocenter position. This laking information transposes to a uniform probability density function for laterality. An

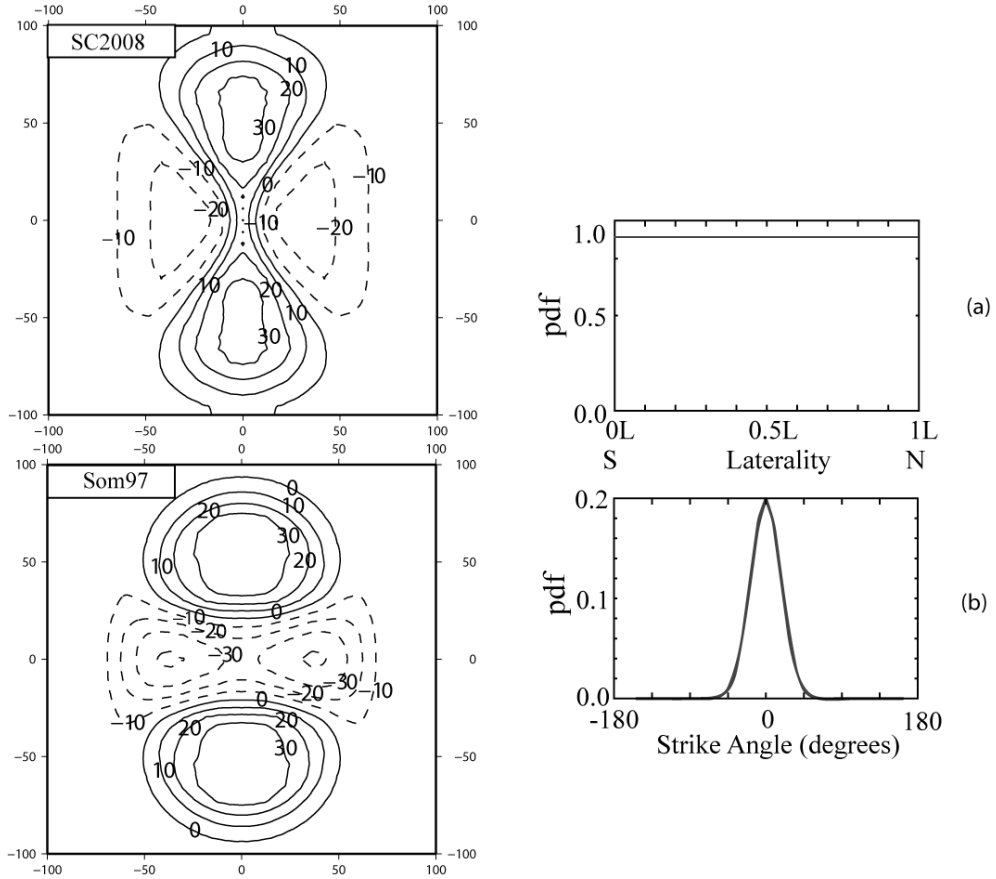

Figure 3.7: Centroid approximation. Maps show the relative percentage difference between hazard maps (SA 5s, probability of exceedance 10% in 50 years) corrected for directivity and hazard maps obtained with a null corrective factor. On the top left the SC2008, on the bottom left Som97.Dashed lines represent negative values, solid lines represent a positive increment.(a) Laterality uniform distribution . (b) Narrow strike-angle Gaussian distribution centered on zero.

uniform distribution means that every point in space has the same probability of nucleating a rupture episode. As shown in figure 3.7 the pattern changes to a bilateral rupture layout leading to a 30% of amplification in case of SC2008 with narrow elongated lobes along the rupture direction. A deamplification up to 20% is observed in the rupture transversal direction. The Som97 and the SC2008 corrective factors in this case are similar except for points very close to the hypocenter. Also in this case the main difference is given by the action of the radiation pattern.

3.3.2 The PSHA implementation in presence of multiple sources

In presence of multiple sources the probabilistic formulation (3.5) is given in the form:

$$E(IM \geq IM_0) = \sum_i^S \alpha_i \int_R \int_M f_{R_i}(r) f_{M_i}(m) P_{IM}[IM(m,r) \geq IM_0 / m, r] dmdr \tag{3.5bis}$$

where for each *i-th* source a description of the seismicity (the activity rate α_i) is given and the solution is acquired summing over all the seismic sources contributing to the ground motion shaking level at the site.

The point strategy can be used to describe the contribution of different sources with the most likely associated orientation and size. Thus, because the source is a point, the [*f(r) dr*] has the form a logical function and the integral over distance reduce to 1for distances equal to the hypocentral distance otherwise it is equal to 0 (figure 3.1a). The computation, in this test, is further simplified removing the integral on magnitude.

The directivity related parameters, the strike and the laterality defining the source-to-site position, vary inside a certain range. The other variables related to the focal mechanism are fixed to a constant value. The same assumption is made on the rupture velocity. In a probabilistic context, it means that their pdf are delta functions. One example is shown in figure 3.8, where three different sources are approximated to their centroid position and their deterministic characteristic are treated probabilistically. Again we make use of ad hoc probability distributions: (1) narrow gaussians centered on the most likely striking angle (145° for source 1; 0°, for source 2; 90° for source 3); (2) narrow gaussians for laterality centered in 0.90 for source 1, in 0.5 for both source 2 and 3.

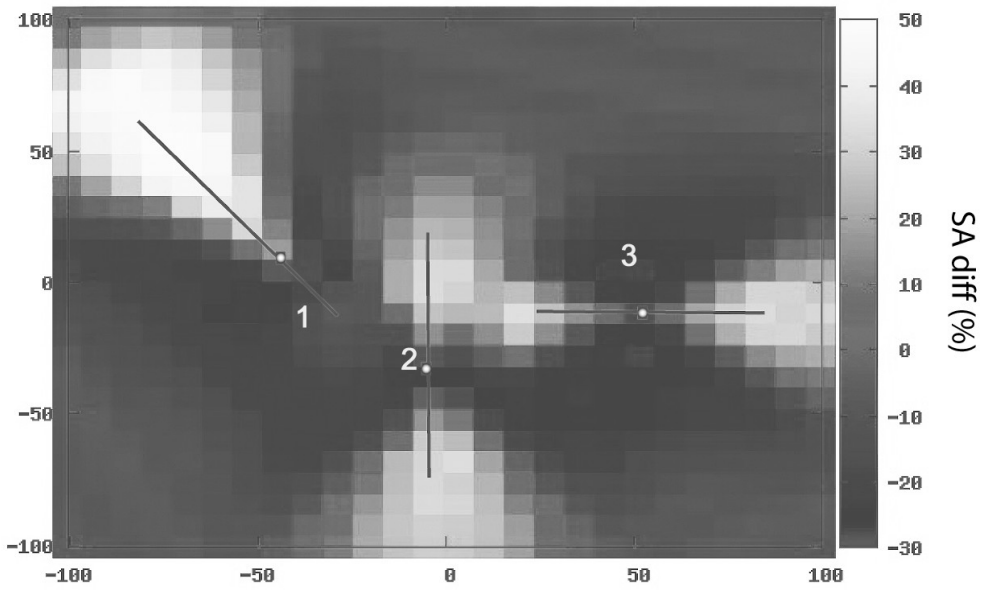

Figure 3.7 The extended areal source. The combined effect of three different sources approximated to their centroid and whose size and orientation is treated probabilistically. Map shows the relative percentage difference between hazard maps (SA 5s, probability of exceedance 10%, 50 years) corrected for directivity and hazard maps obtained with a null corrective factor.

The gray palette highlight in white the positive contributions to the PSHA due to the introduction of the directivity factor relative to a traditional model. In the regions marked in black a insignificant reduction is achieved (about 20%). The applicability of such hazard models depends strongly on the *a-priori* knowledge about the statistical distribution of the parameters involved. Nowadays this informations are available in the catalogs where a full set of geometric (strike, dip, length, width, depth), kinematic (rake) and seismological parameters (single event slip distribution, magnitude, slip rate, recurrence interval) are defined by geological and geophysical data (i.e DISS 2009, Basili et al. 2008). A probabilistic treatment of these informations should lead to a more comprehensive hazard evaluation with respect to the traditional PSHA formulation. This issue will be treated extensively in the discussions (paragraph 3.5 of this Chapter).

3.4 The finite causative fault

The approximation made in paragraph 3.3 has pointed out the strong influence of directivity on the hazard maps. Directivity induces variations that strongly imprint the shaking level and, as a consequence, the PSHA estimation.

Now we turn to the finite fault case in order to test the directivity effect. We use a M=7, 45° reverse dipping fault, 36 km length and 28 km width (figure 3.9) referring to the example proposed by Spudich and Chiou (2008). The directivity corrective factor is computed on the spectral acceleration at 5 seconds.

When no information about the hypocenter position are available an uniform distribution on laterality is used (figure 3.9a). An hypocentral uniform distribution means that every single point of the fault can nucleate a seismic event with the same probability. This strategy is currently used in actual probabilistic seismic hazard analysis. The strike angle dependence is expressed by a Gaussian probability function centered on zero.

Map in figure 3.9a portrays the relative percentage difference of two hazard maps defined at a 10% of probability in 50 years. one computed with a null corrective factor, the second considering the corrective factor for directivity. The resulting pattern shows high (up to 30%) amplification in the up-dip rupture direction along the surface exposure of the fault. A decrease of a 20% outcrops directly in the backward direction.On the off edge of the fault a low directivity effect arises, resulting in a deamplification of the predictions.

The actual probabilistic hazard analyses are based on the uniform distributions of seismicity throughout the seismic zone. Nevertheless recent studies demonstrate that this assumption diverges from the observations (Mai et al. 2005), moreover the location of the hypocenter itself is not safe from a certain degree of uncertainty. Directivity, for both Som97 and SC2008, correlates strongly with the hypocentral position. One advantage of having an hypocentral distance dependency is that it

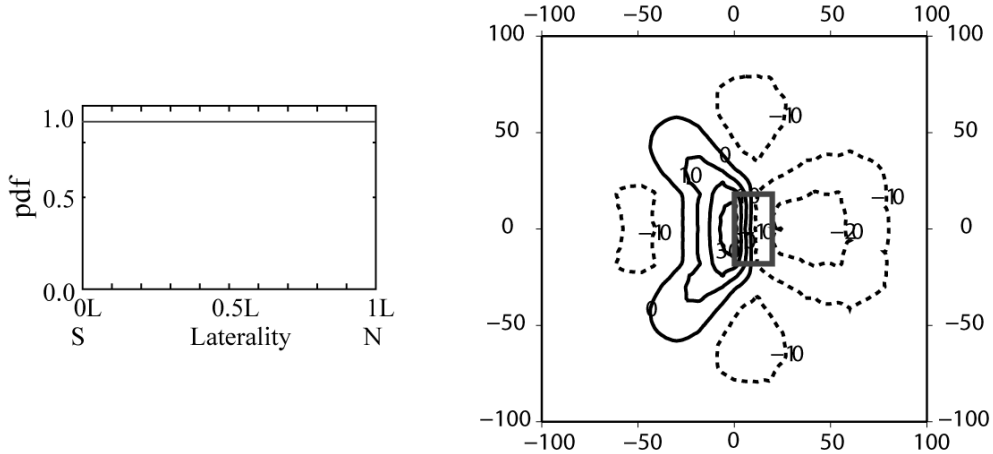

Figure 3.9a: Finite reverse fault 45° dipping. Map to the right shows the relative percentage difference between hazard maps (SA 5sec, probability of exceedance 10%, 50 years) corrected for directivity and hazard maps obtained with a null corrective factor. Uniform distribution for laterality (left panel). Narrow strike-angle Gaussian distribution centered on zero.

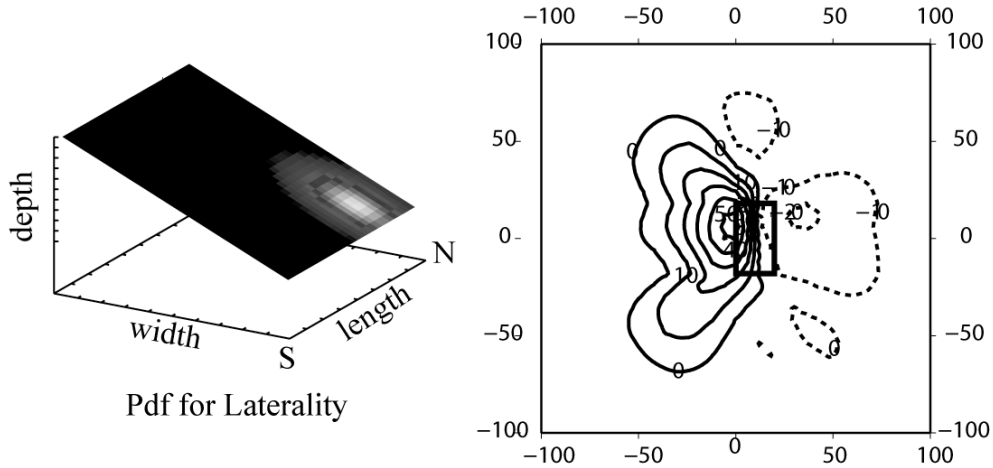

Figure 3.9b: Finite reverse fault 45° dipping. Map on the right shows the relative percentage difference between hazard maps (SA 5sec, probability of exceedance 10%, 50 years) corrected for directivity and hazard maps obtained with a null corrective factor. Gaussian distribution centered on the south-eastern part of the fault (left panel). Narrow strike-angle Gaussian distribution centered on zero.

justifies the introduction of a weighting function for the hypocenter position. We have hypothesize a Gaussian probability density function, the mean centered on a certain hypocentral position, the width defined by the uncertainty over the localization (figure 3.9b). This strategy allows us, to test either the influence of the hypocentral position or the effect of the localization uncertainty on hazard map. This pdf enters the PSHA formulation as a weighting function.The radiation pattern (figure 3.9b) changes significantly around the epicenter, in an area close to the mean value of the Gaussian distribution. The directivity effect leads to an amplification of the prediction of up to a 50% in this region and the pattern spread over a narrower region respect to the uniform model.

3.5 Discussions

Recently Bommer and Abrahamson (2006) and Klugel (2007a) have discussed the apparent increase of the hazard estimates in the modern probabilistic hazard analysis. The former ascribing this behavior to the fact that the ground motion variability is not treated properly. The latter demonstrating that some difficulty arise from the PSHA formulation itself and that the uncertainty is model dependent.

The matter of the debate is the applicability of modern hazard analysis in posing the basis for the structural design specially concerning the critical infrastructure for which the influence of the uncertainties is stronger (i.e. nuclear power plants). In several applications the PSHA methods are considered not sufficiently mature for a meaningful hazard assessment. A valid alternative is found in the deterministic seismic hazard models. Nevertheless the deterministic model requires a detailed description of sources and, although the identification of fault potentially seimogenetic is extremely important (as maybe the vanguard examples of the Italian catalog DISS or the Californian map of active faults), its relevance for predictive purpose is often limited. Even though the most accurate information available for the best identified sources are provided prior the occurrence of the earthquake, rarely the rupture occurs exactly with the expected modalities. Therefore a probabilistic treatment of the fault segments and in general, of the

deterministic parameter is currently indispensable and it is more adequate to deal with "the most likely rupture segments" and of "the most probable rupture scenario" .

In this framework we have exploited the idea of coupling deterministic methods to a probabilistic approach introducing new explanatory variables in the formulation. By one side the introduction of new aleatory variables in GMPEs should lead to a better performance of the PSHA estimations because:

1. The ground motion is better constrained. In fact, as pointed out in 3.1.2, the variability of random variables not included in the computation should systematically increase the conditional probability of exceedance.

2. The reduction of the uncertainties in the GMPEs should affect the hazard estimation as well. In fact, it is common practice to truncate the log-normal distribution, assuming that values above 1 sigma are not reliable. When the sigma is large more scenarios are sheared off.

On the other side it could be postulated that if the statistical distribution of the parameter is not well constrained the hazard estimations could increase with the growth of the dimensionality. Thus the distribution is "non-informative". It takes the form of an uniform distribution meaning that the variable can take all the possible values in its range with the same probability. It has to be noted that the use of uniform distributions is common practice in the PSHA formulation. Other random parameters are *de facto* modeled with non-informative distributions, i.e. the hypothesis of uniform spatial distribution for seismicity in areal sources. The key question is thus: is it useful to use such an approach, which costs much more in terms of computation than a traditional one, if some ingredients, i.e the pdf, are missing?

Thus we propose to test the influence of non -informative distributions on hazard maps, using uniform distributions for both laterality and strike angle (figure 3.10) .

Figure 3.10 shows the percentage relative difference between a null corrective model and the corrected one using uniform distribution for both strike angle and laterality.

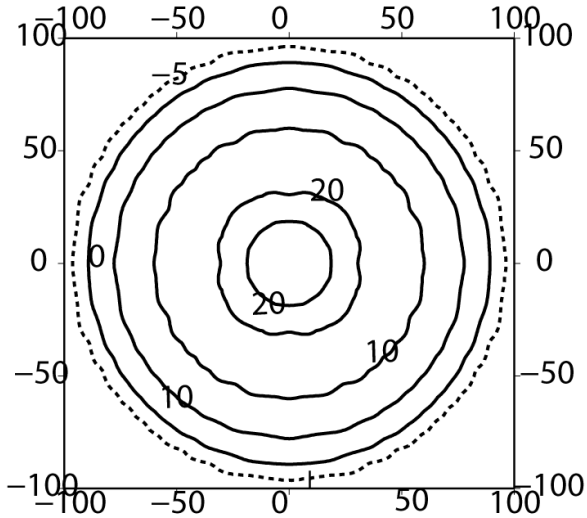

Figure 3.10: shows the percentage relative difference between a null corrective model and the corrected one. The corrective factor used here is the SC2008. The comparison result in curves of constant level around the mid point of the segment.

Maps are computed searching for a probability of 10% of exceedance in 50 years. Compared to the reference map computed with the traditional strategy, the hazard map corrected for directivity results in a difference of 30% for SC2008 around the hypocenter, where the ground motion level is increased on average by the corrective factor. Null difference appears at about 70 km of distance where corrective factor is linearly tapered to zero by its definition. A 5% of decrease is obtained for distances larger that 70 km where the corrective factor is null. We infer that for distances larger than 70km the main difference is given by the reduction of the uncertainty inside the GMPEs. For distances shorter than 70 km two factors compete to the increase of the ground motion level. The first resides in the different formulation of the conditional probability of exceedance of a specified ground motion level, accounting now for the n-dimensional random variable X; The second is attributable to the propagation of uncertainties and to the possible correlation between them. This test may partially answer the question. If the

corrective factor is not associated to a reduction of the standard deviation, then the use of a uniform pdf implies only an increase of the hazard close to the source. The increase is uncontrolled because other sources of errors are introduced and the errors could blend the results achieved when a few better constrained parameters are used. Thus, the use of this correction becomes penalizing with respect to a classical approach. However, if the standard deviation is decreased, then the hazard far from the correction influence is also decreased. Thus the only case when this approach is not advice, is when the corrective factor is not associated to a significant decrease of the standard deviation and ,at the same time, some a priori information is not available.

The a priori information we need to improve the performance of the PSHA is not available for part of the parameters describing the kinematic or the dynamic of source rupture, i.e. the rupture velocity. However the number of studies describing their distributions in the parametric space is growing of importance: Informations about the source time function are becoming available by the inversion procedures; Mai et al. (2005) have handled the distribution of the hypocenters with depth, so that the hypothesis of uniformity, currently adopted in the PSHA should be overcome. Such information could be used in this context. Moreover actually the database are enriched in detailed informations about the style of faulting associated to the majority of the seismogenetic zones of the present seismic hazard maps. By way of example the fault mechanism for the Apennines (Italy) or for the San Andreas fault segments (US-California), the expected style of faulting is not aleatory at all. A good a priori knowledge exists for the distribution of both the dip and the orientation of faults. The information collected for each parameter of interest can be easily converted into pdf to account for in a PSHA formulation.

Chapter 4

Directivity: what deterministic hazard models can tell [1]

The main reason for the increases in the modern estimates of seismic hazard is that the ground motion variability in early applications (and indeed formulations) of PSHA was not treated properly.

Bommer and Abrhamson, 2006

The capability of detecting and codifying a physical constraint has strong implications on ground motion empirical modeling and on the reduction of the uncertainties. Two main problems encourage the use of the deterministic models for predictive purpose.

A first problem is related to the paucity of the number of recordings that is not sufficient to infer a robust parametrization of the ground motion, specifically to capture source complexity. The ergodic hypothesis allows to enlarge the data-set but tends to mask, when present, specific trends. As a result the ground motion predictive equations represent only an average statistical behavior and its associated uncertainty is large. In order to better assess the variability of ground motion the optimum would be having a data-set made of a number of seismic recordings derived from different rupture processes on the same fault. Unfortunately, only few earthquakes have ruptured the same seismogenic fault

1 This chapter is partially published in BSSA June 2010, Vol 100 No. 3: "Variability of kinematic source parameters and its implications on the choice of the design scenario" by G. Cultrera, A. Cirella, E. Spagnuolo, A.Herrero, E. Tinti, F. Pacor

more than once in recent times such that recordings could be obtained in the near-source region with high-quality networks (e.g., 1966 and 2004 Parkfield earthquakes, see Harris and Arrowsmith, 2006; 2004 and 2007 Niigata earthquakes, see Cirella et al., 2008). The lack of such observations limits the detailed analysis of the dependence of ground motion variability on source parameters. As a first approximation it is possible to classify two main sources of ground motion variability at bedrock sites: the heterogeneity of propagation medium and the characteristics of the rupture process. However, it is far from simple to unambiguously distinguish the relative influence of these two factors. For the time being, the use of synthetic simulations may partially overcome the paucity of near-source data (Andrews et al., 2007) and it can help to clearly separate the causes of the ground motion variability. Moreover, the computed synthetic data-set allows us to retrieve multi-parametric synthetic predictive equations valid at close distance from the fault to be used for engineering seismology applications. This is the case of the seismic design of structures and the calculation of Probabilistic Seismic Hazard (PSHA) curves, where the simulated ground motion parameters substitute the predictions from empirical models (Convertito and Herrero, 2004; Convertito et al., 2006; SCEC/CME CyberShake Project, 2007).

The second major problem arises in the probabilistic hazard computation when low annual frequencies of exceedence (or long return periods) are considered. For example, earthquake resistant design for a long span bridge needs very long-period spectral displacement. In this case, the hazard assessment is unlikely because the log-normal distribution associated with ground motion prediction equations is truncated. The synthetic data-set can be exploited to develope hazard solutions conformable to the engineering demand. In the fallowing we show a possible use of the retrieved statistical distributions of synthetic ground motions parameters to select shaking scenarios whose characteristic follow defined criteria, such as scenarios having a particular peak value at one or more sites. In that sense, probabilistic and deterministic hazard analyses compensate each other.

4.1 An Approach to the deterministic modeling

The aim of this chapter is to study the variability of the ground motion due to the variation of several kinematic parameters describing the seismic source. Thus, seismic scenarios from different rupture models of a single finite causative fault have been modeled. The computation of synthetic scenarios is based on a solution of the equations of motion from finite faults embedded in vertically varying media. Different rupture models are obtained varying four kinematic parameters that are: (1) the slip distribution, (2) the rupture velocity, (3) the source time function and (4) the nucleation point. The fault geometry is instead fixed.

A Shaking_chain package has been implemented in order to manage the the variation of the four kinematic parameters on fault. The core of the chain is represented by the computation code. Once that an input file is prepared the Shaking_chain cycles over all the possible combination of parameters and the simulation runs to the final step.

A preliminary step defines the geometry of the problem in a Cartesian fault-oriented system and computes a slip model from a given probability density function.

A second step enters the kernel of the Shaking_chain package that is the code for the earthquake ground motion calculation using complete 1-D Green's function.

A Matlab (the Mathworks, 1984) based source code has been developed in order to infer statistical properties of the ground motion variability. Ground motion intensity measures have been studied in terms of probability distributions and the associated moments.

A de-aggregation technique have been introduced in order to extract ground motion scenarios responding to specific requests. This technique is similar to the disaggregation procedure (Bazurro and Cornell, 1999) used to display the relative contributions to hazard estimations from the range of values of magnitude, M, distance, R, and uncertainty sigma predicted by an attenuation equation.

4.1.1 The Code

Among the simulation methods proposed in literature, we use the Compsyn code, proposed by Spudich and Xu (2003), based on a Discrete Wavenumber / Finite Element (DWFE) technique. It works with the finite fault, allowing us to vary the kinematic source parameters of interest.

The Compsyn code is a deterministic forward modeling code, intended to compute full-wave displacement and velocity time series in the zero-to-intermediate frequency band. It models the effects of shearing motions on a finite fault surface solving the representation theorem integrals, a mathematical statement that relates an observable quantity to the parameters of a seismic source model. It uses the complete solution proposed by Spudich and Archuleta (1984) on a fault surface. Green functions are explicitly computed via a Discrete Waves-number / Finite Element (DWFE) technique of Olson et al. (1984), where the time dependence of the resulting system of equations is solved with the finite difference method and the spatial dependence is calculated through the finite elements method and the discrete waves number technique. The applications assume that the Earth model is defined in a 3-dimensional Cartesian space, and that the Earth structure is a vertically varying media.

4.1.2 Code requirements

The Compsyn code requires some attentions in selecting the proper spatial and time constrains. Some are necessary to avoid numerical noise, same are needed to correctly outline the physical problem.

The spatial resolution is chosen according to numerical dispersion requirements. It is nothing but satisfying the Nyquist sampling criteria in spatial domain. The minimum wavelength component must be sampled with at least two samples (dx). In practice, at least 6 grid points have to be chosen to define the shear wavelength corresponding to the maximum frequency of the computation (fmax) without numerical dispersion effects:

$$\frac{v_r}{10 * f_{max}} \leq dx \leq \frac{v_r}{6 * f_{max}}$$

where v_r is the rupture velocity.

The sampling rate in the time domain must be at least equal to $2f_{max}$ in order to avoid periodic band coalescence and loosing informations, according to the Nyquist sampling criteria. Thus the time step for finite element calculation is driven by the maximum frequency content. But also it should satisfy the Courant stability criterion stating that the length of the time step should be less to the minimum P wave travel time across any element of the finite element grid. An initial choice is given by:

$$dt = 0.15 \frac{\beta}{f_{max} * \alpha}$$

where α and β are the P and S waves velocity respectively.

Every grid point on the fault surface have its how dislocation history and the time the dislocation reaches its maximum value through each grid point is named rise time. Thus, in order to sample the slip evolution (the source time function) the rise time must be greater or equal than the time step (dt). Therefore:

$$\tau > \frac{1}{2 * f_{max}}$$

The time duration must equal or exceed the sum of the extended source duration and the duration of the Green's function in order to avoid noncausal noise before the hypocentral P wave arrivals:

$$t_{max} = t_{propagation} + t_{rupture}$$

4.1.3 The high Frequency Content

The high frequencies radiation from an earthquake source is sensitive to the complications on the fault plane at scales smaller than the overall rupture dimension (Housner, 1955; Haskell, 1964, Sholtz and Aviles, 1986). This behaviour has been interpreted in terms of self-similar rupture process where

source presents hierarchical structures with a spatial fractal geometry (Frankel, 1991).

In order to account for these details we should have a slip model with a resolution of tenths of meters while inversions would have presently a maximal resolved wavelength of typically 10 km for a 100 km fault length (roughly corresponding to M=7), or approximately 300 m for a 1km fault length (roughly corresponding to a M=4).

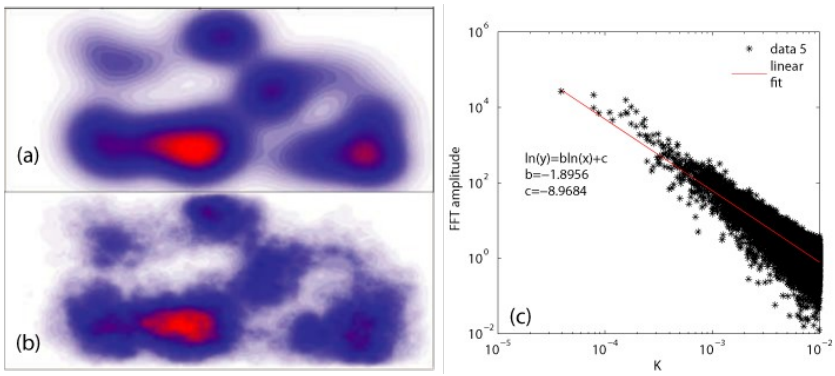

Figure 4.1 (a) contour map of the Gaussian slip distribution (b) contour map of the k2 slip model (c) log-log plot of the spatial Fourier transform of the slip distribution (the x axis represents the radial wavenumber k, and the y axis represents the FFT amplitude). The mean distribution (red line) shows that the bi-dimensional FFT decreases as k^{-2}.

As a consequence, these details are not embodied in the source model, and cannot be propagated from seismic source to surface. In order to overcome this laking information we impose some complexity to the slip distribution following the approach of Zeng et al. (1994) and computing the self-similar k-square model (Herrero and Bernard, 1994) for each slip model proposed in this analysis. The self similar k-square model is used to generate an ω-square *far-field* radiation spectra under the assumption that the amplitude of the slip distribution, high passed at high wave numbers, does not depend on the size of the rupture fault but it is controlled by local heterogeneities at all scale.

A routine has been developed to compute the slip distribution following the k-square model. It reads a list of a given number of Gaussian, defined with their center, their sigma and their weight to create a probability density function (pdf) on

the fault plane (figure 4.1a). The pdf is then used to randomly distribute a fractal distribution of asperities on the fault plane (figure 4.1b). The result is a slip model that decays as k^{-2} as shown in Figure 4.1c.

4.1.4 Ground motion intensity measures

Shaking scenarios for engineering applications are generally provided in terms of Peak Ground Acceleration (PGA), Peak Ground Velocity (PGV), Peak Ground Displacement (PGD) and response spectral ordinates (hereafter referred as ground motion parameters or intensity measures) expected at a selected site. Each ground motion parameter represents different characteristics of the seismogram, and is sensitive to a different frequency content in seismic radiation spectrum: the PGD is related to the low frequency motion ($f < 1$Hz) and mainly correlated to the magnitude and focal mechanism, the PGV is controlled by the coherent low-to-intermediate frequency of ground motion (indicatively 1 – 3 Hz) and by the corner frequency, whereas the peak ground acceleration (PGA) depends on the high frequencies which are strongly affected by small scale heterogeneities of rupture and propagation medium. For this reason, different intensity measures are required for engineering applications, depending on the characteristic earthquake (fault and magnitude) in the region of interest, on the type of structures (e.g., buildings, lifelines, infrastructures) and on the particular seismic design under consideration. For example, earthquake resistant design for a long span bridge needs very long-period spectral displacement, whereas for buildings or tunnels the seismic response mostly depends on the high-frequency motion. For structures having a long vibration period, the seismic action may be represented in the form of a displacement response spectrum (CEN 2004, ANNEX A of EC8-part 1). The same long-period response spectral ordinates are required for displacement-based design approaches and for base isolation devices (Akkar and Bommer, 2007).

In this study we focus on two ground motion parameters, displacement response spectrum (SD) and peak ground velocity (PGV). The first parameter is commonly used for displacement-based design approaches (CEN 2004, ANNEX A of EC8-part 1; Akkar and Bommer, 2007). The second parameter, PGV, is used in

specifying input to engineering design, such as the estimate of macroseismic intensity and structural damage. It is also employed in some methods for the assessment of liquefaction potential and, because of its relationship to ground strains, in the seismic design and assessment of buried pipelines (Bommer and Alacon, 2006; Bommer et al., 2009).

4.2 Variability of kinematic parameters

The range of variability of the kinematic parameters describing the fault rupture is generally constrained by scaling laws derived from observations or physically defined by studies on source dynamics. The definition of their values is extremely important for the modeling of ground motion scenarios, because it allows us to limit the number of physically realistic simulations. The variability of a few kinematic source parameters is well known or has been deeply studied in the recent literature, such as for the source time function (STF), the position of nucleation point (NP), the rupture velocity (Vr) and the slip distribution (SLIP) on the fault plane (Aki and Richards, 2002). However, there are other kinematic parameters whose values are still not well constrained. This is the case of the rise time, whose variability has not investigated in this study.We do not include any variability of ground motion due to the variation in site response (the simulations are computed at bedrock sites considering only one propagation model), being the study of the propagation medium effect and local site conditions beyond the aim of this analyses. The Compsyn code does not account for the wave attenuation of the Earth. However, in this case study the attenuation effect is negligible because we are considering low-frequency motion at close distances from the fault.

In this section we summarize the expected ranges and the reference values of the aforementioned four kinematic source parameters that have been varied to build the synthetic scenarios of this work. We also discuss briefly the issue of the rise time in ground motion modeling.

4.2.1 Position of the nucleation point (NP)

The location of the nucleation point on the fault plane controls the directivity effect by changing the relative source-to-receiver position. This parameter has large

variability: hypocenters are found either in the deeper half-width of the fault but also close to the fault top (Somerville et al., 1999; Manighetti et al., 2005), and a large percentage of them are located either within or close to regions of large slip (Mai et al., 2005). Moreover, repeating fault ruptures can nucleate in different positions, as for the two similar Parkfield earthquakes of 1966 and 2004 that ruptured the same fault plane but with different slip distribution and nucleation position (Custódio and Archuleta, 2007).

4.2.2 Rupture velocity (Vr)

The velocity of the propagating rupture front affects the signal duration and contributes to the directivity effect, which increases as the rupture velocity increases. Moreover, its local variation generates high-frequency radiation.

The description of this parameter is generally simplified, and hence is often assumed constant on the fault plane. However, kinematic rupture histories with variable rupture velocity on the fault have been recently retrieved from non-linear kinematic inversion (e.g., Delouis et al., 2002; Liu and Archuleta, 2004; Piatanesi et al. 2007; Cirella et al., 2008). This behavior is also found in the spontaneous dynamic models, where the variability of the rupture velocity depends on the heterogeneous distribution of dynamic parameters on the fault plane. For example, Ruiz (2007) obtains a rupture velocity proportional to the 4th power of the slip gradient through spontaneous dynamic simulations. For both constant and heterogeneous rupture models, the rupture velocity is defined in general as a fraction of the shear-wave velocity (Vs), ranging between 0.6·Vs and 0.92·Vs (the latter corresponds to the Rayleigh waves velocity). This range is constrained by spontaneous dynamic simulations (Andrews, 1976; Bouchon et al., 2001; Bizzarri et al., 2001 and references therein). The dynamic models predict also rupture velocities greater than the shear velocity under particular values of the constitutive parameters (Andrews, 1976; Rosakis et al., 1999 among many others): in all these models, very high peaks of slip velocity are found and they are believed to be responsible of anomalous wave amplitudes (Bizzarri and Spudich, 2008), as confirmed by kinematic models of recent earthquakes (e.g., 1999 Izmit earthquake in Bouchon et al., 2002; 1999 Duzce earthquake in Birgören et al., 2004; 2002

Denali earthquake in Oglesby et al., 2004).

4.2.3 Slip distribution on the fault (SLIP)

The slip distribution of essentially all earthquakes, imaged by kinematic inversion techniques, is heterogeneous on the fault plane. This heterogeneity can be observed at all scales and it has been modeled by different authors (Hanks, 1979; Andrews, 1980; Frankell, 1991; Zeng et al., 1994; Ma et al., 2000; Shakal et al., 2005). In particular, Herrero and Bernard (1994) proposed a simple method to account for the details of slip in a large range of wavelengths, by using the self similar slip distribution (k-2) on the fault plane.

The heterogeneity often results in different-sized slip patches, whose relative positions with respect to the hypocenter location affect the near-source ground motion and control directivity effects (e.g., Manighetti et al., 2001; Mai et al., 2005).

4.2.4 Source time function (STF)

In a first approximation, the rupture behavior can be described as a simple phenomenon: each point on the fault plane starts to slide when the rupture front reaches its position; the final slip at each point on the fault plane is reached in a specific time interval (called rise time) and its evolution is described through a slip velocity function varying on the fault.

Several authors have proposed different analytical models to parameterize the slip velocity function, on the basis of dynamic rupture modeling: crack-like models (Andrews 1976; Das and Aki, 1977; Day, 1982) and pulse-like models (Heaton 1990; Nielsen and Madariaga, 2003). In the crack-like models the healing is due to the rupture front back-propagating from the fault boundaries; in this case the maximum rise time is comparable to the rupture duration and it depends on the dimension of the fault. In the pulse-like models the rupture front is followed by a healing front and the rise time is shorter and independent from the rupture duration; these models are used in kinematic simulations, the rise time being assumed either variable (e.g. Bernard et al.,1996; Cirella et al. 2008) or constant on the fault (e.g., Beroza and Spudich, 1988; Somerville, 1999). We underline that a realistic

characterization of the slip-velocity function is a critical component of earthquake rupture modeling (Guatteri et al., 2004; Tinti et al., 2009) Moreover, waveform inversion procedures cannot well invert and resolve the rise time values both because of the limited frequency band considered during the inversion and because of an evident trade-off between rise time and the peak slip velocity.

The functional form of the slip velocity is defined by the source time function (STF). In the singletime window approaches (Cohee and Beroza; 1994), the temporal evolution of slip velocity is described by an analytical expression of STF, usually defined as a boxcar, an exponential, a cosine or a triangle. In this work we also consider a new source time function recently proposed in literature, the regularized Yoffe function (Tinti et al., 2005; Cirella et al., 2006). This is a flexible STF defined by three independent parameters: the final slip, the slip duration and the duration of the positive slip acceleration Tacc. This new source time function is consistent with dynamic, pulse-like earthquake rupture and it allows the dynamic interpretation of the kinematic slip models (Nielsen and Madariaga, 2003; Piatanesi et al., 2004). Moreover the regularized Yoffe functions have a greater high frequency content and therefore they are able to better constrain the details of the rupture in near field region (Cirella et al, 2009).

4.2.5 On the Rise Time

The rise time represents the time needed to reach the maximum slip in each point of the fault. In this study we have decided to fix the rise time to the constant value of 1 Hz. This decision is supported by the fact that exists a trade-off between the peak slip velocity and the rise time and varying the two at the same time could blend the results. Because in the inversion methods the rise-time is not as constrained as the peak slip velocity it is hard to assign a statistical behavior to its variability. Major informations on the ground motion variability could be achieved instead varying the source time function. Moreover, as aforementioned, it is of interest discerning among all the proposed interpretations of the source time function in relation with their effects on the ground motion variability.

It has also to be noted that the rise time acts on the signal like a filter. The assignation of a certain rise time guarantees a frequency content up to about its

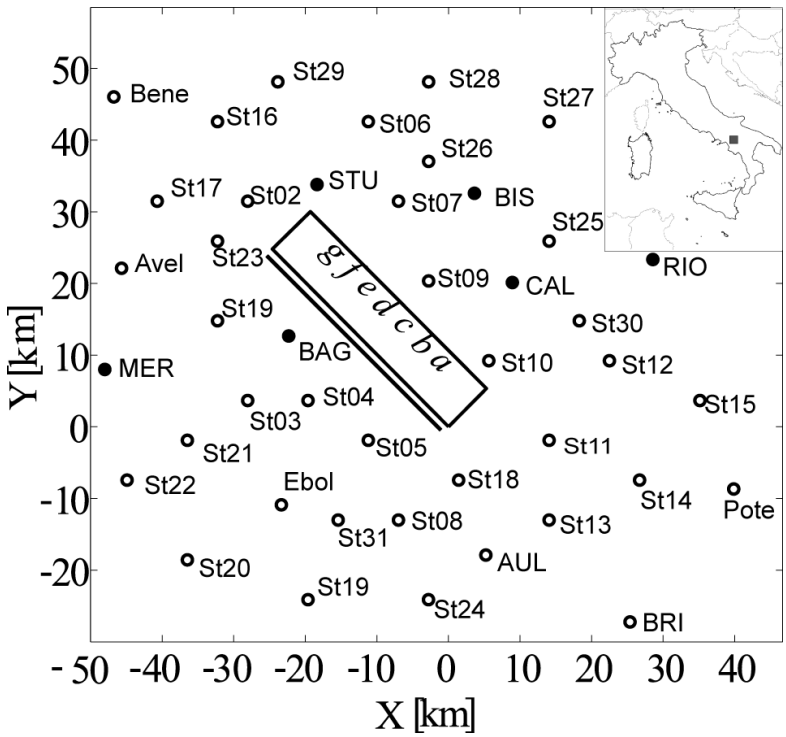

Figure 4.2: Stations' location and fault projection with geometry similar to the 1980 Irpinia, Italy, earthquake. Letters a to g on the fault shows the position of 7 nucleation points, located at 10 km down-dip from the upper edge of the fault and equally spaced along the strike direction (7.0-10.5-14.0-17.5-21.0-24.5-28.0 km, named from a to g respectively). The line running along the southwest edge of the fault indicates its projection to the surface.

inverse value. Because we attempt to push the simulation up to the highest frequencies allowed by the computational time and by the resolving resolution. we have tested a rise time of 0.01s. We have observed that the four proposed source time functions lead to exactly the same results. This is because a small rise time transforms the source time functions into delta functions and the shape of the dislocation history is therefore indistinguishable.

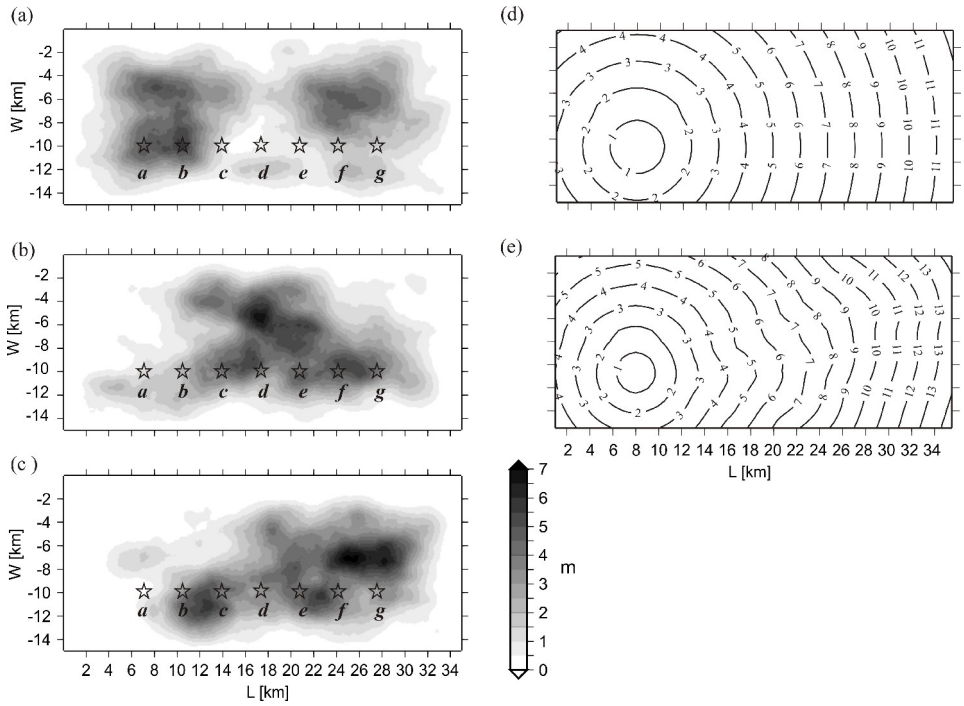

Figure 4.3: Three distributions of final slip considered in this study, each of them ha ving asperities in different positions: (a) model A, (b) model B, (c) model C. Black contours in panels (d) and (e) represent the rupture fronts associated to the rupture velocity model Vr2 and Vr5, respectively, andfor nucleation point #a (Figure 1); Vr5 depends on the peak slip velocity distribution corresponding to the slip model B.

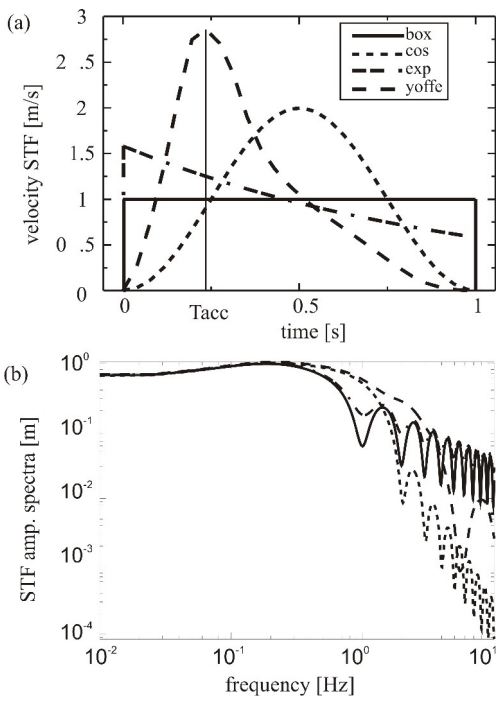

Figure 4.4: Source time functions: boxcar (box), exponential (exp), cosine (cos), and regularized Yoffe function with Tacc= 0.225s (yoffe): (a) in time domain (normalized to unit area); (b) in frequency domain.

4.3 Geometry and Parameters setting

We model all scenarios for a single fault plane with a focal mechanism similar to the 1980 Irpinia, Italy, earthquake (Mw 6.9): normal fault of (35x15) km2, 60° dip, 315° strike, -90° rake, and fault top depth at 2.2 km (figure 4.2). The kinematic parameters are assigned at nodal points of the fault plane equally spaced every 100 m along strike and dip directions.

The main goal of this chapter is to study the ground motion variability due to the variations of kinematic rupture parameters. We therefore assume a simplified 1-D crustal model valid for the area to compute the Green's functions (Table 1; Amato and Selvaggi, 1993; Improta et al., 2003; Improta, 2009, personal communication) and we do not include any variability in ground motions due to variations in site response.

Synthetic seismograms are computed at bedrock in the frequency band 0-2.0 Hz, for 31 virtual sites and for 12 sites having the same location of the Accelerometric Italian Network stations (ITACA Working Group, 2008; Figure 4.2). For all sites, the fault distance R_{JB} (defined as the closest distance to the surface projection of the fault plane; Joyner and Boore, 1981) ranges between 7 km and 70 km. The different rupture models are obtained by varying the position of the nucleation point, the rupture velocity, the source time function and the final slip distribution. For all cases the rise time is chosen to be constant on the fault and equal to 1 sec. We consider 7 nucleation points (NP) in the deeper portion of the fault, equally spaced along the fault length to account for the potential directive and anti-directive effects (Figure 4.2). Three distributions of final slip on the fault plane (SLIP model A, model B, model C; Figure 4.3) are considered; they are computed using a self similar k-square slip model (Herrero and Bernard, 1994). We assume 4 analytical source time functions (STF) describing the slip velocity evolution (Figure 4.4): a boxcar, an exponential, a cosine and a regularized Yoffe function (Tinti et al., 2005; Cirella et al., 2006) with constant Tacc=0.225s. Finally, we consider 3 constant rupture velocities (V_r1, V_r2, V_r3), defined as 70%, 80% (Figure 4.3d) and 90% of S-wave velocity (V_s= 3.0km/s), and 2 heterogeneous

distributions of rupture velocity whose variations depend either on the distance dis(x,y) of the rupture front from the nucleation point (V_r4) or on the final slip distribution D(x,y) on the fault plane (V_r5, Figure 4.3e):

(1) $$V_r 4(x,y) = dis(x,y)0.035 + 0.6 V_s \quad (V_r(x,y) < 0.92 V_s)$$

(2) $$V_r 5(x,y) = (0.32 \times (D(x,y)/D_{max})2 + 0.6) \times V_s$$

where D_{max} is the maximum slip reached on the fault plane and (x,y) are the local coordinates on the fault. We decrease the slip on the upper part of the fault to avoid super-shear condition of the rupture velocities.

The rupture velocity described in Equation (1) is derived from dynamic spontaneous modeling (Ohnaka and Shen, 1999): at larger distances from the nucleation, the dynamic loading of the breaking points increases and hence accelerates the rupture front; the constant parameters in the equation are chosen to fix a minimum velocity value at zero distance and to ensure a slowly growing of rupture velocity. The variable rupture velocity defined in Equation (2) is based on modifying the formulation of Ruiz (2007) using a 2nd order dependence of Vr on the total slip, in order to avoid the generation of strong stopping phases. The source model of Irpinia mainshock, inferred from the inversion of strong motion data (Cocco and Pacor, 1993) is characterized by two main asperities (Slip A of Figure 4.3), with the position of the nucleation point corresponding to the instrumental hypocenter (40.76N, 15.31E, depth of 15km, NP=a in Figure 4.2; Working group ITACA, 2008) and producing a quasi-unilateral rupture propagation toward northwest.

4.4 Statistic and reliability

The number of simulated scenarios at bedrock, resulting from different choices of rupture parameters, leads to 420 three-component time series at each site, both in displacement and velocity. Spectral displacement with 5% damping ratio (SD) and peak velocity values (PGV) are derived from the geometric mean of the horizontal components. The shaking_chain package has been accompanied by a robust

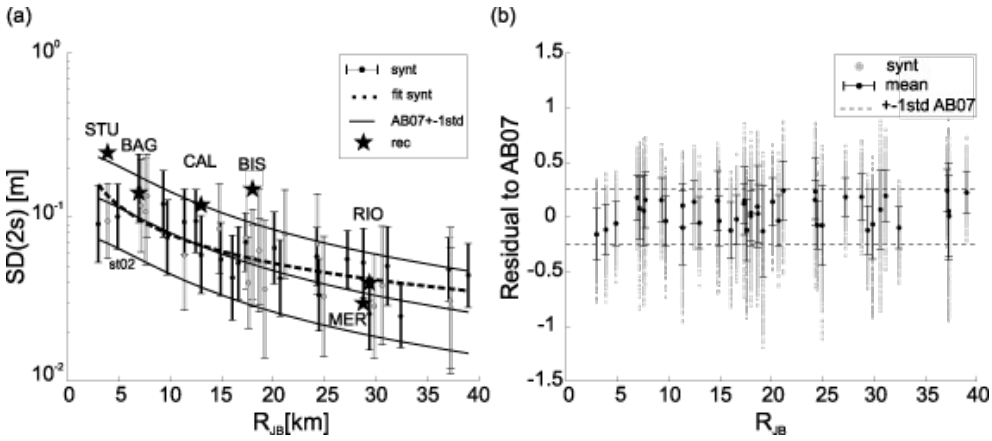

*Figure 4.5: Mean horizontal SD (5% damping) at 2s computed at all sites for all simulated scenarios and ordered by fault distance RJB (closest distance to the surface projection of the fault plane). (a) Geometric mean (± 1 standard deviation) at each site and its fit (logSD(R) = -0.5792 * log(R) - 0.5274), compared with the Akkar and Bommer (2007) empirical predictive model for normal faulting (AB2007); gray bars refer to the sites in the strike directions. Stars indicate the same intensity measure as recorded during the first 35 s of the 1980 Irpinia earthquake. (b) Residuals between the empirical estimates from AB07(Akkar and Bommer, 2007) and the simulations; for each site, gray dots are the residual for each scenario and error bars represent the standard deviation compared with the AB07 standard deviation.*

statistical analysis developed with Matlab computing language (The MathWorks, 1984) and running over the 420 shaking scenarios. The distribution of the ground motion intensity measure has been computed in order to test the reliability of the synthetic data-set respect to the observations. Moreover, through the statistical analysis of the variate, it is possible to separate each different contribution of the four presented parameters to ground motion variability.

We first examine the reliability of our ground-motion simulations by comparing the SD values at 2 seconds at all sites as a function of fault distance R_{JB} with the AB07 (Akkar and Bommer, 2007) ground motion predictive equation (GMPE), derived from European/Middle East strong-motion records (Figure 4.5). Other empirical equations for response spectra, using the same distance metrics, give similar results for the chosen period (Boore and Atkinson, 2008; Bommer et al., 2009). The chosen period (T=2s) defines the beginning of the constant displacement range of the spectrum (CEN, 2004), it allows the comparison with the

data recorded during the 1980 Irpinia earthquake (not reliable at periods larger than 3-5 s; ITACA Working Group, 2008) and it is within the frequency range used in this study. The mean values of the simulated motions combining all scenarios follow very well the AB07 mean prediction (Figure 4.5a). Moreover, the majority of the recorded data are within one standard deviation of the synthetics and of the AB07 equation.

In order to quantify the comparison with the empirical model, we computed the residuals of the logarithmic SD values between the empirical estimates obtained from AB07 (Akkar and Bommer, 2007) and the simulations (residual = log10[SD_AB07] − log10[SD_synthetic], Figure 4.5b). The standard deviation of the residuals is comparable with the empirical standard deviation (gray bars in Figure 4.5b). To investigate the source of variability in the synthetic values, we analyze the distributions of peak ground motion obtained from all shaking

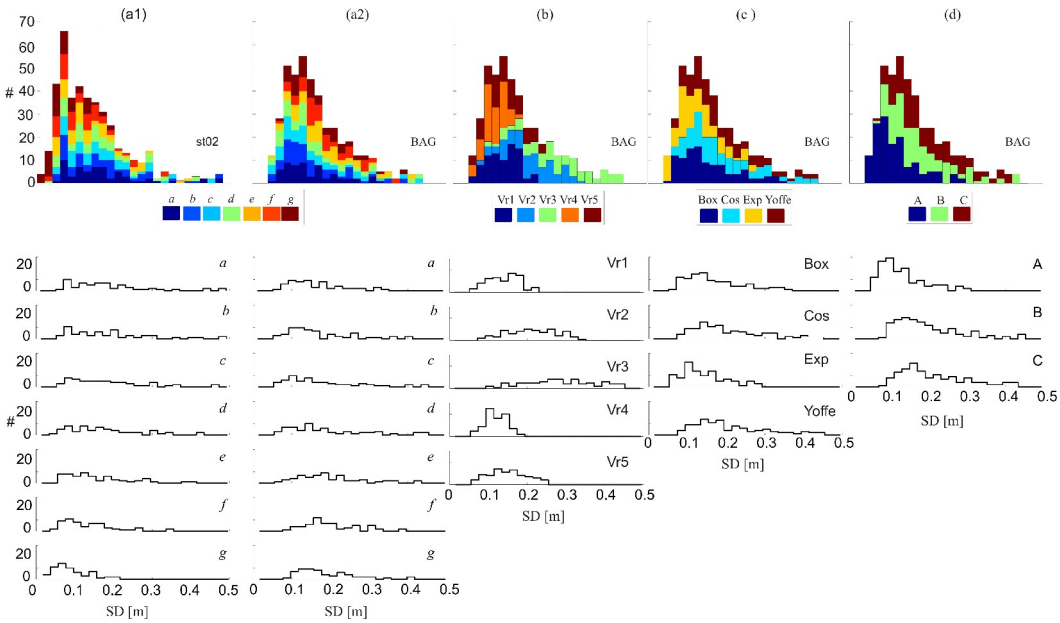

Figure 4.6: Distribution of SD for 5% damping at 2s at stations S02 (panel a1) and BAG (panels a2 to d). Color histograms (top plots) represent the cumulative distribution of all scenarios with colors indicating the contribution of a specific kinematic parameter: a) position of nucleation point (NP), b) rupture velocity (Vr), c) source time function (STF), d) slip model (SLIP). Black histograms (single line) on each column represent the distribution of each source parameter alone.

scenarios at each site and we examine which is the contribution of each kinematic source parameter to the peak distribution. Because in this study the whole variability of the simulated intensity measures is referred to the source rupture modeling, we show in Figure 4.6 how different choices of nucleation point (panel a), rupture velocity (panel b), source time function (panel c) and slip model (panel d) affect the SD values expected at a single site (BAG for all the studied kinematic source parameter and st02 only for the nucleation point). The sensitivity of ground motions to kinematic source parameters depends on the source parameter itself; for example, the different positions of rupture initiation (NP) have large influence: site st02 (panel a1 of Figure 4.6) experiences decreasing SD values as the nucleation point moves from a to g position (Figure 4.2), i.e. the lowest SD is observed when the earthquake nucleates close to the fault edge adjacent to the site and the rupture front moves far from it (nucleation point g in panel a1, Figure 4.6); conversely at BAG site (panel a2 of Figure 4.6) the nucleation points located at the eastern positions on the fault plane contribute to the lowest values, while the central nucleation points produce an increase of the SD.

The different source time functions, give similar shapes of the distributions. Moreover, the regularized Yoffe and cosine functions yield the highest values of SD. This feature is due to the spectral and dynamic properties of these two source time functions, whose slip velocities have a larger high-frequency content than for the boxcar and exponential functions and contribute to the maximum values of the simulated ground motion. Finally, the slip models B and C produce higher motion than model A because the slip patches are closer to the selected site BAG.

The observed results partially can be explained in terms of directivity. The relative source-site position, the radiation pattern, and the fraction of surface suitable of rupture toward the station modulates the amplitude and the frequency content of the seismic radiation.

4.5 The role of directivity

The contribution of finite fault source parameters to ground motion variability is an extensively debated problem. As I have discussed in Chapter 1, the rupture

complexity produces a highly heterogeneous pattern at the Earth surface in the near source region. This pattern is partially due to the directivity effect.

The proposed analysis allows us to relate the ground motion variability to the source-to-site geometry, to the rupture direction and to the rupture surface geometry. These parameters appear to control the directivity effect (Spudich and Chiou, 2008). The sites with the same fault distance R_{JB} can experience very different variability (e.g. in the case study:BAG and st02) due to different azimuth, and the larger standard deviations are associated to sites in the strike direction (Figure 4.5a) where forward and backward directivity effects are stronger.

The ground motion experienced at Sturno (STU) is controlled by the maximum directivity effect and is simulated by the synthetic scenarios producing the extreme values; Bisaccia (BIS), instead, is classified as rock site but it is affected by site effects due to a velocity inversion (clay shale formation underlying the conglomerate slab; Olivares and Silvestri, 2001), not simulated in our synthetics.

The directivity effect also explains the strong dependence of SD values on the five rupture velocities, Vr (panel b of Figure 4.6): the SD increases as the constant rupture velocity increases (rupture velocity Vr3 contributes to the highest values). Moreover, the Vr4 rupture velocity produces a distribution similar to the constant rupture velocity Vr1 (2.1 km/s) but with smaller variability; in fact, the average velocities along strike and dip directions are 1.82-2.26 km/s and 1.94-1.98 km/s, respectively, depending on the nucleation position. Similar behavior is observed for Vr5. Figure 4.7 shows the spatial distribution of the directivity correction factor defined by Spudich and Chiou (2008) overlapping the SD values averaged over all the computed scenarios at each site (black circles). SD values at sites on the foot-wall position are larger than hanging-wall ones. This feature is mainly due to the combined effects of prevailing up-dip rupture propagation, source-to-receiver geometry and earthquake source radiation pattern (Spudich and Chiou, 2008). The coefficient proposed by Spudich and Chiou (2008) to calculate a directivity correction factor to the ground motion prediction equations, qualitatively explains the spatial variation of the simulated data: (i) the sites in the footwall fall in the positive area of the coefficient that indicates the increased directivity effects in the

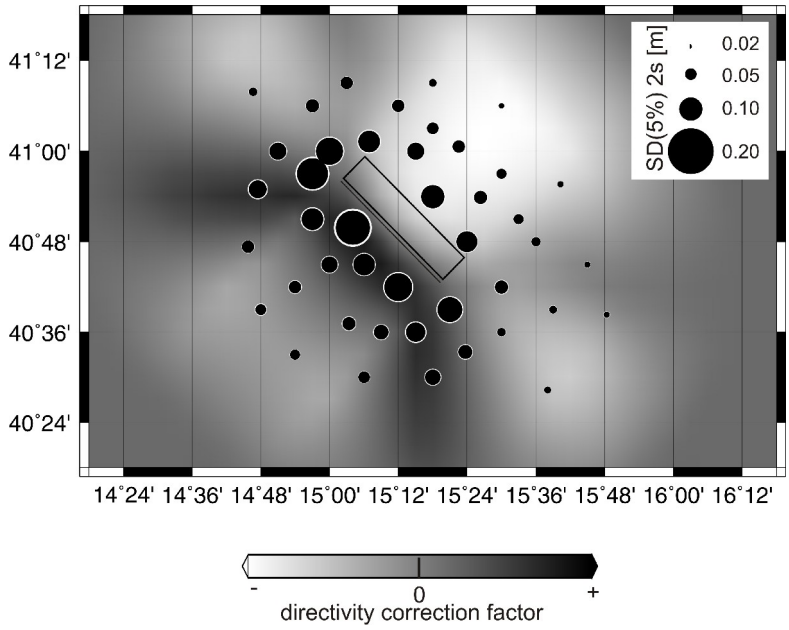

Figure 4.7: Spatial distribution of mean values of SD at 2s averaged over all the computed scenarios at each site (black circles are proportional to the mean value). Gray scale indicates the combined effect of the directivity and the radiation pattern computed using the definition given by Spudich and Chiou (2008) for the same fault geometry and averaged over the different nucleation point positions.

updip direction, and (ii) the synthetic mean values at sites located on the hanging wall are strongly lowered by the S-wave nodal plane of the radiation pattern (Figure 4.7).

Observational data suggest a different behavior. The higher ground motion on the hanging wall observed for dip-slip earthquakes has been explained by the dynamic modeling, which showed that, for typical non vertical dip-slip faults, the breakdown of symmetry with respect to the free surface allows radiated seismic waves to reflect off the free surface and to hit the fault again, altering the stress field on the fault; this process can lead to time-dependent normal stress and a feedback between the friction/rupture processes and seismic radiation (Oglesby et al., 2000). A kinematic model is not able to model these dynamic implications. However it allow us to confirm the hypothesis that directivity effect strongly controls the ground motion variability from a kinematic point of view.

4.6 Hazard solutions conformable to the engineering demand: The scenario selection

The statistical distributions of ground motion parameters, obtained from a large number of simulated scenarios, can help for the selection of shaking scenarios whose characteristics follow defined criteria. A typical example is the choice of a subset of scenarios whose peak value or spectral ordinates match a given value inferred from empirical predictive models, from probabilistic seismic hazard analysis (CEN 2004) or directly from the distribution itself. In this case it is possible to select the scenarios which produce the modal value (maximum probability of occurrence), or the extreme value, or mean value, or the percentiles of the distribution inferred from the histograms. This approach is similar to the de-aggregation of seismic hazard for extracting those scenarios that contribute most to the seismic hazard at a given site. In general, there is more than one scenario giving similar values of the selected ground motion parameter at one site. As an example, Figure 4.8 shows the distributions of SD at 2s and PGV for BAG site. Three different groups of shaking scenarios are highlighted: group I (figure 4.8b), which collects the ensemble of scenarios producing the maximum probability of SD occurrence within ±10% of the total range (42% of all scenarios), group II (figure 4.8c) and group III (figure 4.8e), representing the ensemble of scenarios within the 20% of the total range below the maximum value of SD (4% of all scenarios) and of PGV (3% of all scenarios), respectively. The selected scenarios are characterized by different combination of kinematic rupture parameters and for each group we can separate the contribution of rupture velocity, slip model, nucleation point and source time function. Scenarios belonging to group I (maximum probability of occurrence of SD at 2s, Figure 4.8b) mostly depend on the lowest rupture velocities (Vr1, Vr4 and Vr5), and there is a slightly dependence on the boxcar and exponential source time functions and on the nucleation points located towards the fault edges. On the contrary, scenarios of group II (maximum SD values, Figure 4.8c) are characterized by the largest rupture velocity (Vr3), slip model B and C having the slip patches close to the site, nucleation points in the directive position (c and d in figure 4.2) and the cosine and regularized Yoffe

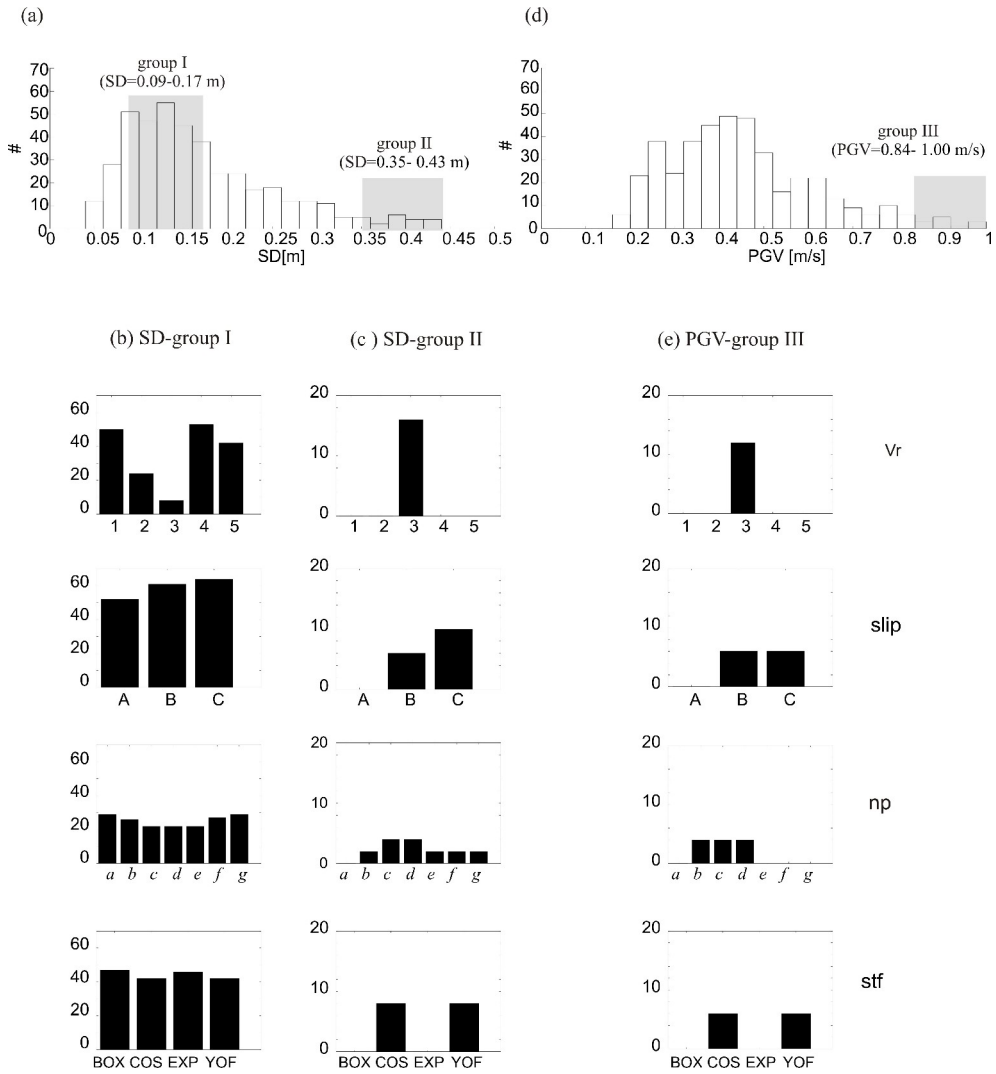

Figure 4.8:(a) Histograms of SD for 5% damping at 2s and PGV at BAG; gray shades shows three different groups of scenarios: group I (177 scenarios with SD(5%) at 2 s ranging around ±10% of the maximum probability of occurrence), group II (16 scenarios with SD(5%) at 2 s above the 80% of the total range, e.g. 20% below the maximum value),), group III (12 scenarios with PGV above the 80% of the total range, e.g. 20% below the maximum value). The figure displays also the selection of kinematic parameters contributing to the shaking scenarios of (b)group I, (c)group II and (d)group III: rupture velocity (Vr), the total slip (slip), the nucleation point (np) and the source time function (stf).

source time functions, which have a larger high frequency content (figure 4.4 and 4.6d).

The scenario selection can require a combination of several conditions to be satisfied (e.g., Bazzurro and Cornell, 2002). As an example, we should look for the scenarios simultaneously producing a given value of two ground motion parameters (such as SD and PGV) at the same site, or a given value of spectral displacement at two sites with the same fault distance. The first example regards the selection of scenarios producing the maximum value of both SD at 2s and PGV at the site BAG (group II and III, Figure 4.8); this is necessary, for example, when a seismic response study is performed on different type of structures at the same location. These scenarios are characterized by the maximum rupture velocity (Vr3) and by the slip distributions B or C (Figures 4.8c and 4.8e). However, a smaller number of nucleation points contributes to the maximum PGV, leading to 10 common set of rupture parameters producing both maximum SD and PGV.

In the case of earthquake scenarios for extended areas (such as an urban district), the selection of a scenario whose peak values are the same at more then one site (multiple sites selection) is not straightforward, especially for sites in near source region. As an example, we select the two sites BAG and st02, which have the same fault distance (Rfault ~ 7 km) but different azimuth (Figure 4.2). The scenarios producing the spectral values expected from the AB07 empirical predictive model (SD±5%=0.099±0.005 m; Akkar and Bommer, 2007) are the 6% and 4% of the simulated scenarios for BAG and st02, respectively. Among the selected scenarios, only 3 of them (0.7% out of 420 scenarios) have same rupture velocity (Vr2,Vr3 and Vr5), slip (model A, B and C) and nucleation point (b and d in figure 4.2). However, none of the rupture models producing maximum spectral displacement at both BAG and st02 sites have the same source time function; this means that there is not a common set of rupture parameters producing similar SD at two sites with the same fault distance.

4.7 Discussion

With the increasing use of dynamic non-linear analysis techniques in the seismic design of structures, the prediction of ground motion time series has become indispensable for the complete determination of structural response and damage estimation for future large earthquakes. The use of synthetic approach may help us to study the variability of the strong ground motion (e.g. Andrews et al., 2007; Søresen et al., 2007) and to infer a robust classification of the ground motion based on the source parameters describing the rupture process, which are in general affected by the uncertainties on the kinematic source parameters (Irikura et al., 2004).

Our work aims at contributing to this open debate, with the main objectives of studying and quantifying the effect of kinematic source variability on the ground motion parameters. We have modeled scenarios for a fault mechanism similar to the 1980 Irpinia, Italy, earthquake source (Mw 6.9), using a discrete wave-number/finite element technique to compute the full-wave displacement and velocity time series in the zero-to-intermediate frequency band. We have used a massive computation of synthetic seismograms at several sites located in the near-source region, resulting from hundreds of rupture models with different combination of rupture velocity, nucleation position, source time function and slip distribution. The values of the rupture parameters were chosen within a range defined in previous studies, depending on the degree of knowledge of the physical mechanisms controlling the process and accounting for the correlation between them (like high slip is associated to higher-than-average rupture velocity). The obtained shaking scenarios, including the worst case scenario (Andrews et al., 2007), represent a set of possible earthquakes which may rupture the same seismogenic fault. The same approach described in this study can be applied to study other source-to-receiver geometries, magnitudes and style of faulting. We chose two intensity measures which account for different characteristic of the ground motion: spectral displacement of 5% damping at 2 s and the peak ground velocity.

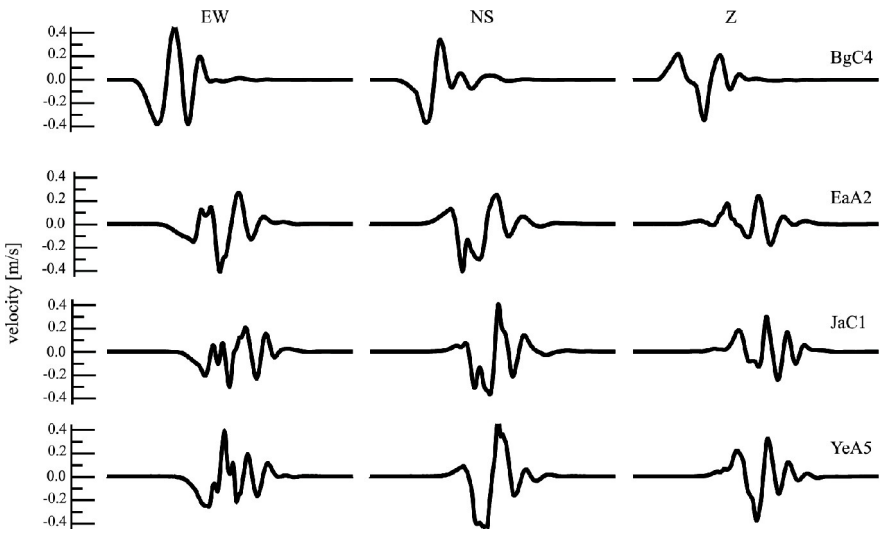

Figure 4.9 Example of seismograms computed at BAG, having similar PGV values ranging around the maximum probability of occurrence (PGV=0.41 0.02) but different rupture models. four letters code L1, L2, L3, L4 represents: L1=STF (B=box,E=Exponential, J=Cosine, Y=Yoffe), L2=NP (Figure 4.2), L3=SLIP (Figure 4.3) and L4=v_r. The seismograms duration is 30 s.

Kinematic source parameters have a significant influence on the resulting ground motions, either in terms of mean values or of the shape of the ground motion distributions. We have shown how peak distributions depend on both azimuth and distance, changing significantly in shape and mean values with the position of the recording site with respect to the fault. The decrease with distance of the peak ground motion is not isotropic in the near source range and the azimuthal variability depends on the rupture model, whereas the majority of the ground motion predictive equations assume an isotropic behavior. The analysis of the effect of the source parameters on the ground motion scenarios may be used to reduce the number of simulations by varying only those rupture parameters which mostly contribute to a specific ground motion measure or which are likely to give values of interest for the particular case study.

However, the large amount of synthetic data provides a detailed description of the variability that could be observed at a given site, or at several sites, for different earthquakes. This variability can largely affect the scenario prediction and it should

be considered when dealing with damage assessment in urban areas or for large structures (Ansal et al, 2009). For these studies it is important to assess the synthetic databases including different intensity measures and whose values have a specific significance (e.g. associated to mean motions, all simulation results, 84% percentile, etc.). We have then used the histograms of the simulated ground motion parameters to select one or more representative rupture scenarios matching specific properties in terms of peak or spectral ordinates values at a given site. In this case the same intensity value can be related to seismograms generated by different rupture models; in other words, seismograms with the same peak value can be produced by different possible earthquakes on the fault and may have different characteristics in terms of frequency content and duration (Figure 4.9).

Moreover, it can be possible to select seismograms satisfying more than one ground motion parameter (e.g., given values of SD and PGV simultaneously), even though it is not always possible to select a scenario satisfying more than one request. This quantitative selection procedure may be useful for finding several temporal signals to be used, for example, in the dynamic analysis of structures.

The present study contributes to improve our understanding on the seismic source and on its effects on the ground motion predictions, even though the behavior of the peak ground motion distributions depends on the specific fault and site configuration and cannot be "extrapolated" to other geometries. Many efforts are still needed to improve our ability to accurately estimate the most critical source parameters influencing the ground motion; a robust evaluation of the kinematic source parameters, not only in terms of mean value but also in terms of distribution functional shape as well as its range limits, is essential to define ground shaking scenarios for seismic-hazard assessment and risk analysis, along with a correct modeling of the variation on propagation wave path. However, we believe that seismologists can give a large contribution to the seismic engineering studies by reproducing and explaining the large variability of expected ground motion in the near source region.

Conclusions

The empirically derived ground motion predictive equations are made of a sum of terms. They can be assimilated to the polynomial approximation where the ground motion is expressed by several first order explicit parameters; the other variables, not treated explicitly in the formulation, results embedded in a generic *n*-th order term, named the uncertainty sigma. Belong to this uncertainty also the errors in retrieving the predicted values, a possible correlation between them and some degrees of randomness of unidentified nature. The uncertainty represents a measure of the overall ground motion variability that is strong especially in the near source region. In this zone the ground motion amplitude is partially modulated by the directivity effect resulting from waves interference or diffraction. The directivity effect has been identified by ground motion modeling where it comes out as a direct result of the rupture history on the fault. On the contrary in the GMPEs, that are widely used in the hazard assessment practice, the parameters related to the directivity effect are not accounted for and the variables related to the rupture propagation are hidden in the uncertainty.

Better performance can be achieved when new first order effects are taken out from the enveloping uncertainty and added to the description of the functional form. When these variables are linked by a physical relation the degrees of freedom of the system are reduced. This reduction leads to a more comprehensive definition of the median ground motion value. On the other hand, the introduction of new explanatory variables either incorporates new sources of uncertainty, or moves parts of the overall uncertainty to a quantifiable term. In any case, managing the propagation of this uncertainties is not trivial and mostly depends on the applications.

In PSHA practice both the definition of the mean value and the uncertainty in the prediction compete to the hazard assessment. When only few variables define the ground motion prediction, the other variables, embedded implicitly in the

uncertainty, augment the chances of having a certain ground motion level. If for example, only the magnitude and distance couple is considered, the same ground motion will be predicted for earthquakes with the same magnitude, even if the shaking distribution depends on a specific rupture process. In a PSHA framework, that means systematically increasing the chances of a certain ground motion level to be exceeded. At the same time the introduction of new variables is not necessarily correlated to a reduction of the uncertainty. Thus, there is a penalty to be paid in terms of parametric uncertainty (Strasser, 2009) that may affect the PSHA assessment, unless the introduction of new explanatory variables is accompanied to a significant reduction of the uncertainty. Otherwise is preferable to avoid the introduction of new variables carrying the penalty of having a less accurate median value definition. Fortunately in a few cases the introduction of new explanatory variables and the reduction of the uncertainty goes together (i.e. Spudich and Chiou, 2008). As pointed out in Chapter 3 the introduction of a directivity term as modeled by Spudich and Chiou (2008) leads to a reduction of the uncertainty and a meaningful use of the rupture related parameters has demonstrated its effectiveness in a PSHA framework.

Different are the considerations on the introduction of new explanatory variables in the GMPEs when the predictions are exploited in real time applications, like the rapid shaking response representation where the prediction are used to augment the number of observations in presence of a sparse instrumental coverage. In such cases, only the overall mean trend is considered, the variability being confined in the sigma value that, in these applications, is neglected. Thus an accurate definition of the median value is of great importance to better characterize the ground motion even if it could be affected by a worst definition of the variability. In particular the ShakeMap application in Chapter 2 has shown that the effects whose parametrization is not defined tend to envelope a regional specific trend leading to blending results. When first order effects (i.e. propagation effect) are neglected, the use of different relations or the introduction of directivity modifiers could be of less relevance. However, it has to be emphasize that ShakeMap should not be considered in the same way as the deterministic methods because its estimations

are associated to a predictability degree of 50% of exceedance (the GMPE uses the mean value). This consideration is true also in case of the scenario studies because a unique scenario is not representative of the potentiality of a fault or seismic zone (Chapter 4). The deterministic scenarios are more reliable if accompanied to a statistical description of the chances of a ground motion level to be exceeded. The same synthetic simulations are currently used to set up a data -set which is well-distributed across the parametric space. This dataset is used both to replace the predictive equations in a probabilistic framework or it is used to identify physical relations linking the explanatory variables to the ground motion to be incorporated in the empirical regression analyses.

Nowadays, deterministic and probabilistic models are more and more closer with respect to the past. Effects like focal mechanism, hanging wall or directivity terms, which belong to the deterministic approaches, have been progressively incorporated in the predictive equations, with direct consequences on PSHA estimations and on ground motion prediction. On the other side, statistical methods have driven the deterministic modeling to produce more meaningful hazard analysis. This effort is also motivated by the fact that the data-bank is now sufficiently rich in data to avoid the use of “non informative” distribution (Chapter 3) in making hazard assessment both for PSHA and in terms of scenario selection (Chapter 4). Thanks to the great progress made by the inversion techniques, larger earthquakes have been inverted for rupture parameters (i.e. slip, rise time and rupture velocity) and tomographic analyses refined by the instrumental improvement are able to characterize with a certain detail the propagation of waves inside a region.

These informations have a corroborated relevance in the hazard assessment so that their introduction in an hazard framework “closes the loop” (McGuire, 1995) between the original perception of the seismic hazard, the consideration of all possible effects that might contribute to the ground motion variability, and their representation with a single (or few) set of parameters derived from current diagnostic procedures and/or by the use of modern database that help to better constrain the real world.

Acknowledgments

I thank the Genova university, the Professor Claudio Eva and Daniele Spallarossa, for giving me the opportunity of performing the present studies and for supporting my professional growth.

I would like also to thank the INGV of Rome, André Herrero and Giovanna Cultrera, for having involved me in the Italian Civil Protection projects (2007-09 DPC-INGV agreement) this thesis is partially performed within. In particular, Chapter 3 has been developed following the guidelines of the S2 project " Realizzazione di un modello dinamico sperimentale di valutazione della pericolosità sismica a scala nazionale" (Realization of a sperimental dynamic model of hazard assessment on national scale); Chapter 2 has been developed in the S3 project framework "Valutazione rapida dei parametri e degli effetti dei forti terremoti in Italia e nel Mediterraneo" (Fast evaluation of parameters and effects of strong earthquakes in Italy and in the Mediterranean); the analysis in Chapter 4 started during the S3 project of period 2004-2006 "Scenari di scuotimento in aree di interesse prioritario e/o strategico" (Shaking seismic scenarios in area of strategic and/or priority interest).

I would like also to acknowledge the ITACA Working Group (2008 http://itaca.mi.ingv.it) and the National Research Institute for Earth Science and Disaster Prevention (NIED - http://kik-net.bosai.go.jp and http://knet.bosai.go.jp) for providing the databases I have used to conduct this study.

Bibliography

Abrahamson, N. A. & R. R. Youngs, R. R. (1992), 'A stable algorithm for regression analyses using the random effects model', *Bulletin of the Seismological Society of America* **82**, 505-510.

Abrahamson, N. A. & Somerville, P. G. (1996), 'Effects of the hanging wall and footwall on ground motions recorded during the Northridge earthquake', *Bulletin of the Seismological Society of America* **86**, S93-S99.

Abrahamson, N.A. (2000). Proc. of 6th Int. Conf. on Seismic Zonation, Palm Springs, Earthq. Eng. Res. Inst.

Abrahamson, N. & Silva, W. (2008), 'Summary of the Abrahamson & Silva NGAGround-Motion Relations', *Earthquake Spectra* **24**(1), 67-97.

Aki, K. (1968), 'Seismic Displacements Near a Fault', *J. Geophys. Res.* **73**, 5359?5376.

Aki, K. (1967), 'Scaling law of seismic spectra', *J. Geophys. Res.* **72**, 1217-1231..

Aki, K., Richards, P.G., 1980. Quantitative Seismology, Freeman and Co., New York

Aki K. and P.G. Richards, (2002). Quantitative Seismology: Theory and Methods, second edition.University Science Books.

Akkar, S. & Bommer, J. J. (2007), 'Empirical Prediction Equations for Peak Ground VelocityDerived from Strong-Motion Records from Europe and the Middle East', *Bulletin of the Seismological Society of America* **97**(2), 511-530.

Amato, A., and Selvaggi G. (1993). Aftershock location and P-velocity structure in the epicentral region of the 1980 Irpinia earthquake. *Annali di Geofisica*, 36, 3-15.

Ambraseys, N.; Simpson, K. & Bommer, J. (1996), 'PREDICTION OF HORIZONTAL RESPONSE SPECTRA IN EUROPE', *Earthquake engineering and Structural Dynamics* **25**, 371-400.

Ameri, G., Akinci A., Cocco M., Cultrera G., Franceschina G., Pacor F., Pessina, V., Lombardi A.M., (2007). Ground motion scenario for selected cities (pp 41-58). In: Technical dissemination N. 8 SP11 - Prediction of ground motion and loss scenarios for selected infrastructure systems in European Urban

Environment/ (Eds: Faccioli E.) IUSS Press, ISBN 978-88-6198-012-9, pp. 210.

Ameri, G., Pacor, F., Cultrera, G. and G. Franceschina (2008). Deterministic Ground-Motion Scenarios for Engineering Applications: The Case of Thessaloniki, Greece. *Bull. Seism. Soc. Am.*, **98**, 3, 1289–1303.

Andrews, D. J. (1976). Rupture velocity of plane strain shear cracks, *J. Geophys. Res.*, 81, No. 32, 5679-5687

Andrews, D.J., T. C. Hanks, and J.W. Whitney (2007). Physical limits on ground motion at Yucca Mountain, *Bull. Seism. Soc. Am.*, 97, 1771-1792.

Baker, G. (2008), 'Improving our understanding of near-surface seismic reflection data quality.', *Invited contribution to The Leading Edge Special Issue* **27**, 1526-1534.

Baker, J. W. & Cornell, A. C. (2005): 'A vector-valued ground motion intensity measure consisting of spectral acceleration and epsilon', *Earthquake Engng Struct. Dyn. 2005; 34:1193–1217*, Published online 21 April 2005 in Wiley InterScience (www.interscience.wiley.com). DOI: 10.1002/eqe.474

Baker, J. W. & Cornell, A. C. (2006); 'Vector-Valued Ground Motion Intensity Measures forProbabilistic Seismic Demand Analysis', Stanford University.

Bakun, W. H.; Stewart, R. M. & Bufe, C. G. (1978): 'DIRECTIVITY IN THE HIGH-FREQUENCY RADIATION OF SMALL EARTHQUAKES', *Bulletin of the Seismological Society of America* **68**, 1253.

Bazurro, P. & A., Cornell, A. (1999): 'Disaggregation of Seiemic Hazard', *Bulletin of Seismological Society of America* **89**(2), 501-520.

Ben-Menahem, A. (1961): 'Radiation of seismic surface-waves from finite moving sources', PhD thesis, California Institute of Technology.

Ben-Menahem A. (1962): 'Radiation of seismic body waves from a f inite moving source in the earth',. *J. Geophys. Res., 67, 345-350*

Benioff, H. (1955), 'Earthquakes in Kern County California during 1952', *Department of natural resources - Division of Mines* **171**, 199-204.

Berge C., Herrero A., Bernard P., Bour M. & Dominique P., (1998), 'The spectral Source model: A Tool for deterministic and Probabilistic Sesimic Hazard Assesment', *Earthquake Spectra* **14**(1), 35-57.

Bernard P., Herrero A., & Berge C. (1996). 'Modeling Directivity of Heterogeneous EarthquakeRuptures', *Bulletin of the Seismological Society of America* **86**(4), 1149-1160.

Bernard, P. & Herrero, A. (1994), 'Slip heterogeneity, body-wave spectra, and directivity of earthquake ruptures', *Annals of Geophysics* **37**, 1679-1690.

Bernard, P.; Herrero, A. & Berge, C. (1996), 'Modeling Directivity of Heterogeneous EarthquakeRuptures', *Bulletin of the Seismological Society of America, Vol. 86, No. 4, pp. 1149-1160, August 1996* **86, No 4**, 1149-1160.

Beroza, G. C., & P. Spudich (1988). Linearized Inversion for Fault Rupture Behavior - Application to the 1984 Morgan-Hill, California, Earthquake. J. Geophys. Res., 93 (B6):6275-6296.

Bizzarri, A. & Spudich, P. (2008). Effects of supershear rupture speed on the high–frequency content of *S* waves investigated using spontaneous dynamic rupture models and isochrone theory. J. Geophys. Res., 113, B05304, doi:10.1029/2007JB005146

Bizzarri, A., Cocco M., Andrews D. J. & Boschi E., (2001). Solving the dynamic rupture problem with different numerical approaches and constitutive laws. *Geophys. J. Int.* 144, 656-678.

Birgören, G., Sekiguchi H., and K. Irikura, (2004). Rupture model of the 1999 Duzce, Turkey, earthquake deduced from high and low frequency strong motion data. *Geoph. Res. Lett.,* 31, L05610, doi:10.1029/2003GL019194.

Boatwright, J. (2007), 'The Persistence of Directivity in Small Earthquakes', *Bulletin of the Seismological Society of America* **97, No 6**, 1850-1891.

Boatwright, J. & Boore, D. M. (1982), 'Analysis of the ground accelerations radiated by the 1980 Livermore Valley earthquakes for directivity and dynamic source characteristic', *Bulletinofthe Seismological Society of America* **72a**, 1843-1865.

Bommer J. J. (2003) 'Uncertainty about the uncertainty in seismic hazard analysis', Engineering Geology, Volume 70, Issues 1-2, October 2003, Pages 165-168

Bommer et al. (2000), Proceedings of the 12th World Conference on Earthquake Engineering, paper no. 207

Bommer JJ, Alarcón JE (2006). The prediction and use of peak ground velocity. J Earthq Eng 10(1):1–31. doi:10.1142/S1363246906002463

Bommer. J. & Abrhamson., A. N. (2006), 'Why Do Modern Probabilistic Seismic-Hazard Analyses Often Leadto Increased Hazard Estimates?', *Bulletin of the Seismological Society of America, , pp. , doi:* **96**(6), 1967?1977.

Bommer, JJ, Stafford, PJ, Akkar, S. (2009). Current empirical ground-motion prediction equations for Europe and their application to Eurocode 8, Bulletin of Earthquake Engineering. Published online: 28 May 2009. DOI: 10.1007/s10518-

009-9122-9

Bommer. J. & Abrhamson., A. N. (2006), 'Why Do Modern Probabilistic Seismic-Hazard Analyses Often Leadto Increased Hazard Estimates?', *Bulletin of the Seismological Society of America, , pp. , doi:* **96**(6), 1967?1977.

Boore, D. & Joyner, W. (1978), 'The influence of rupture incoherence on seismic directivity', *Bulletin of the Seismological Society of America;* **68**(2), 283-300.

Boore, D. M. and W. B. Joyner (1982). The empirical prediction of ground motion, *Bull. Seism. Soc. Am.* **72**, S43-S60

Boore, D.; Joyner, W. & T.E.Fumal (1997), 'Equations for Estimating Horizontal Response Spectra and Peak Acceleration from Wester Noth American Earthquake: A Summary of Recent Work', *Seismological Research Letters* **68**(1), 128-153.

Boore, D. M.; Watson-Lamprey, J. & Abrahamson, N. A. (2006), 'Orientation-Independent Measures of Ground Motion', *Bulletin of the Seismological Society of America* **96, 4A**, 1502-1511.

Boore, D. M. & Atkinson G. M. (2007), 'NGA Ground Motion Relations for the Geometric Mean Horizontal Component of Peak and Spectral Ground Motion Parameters', Technical report, PACIFIC EARTHQUAKE ENGINEERING RESEARCH CENTER.

Bordchert, R. D. (1994), 'Estimates of Site-Dependent Response Spsectra for Design (Methodology and Justification)', *Earthquake Spectra* **10**, 617.

Bouchon M., M. N. Toksöz, H. Karabulut, M.-P. Bouin, M. Dietrich, M. Aktar and M. Edie, (2002). Space and Time Evolution of Rupture and Faulting during the 1999 Izmit (Turkey) Earthquake. *Bull. Seism. Soc. Am.,* 92; 1; 256-266; DOI: 10.1785/0120000845.

Bouchon, M. Bouin, M.-P. Karabulut, H. Toksoz, M. N. Dietrich, M.; Rosakis, A. J., (2001). How Fast is Rupture during an Earthquake? New Insights from the 1999 Turkey Earthquakes, *Geoph. Res. Lett*., 28, 14, 2723-2726.

Bray, J. & Rodriguez-Marek, A. (2004), 'Cahracterization of forward-directivity ground motions in the near fault region', *Soil Dynamics and Eartquake Engineering Geology* **24**, 815-828.

Brune, J. N. (1971), 'Correction. Tectonic stress and spectra of seismic shear waves from earthquakes', *J. Geophys. Res* **76**, 5002.

Brune, J. N. (1970), 'Tectonic Stress and the spectra of seismic Shear Waves from earthquakes', *Journal of Geophysical Research* **75**, 4997-5009.

Bullen K. E. & Bolt B.A., (1985), 'An Introduction to the theory of seismology', fourth edition, Cambridge University Press.

Campbell, K.W. (1985). Strong motion attenuation relations: a ten-year perspective, *Earthquake Spectra*, 1(4), 759–804.

Campbell, K. W. 1987. "Predicting Strong Ground Motion in Utah: Assessment of Regional Earthquake Hazards and Risk along the Wasatch Front, Utah," Open-File Report 87-585, Vol 2, U.S. Geological Survey, Reston, VA, pp L1-L90.

Campbell, K. & Bozorgnia, Y. (2003), 'Updated Near-Source Ground-Motion (Attenuation) Relations for the Horizontal and Vertical Components of Peak Ground Acceleration and Acceleration Response Spectra', *Bulletin of the Seismological Society of America* **93**(1), 314-331.

Causse M., F. Cotton, C. Cornou, and P.-Y. Bard, (2008). Calibrating Median and Uncertainty Estimates for a Practical Use of Empirical Green's Functions Technique. *Bull. Seism. Soc. Am.*, 98, 1, 344–353, doi: 10.1785/0120070075

CEN (2004). Eurocode 8: Design of structures for earthquake resistance - Part 1: General rules, seismic actions and rules for buildings. *Bruxelles* , 6291-6302.

Chen, X. (1995), ' Near-fault ground motion for the Landers earthquake', (Chapter 2: Nature of the near-field ground motion), EERL 95-02 Earthquake Engineering Research Laboratory, Caligfornia Institute of Technology, Pasadena, CA: 169 pp.

Chiou, B. S.-J. & Youngs, R. (2008), 'An NGA Model for the Average HorizontalComponent of Peak Ground Motionand Response Spectra', *Earthquake Spectra* **24**(1), 173-215.

Chopra, A. K. & C. Chintanapakdee, C. (2001), 'Comparing response of SDF systems to near-fault and far-fault earthquake motions in the context of spectral regions', *Earthquake Eng. Struct. Dyn.* **30**, 1769 -1789.

Cirella, A., A. Piatanesi, E. Tinti and M. Cocco (2006). Dynamically consistent source time functions to invert kinematic rupture histories. *Eos, Trans. AGU 87*(52), Fall Meet. Suppl., Abstract S41B-1323.

Cirella, A., A. Piatanesi, E. Tinti, and M. Cocco, (2008). Rupture process of the 2007 Niigata-ken Chuetsu-oki earthquake by non-linear joint inversion of strong motion and GPS data. *Geophys. Res. Lett.*, 35, L16306, doi:10.1029/2008GL034756.

Cocco, M. and F. Pacor (1993): The rupture process of the 1980, Irpinia, Italy earthquke from the inversion of strong motion waveforms, Tectonophysics, 218, 157-177

Cohee, B. P., and G. C. Beroza, (1994). Slip distribution of the 1992 Landers

earthquake and its implications for earthquake source mechanics. *Bull. Seismol. Soc. Am.*, 84, 693–712.

Convertito, V. and A. Herrero (2004). Influence of focal mechanism in probabilistic seismic hazard analysis, Bull. Seism. Soc. Am. 94, no. 6, 2124-2136

Convertito, V. , Emolo, A. & Zollo, A. (2006), 'Seismic-Hazard Assessment for a Characteristic Earthquake Scenario: An Integrated Probabilistic–Deterministic Method', *Bulletin of the Seismological Society of America* **96**(2), 377?391.

Cook, R. D. (1982). Residuals and Influence in Regression, Chapman and Hall, New York.

Cornell. A. C. (1968), 'ENGINEERING SEISMIC RISK ANALYSIS', *Bull. Seismol. Soc. Am.* **58**(5), 1583-1606.

Cox,C. & Ashford, S. A. (2001), 'Characterization of Large Velocity Pulses for Laboratory Testing'(Structural Systems Research Report No. SSRP-2001/11), Technical report, Department of Structural Engineering, UCSD.

Custódio, S., and R. J. Archuleta (2007). Parkfield earthquakes: Characteristic or complementarity?. *J. Geophys. Res.,* 112, B05310, doi: 10.1029/2006JB004617.

Cultrera, G.; Pacor, F.; Franceschina, G.; Emolo, A. & Cocco, M. (2009), 'Directivity effects for moderate- magnitude earthquakes (Mw 5.6-6.0) during the 1997 Umbria-Marche sequence, Central Italy', *Tectonophysics*, 1-2/476(2009)

Das S., & Aki K., (1977), 'A Numerical study of two-dimensional spontaneous rupture rpopagation', *Geophysical Journal International* **50**(3), 643-668.

Day S. (1982). Three-dimensional finite-difference simulation of fault dynamics: rectangular faults with fixed rupture velocity. *Bull. Seismol. Soc. Am.*, 72, 705-727.

Delouis, B, Giardini D., Lundgren P. and Salichon J. (2002). Joint inversion of Insar, GPS, teleseismic and strong-motion data for the spatial and temporal distribution of earthquake slip: application to the 1999 Izmit mainshock. *Bull. Seismol. Soc. Am.*, 92(1), 278-299.

Douglas A., J. A. Hudson J. A., & R. G. Pearce (1988)., 'Directivity and the Doppler effect', *Bull. Seismol. Soc. Am.* 78, 1367-1372

Douglas, J., and P. M. Smit (2001). How accurate can strong ground motion attenuation relations be? *Bulletin of the Seismological Society of America* 91 (6), 1,917–1,923.

Douglas, J. (2003). Earthquake ground motion estimation using strong motion records: a review of equations for the estimation of peak ground acceleration and

response spectral ordinates, *Earth-Science Reviews,* 61, p. 43-104

Douglas, J. (2006). Errata of and Additions to "Ground Motion Estimation Equations 1964–2003." Report BRGM/RP-54603-FR, Bureau des Recherches Géologiques et Minières, France, 103 pps.
http:// www.brgm.fr/publication/pubDetailRapportSP.jsp?id=RSP-BRGM/ RP-54603-FR

Filson J. & McEvilly TV (1967): ' Love wave spectra and the mechanism of the 1966 Parkfield sequence ', *Bull. Seismol. Soc. Amer.* 57, 1245-59

Frankel, A. (1991). High-frequency spectral falloff for earthquakes fractal dimension of complex rupture,b -value, and the scaling of strength on faults Jour. Geophys. Res. 96

Frankel, A.; Stephenson, W.; Carver, D.; Williams, R.; Odum, J. & Rhea, S. (2007), 'Seismic Hazard Maps for Seattle, Washington,Incorporating 3D Sedimentary Basin Effects, NonlinearSite Response, and Rupture Directivity', *Open-File Report 2007–1175U.S. Department of the InteriorU.S. Geological Surveyhttp://pubs.usgs.gov/of/index_old.html* , Technical report, USGS-Open file report.

Guatteri M., Mai P.M., and Beroza G.C., (2004). A pseudo-dynamic approximation to dynamic rupture models for strong ground motion prediction. Bull. Seis. Soc. Am., 94,6,2051-2063

Gutenberg B. and Richter C.F. (1954). Seismicity of the Earth and Associated Phenomena, 2nd ed., Princeton, N.J.: Princeton University Press, pages 17-19.

Hall, J. T.; J., T. H.; Halling, M. & Wald, D. (1995), 'Near-source ground motions and its effects on flexible buildings,', *Earthquake Spectra* **11**, 569-605.

Hanks, T. (1974), 'The faulting mechanism of the San Fernando earthquake', *Journal of Geophysical Research* **79**, 1215-1229.

Hanks, T. (1975), 'Strong ground motion of the San Fernando, California, earthquake: Ground displacements', *Bull. Seism. Soc. Am* .65 193-225

Haskell, N. A. (1964), 'Total energy and energy spectral density of elastic wave radiated from propagating faults', *Bulletin of the Seismological Society of America* **54, No 6**, 1811-1841.

Haskel, N. A. (1966), 'Total energy and energy spectral density of elastic wave radiation from propagating faults: part II. A statistical source model', *Bull. Seism. Soc. Am.* **56**, 125-140.

Harris R.A. and J. R. Arrowsmith, (2006). Introduction to the Special Issue on the

2004 Parkfield Earthquake and the Parkfield Earthquake Prediction Experiment. *Bull. Seism. Soc. Am*, 96, 4B,1-10, doi: 10.1785/0120050831

Heaton, T. H. (1990). Evidence for and implication of self-healing pulses of slip in earthquake rupture. *Phys. Earth Planet. Int.*, 64, 1-20.

Hirasawa, T. & Stauder, W. (1995), 'On the seismoic body waves from a finite moving source', *Bulletin of the Seismological Society of America* **55, No 2**, 237-262.

Housner, G.W., (1955). Properties of strong-motion earthquakes, *Bull. seism.Soc. Am.,* **45,** 197–218.

Howard, J. K.; Tracy, C. A. & Burns, R. G. (2005), 'Comparing Observed and Predicted Directivity in Near-Source Ground Motion', *Earthquake Spectra* **21**, 1063-1092.

Iervolino, I. & Cornell, C. A. (2008), 'Probability of Occurrence of Velocity Pulses in Near-Source Ground Motions', *Bulletin of the Seismological Society of America,* **98**(5), 2262-2277.

Improta L., M. Bonagura, P. Capuano and G. Iannaccone (2003). An integrated geophysical investigation of the upper crust in the epicentral area of the 1980, Ms=6.9, Irpinia earthquake (Southern Italy). *Tectonophysics*, 361,1-2, pp.139-169.

ITACA Working Group (2008) - Data Base of the Italian strong motion data: http://itaca.mi.ingv.it

Iwata, T., H. Sekiguchi, Y. Matsumoto, H. Miyake, and K. Irikura (2000). Source process of the 2000 western Tottori Prefecture earthquake and near-source strong ground motion, paper presented at 2000 Fall Meeting Seismol. Soc. of Jpn., Tsukuba.

Joyner, W.B. and D.M. Boore (1988). Measurement, characterization, and prediction of strong ground motion, in Earthquake Engineering and Soil Dynamics II, Proc. Am. Soc. Civil Eng. Geotech. Eng. Div. Specialty Conf., June 27--30, 1988, Park City, Utah, 43--102. (4.7 Mb)

Joyner, W. B. (1991), 'Short Notes: Directivity For Non Uniform Ruptures', *Bulletin of the Seismological Society of America* **81**, 1391-1395.

Kanno, T.; Narita, A.; Morikawa, N.; Fujiwara, H. & Fukushima, Y. (2006), 'A New Attenuation Relation for Strong Ground Motion in Japan Based on Recorded Data', *Bulletin of the Seismological Society of America, Vol. 96, No. 3, pp. , June 2006, doi: 10.1785/0120050138* **96**, 879?897.

Kasahara, K. (1960), 'An Attempt to Detect Azimuth Effect on Spectral Structures

of Seismic Waves (The Alaskan Earthquakes of April 7, 1958)', *Bull. Earthquake Res. Inst.,* **38**, 207-218..

Klügel, J.-U. (2007), 'Comment on “Why Do Modern Probabilistic Seismic-Hazard Analyses Often Lead to Increased Hazard Estimates?” by Julian J. Bommer and Norman A. Abrahamson', *Bulletin of the Seismological Society of America, Vol. 97, No. 6, pp. 2198–2207, December 2007, doi: 10.1785/0120070018* **97**, 2198-2207.

Klügel, J.-U. (2007), 'Error inflation in Probabilistic Seismic Hazard Analysis', *Engineering Geology* **90**, 186-192.

Liu, P., and R. Archuleta (2004). A new nonlinear finite fault inversion with three-dimensional Green’s functions: application to the 1989 Loma Prieta, California, earthquake. *J.Geophys. Res.*, 109, B02318, doi:10.1029/2003JB002625.

Ma, K. F., Song, T. R., Lee, S. J. and Wu, H. I. (2000). Spatial slip distribution of the September 20, 1999, Chi-Chi, Taiwan earthquake Mw = 7.6 - inverted from teleseismic data. *Geophys. Res. Lett*., 27, 3417-3420.

Mai M.P., Spudich P. &Boatwright J (2005). 'Hypocenter Locations in Finite-Source Rupture Models', *Bull. Seismol. Soc. Am.* 95 965-9

Manighetti, I.; Campillo, M.; Sammis, C.; Mai, M. & King, G. (2005), 'Evidence for self-similar, triangular slip distributions on earthquakes: Implications for earthquake and fault mechanics', *Journal of Geophysical Research* **110**, B05302.

Malagnini, L., R.B. Herrmann and M. Di Bona; (2000). Ground-Motion Scaling in the Apennines (Italy). Bull. Seism. Soc. Am., 90, 1062-1081.

Michelini A, Faenza L., Lauciani V., and Malagnini L., (2008). Shakemap Implementation in Italy, Seismological Research Letters; September/October 2008; v. 79; no. 5; p. 688-697; DOI: 10.1785/gssrl.79.5.688

McGuire, R.K(1975), 'Fortran Computer Program for seismic risk analysis', *Open-File Report 1976–67 U.S. Department of the InteriorU.S. Geological Survey*, Technical report, USGS-Open file report.

McGuire. R.K., (1995), 'Probabilistic Seismic Hazard Analysis and Design Earthquakes: closing the Loop', *Bulletin of Seismological Society of AMerica* **85**(5), 1275-1284.

McGuire. R.K., (1976), 'Fortran Computer Program for Seismic Risk Analysis', United States Department of the interior Geological Survey, Open File Report.

McGuire, R. K. (2004), 'Estimating Finite Source Properties of Small Earthquake Ruptures', *Bulletin of the Seismological Society of America* **94**, 377-393.

McGuire, R. K. & Arabasaz W.J., (1990). an introduction to probabilistic seismic hazard analysis, in SH Ward, ed. Geotechnical and Environmental Geophysics, Society of Exploration Geophysicists, Vol 1, pp. 333-353.

Newmark. M. N, & Hall, W. J. (182), 'arthquake Spectra and Design'(EEERI Monograph 3), Technical report, Earthquake Engineering Research Institute, Oakland, CA..

Nielsen S. and R. Madariaga, (2003). On the Self-Healing Fracture Mode. *Bull Seismol Soc Am*, 93:2375–2388.

Oglesby, D. D., R. J. Archuleta, and S. B. Nielsen (2000). The dynamics of dip-slip faulting: explorations in two dimensions, J. Geophys. Res., 105, B6, 13643-13653.

Ohnaka M. and L. Shen (1999). Scaling of the shear rupture process from nucleation to dynamic propagation: Implications of geometric irregularity of the rupturing surfaces. *J. Geophys. Res.*, 104, B1, 817–844, 1999.

Okada T., Umino N., Hasegawa A. (2009) Deep structure of the Ou mountain range strain concentration zone and the focal area of the 2008 Iwate-Miyagi Nairiku earthquake, NE Japan – Seismogenesis related with magma and crustal fluid, Earth, Planets and Space, accepted.

Olivares L. and F. Silvestri (2001). Analisi della risposta sismica e della subsidenza post-sismica del colle di Bisaccia a seguito del terremoto irpino-lucano del 1980. Proc. X National Conference of Italian National Association of Earthquake Engineering, Potenza-Matera, Italy, 9- 13 sept. 2001.

Olson A.H., Orcutt. J.A. & Frasier. G.A., (1984), 'The discrete wavenumber/finite element method for synthetic seismograms', *Geophysical journal of the Royal Astronomical Society* **77**(2), 421-460.

Ordaz M. Aguillar A., Arboleda J. (2001) CRISIS 99-18 v.1.018 Program for computing seismic risk, Instituto de Ingenieria, Universidad Nacional Autonoma de Mexico.

Panza G.F., Romanelli F., Vaccari F., Decanini L., Mollaiolis F. (2003). Seismic ground motion modelling and damage earthquake scenarios: A bridge between seismologist and seismic engineers. OECD/NEA Workshop on Relation between Seismological Data and Seismic Engineering. 16-18 October 2002. (vol. 1, pp. 241-266).

Piatanesi, A.; Cirella, A.; Spudich, P. & Cocco, M. (2007), 'A global search inversion for earthquake kinematic rupture history: application to the2000 western Tottori, Japan earthquake', *JOURNAL OF GEOPHYSICAL RESEARCH* **112**, B07314.

Piatanesi, A.; Tinti, E.; Cocco, M. & Fukuyama, E. (2004), 'The dependence of

traction evolution on the earthquake source time function adopted in kinematic rupture models', *Geophysical Research Letters* **31**, L04609.

Power M., Chiou B., Abrahamson N., Bozorgnia Y., Shantz T., & Roblee C. (2008): ' An Overview of the NGA project', *Earthquake Spectra*, **24**, pp. 3-21

Priestley M. J. N. (2003). Myths and Fallacies in Earthquake Engineering, Revisited, The Mallet Milne Lecture, IUSS Press, Pavia, Italy.

Pulido, N. & Dalguer, L. A. (2009), 'Estimation of the High-Frequency Radiation of the 2000 Tottori (Japan) Earthquake Based on a Dynamic Model of Fault Rupture: Application to the Strong Ground Motion Simulation', *Bulletin of the Seismological Society of America* **99**, 2305-2322.

Reiter, L. (1990). Rarthquake Hazard Analysis: Issues and Insight. New York Columbia University Press.

Ripperger J., P. M. Mai, and J.-P. Ampuero, (2008). Variability of Near-Field Ground Motion from Dynamic Earthquake Rupture Simulations. Bulletin of the Seismological Society of America, Jun 2008; 98: 1207 - 1228.

Rodgers, A J, Xie, X, Petersson, A (2007). Bounding Ground Motions for Hayward Fault Scenario Earthquakes Using Suites of Stochastic Rupture Models. S21A-0232, AGU Fall Meeting 2007

Rosakis, A. J. Samudrala, O. Coker, D. (1999). Cracks Faster than the Shear Wave Speed. *Science*, 5418, 1337-1339.

Rowshandel, B. (2006), 'Incoporating Source Rupture Characteristic into Ground-Motion Hazard Analysis Models', *Seismological Research Letters* **77**(6), 708-722.

Ruiz J. A. (2007). Modélisation d'accélérogrammes synthétiques large-bande par modélisation de la cinématique de la rupture sismique. PhD thesis, Institut de Physique du Globe de Paris, France.

Sadigh, K.; Chang, C. Y.; Egan, J. A.; Makdisi, F. & Youngs, R. R. (1997), 'Attenution Relationships for Shallow Crustal Earthquake Based on California Strong Motion Data', *Seismological Research Letters* **68**(1), 180-190.

Savage, J. C. (1967), 'SPECTRA OF S-WAVES RADIATED FROM BILATERAL FRACTURE', *Bulletin of the Seismological Society of America* **57**, 39-54.

SCEC/CME Cyber Shake Project,
http://epicenter.usc.edu/cmeportal/CyberShake.html

Scholz, C. H., Aviles, C. & Wesnousky, S. Bull. seism. Soc. Am. 76, 65 □ 70

(1986)

Sekiguchi H. (2007). Validation of a broadband source modeling method of interplate earthquakes. S34A-06, AGU Fall Meeting 2007

Semmane, F., F. Cotton, and M. Campillo. 2005. The 2000 Tottori earthquake: A shallow earthquake with no surface rupture and slip properties controlled by depth. J. Geophys. Res. 110 (B3): B03306, doi:10.1029/2004JB003194.

Shakal, A., V. Graizer, M. Huang, H. Haddadi, and K. Lin (2005), Strong-motion data from the M6.0 Parkfield earthquake of September 28, 2004*, Proceedings of SMIP05 Seminar on Utilization of Strong Motion Data, Los Angeles, CA*, 1-18.

Smith, W. H. F., and P. Wessel (1990). Gridding with continuous curvature splines in tension, Geophysics 55, 293-305.

Sørensen, B.; Pulidio, N. & Atakan, K. (2007), 'Sensitivity of Ground Motion Simulations to Earthquake Source Parameters: A case of study for Istambul, Turkey.', *Bulletin of Seiemological Society of America* **97**, 881-900.

Somerville, P. (2003), 'Magnitude scaling of the near fault rupture directivity pulse', *Phys. Earth Planet. Inter.* **137**, 201?212.

Somerville, P.; Smith, N. & Graves, R. (1997), 'Modification of empirical Strong Ground motion Attenuation Realtions to include the Amplitude and Duration Effects of rupture Directivity', *Seismological Research Letters* **68, N°1**, 199-222.

Somerville, P. Irikura, K. Graves, R. Sawada, S. Wald, D. Abrahamson, N. Iwasaki, Y. Kagawa, T. Smith, N. Kowada, A., (1999). Characterizing Crustal Earthquake Slip Models for the Prediction of Strong Ground Motion. *Seism. Res. Lett*., 70, 1, 59-80.

Spudich, P., Xu, L., (2002). Documentation of software package Compsyn sxv3.11: programs for earthquake ground motion calculation using complete 1-d green's functions, International Handbook of Earthquake and Engineering Seismology CD, Int. Ass. Of Seismology and Physics of Earth's Interior, Academic Press.

Spudich, P. & Archuleta, R. (1987), 'Techniques for Earthquake Ground-Motion Calcualtion with Applications to Source Parametrization of finite Faults', *Academic Press, Orlando* in Seismic Strong Motion Synthetics,Orlando**,**, 205-265.

Spudich, P. & Chiou, B. S. (2008), 'Directivity in NGA Earthquake Ground Motions: Analysis Using Isochrone Theory', *Earthquake Spectra* **24**(1), 279-298.

Spudich, P. & Frazer, L. (1984), 'Use of ray theory to calculate high-frequency radiation from earthquake sources having spatially variable rupture velocity and

stress drop', *Bulletin of the Seismological Society of America* **74**(6), 2061-2082.

SSHAC – Senior Seismi Hazard Commission, 'Guidance for Performing Probabilistic Seismic Hazard Analysis for a Nuclear Plant Site: Example Application to the Southeastern United States', NUREG/CR-6607, UCRL ID-133494, Division of Engineering Technology Office of Nuclear Regulatory Research U.S. Nuclear Regulatory Commission Washington, DC 20555-0001.

Strasser, F. O., N. A. Abrahamson, and J. J. Bommer (2009). Sigma: Issues, insights, and challenges. *Seismological Research Letters* 80, 41–56.

Tinti, E.; Fukuyama, E.; Piatanesi, A. & Cocco, M. (2005), 'A Kinematic Source-time Function Compatible with eartquake Dynamics', *BSSA* **95**, 1211-1223.

Tinti, E.; Spudich, P. & Cocco, M. (2005), 'Earthquake fracture energy inferred from kinematic rupture models on extended faults', *Journal of Geophysical Research* **110**, B12303.

Tinti E., Cocco M., Fukuyama E., and Piatanesi A., (2009). Dependence of slip weakening distance (Dc) on final slip during dynamic rupture of earthquakes. Geophys. J. Int., 177,1205-1220.

Tothong, P.; Cornell, C. A. & Baker, J. (2007), 'Explicit Directivity-Pulse Inclusion in Probabilistic Seismic Hazard Analysis', *Earthquake Spectra* **23**(4), 867-891.

Trifunac, M. D. & Brune, J. N. (1970), 'COMPLEXITY OF ENERGY RELEASE DURING THE IMPERIAL VALLEY, CALIFORNIA, EARTHQUAKE OF 1940', *Bulletin of the Seismological Society of America* **60**, 137-160.

Venkataraman, A. & Kanamori, H. (2004), 'Effect of directivity on estimates of radiated seismic energy', *JOURNAL OF GEOPHYSICAL RESEARCH* **109**, B04301.

Venkataraman, A.; Rivera, L. & Kanamori, H. (2002), 'Radiated Energy from the 16 October 1999 Hector Mine Earthquake:Regional and Teleseismic Estimates', *Bulletin of the Seismological Society of America* **92**(4), 1256?1265.

Wald, J.; Worden, B.; Quitoriano, V. & Pankow, K. (2006), 'ShakeMap Manual - Version 1.0 6/19/06TECHNICAL MANUAL, USERS GUIDE, AND SOFTWARE GUIDE'.

Wang, H., H. Igel, F. Gallovic, A. Cochard, and M. Ewald (2008). Source related variations of ground motions in 3-D media: Application to the Newport–Inglewood fault, Los Angeles basin, Geophys. J. Int. 175, 202–214.

Wang, Z.; Fukao, Y. & Huang, R. (2008), 'Role of fluids in the initiation of the

2008 Iwate earthquake (M7.2) in northeast Japan', *GEOPHYSICAL RESEARCH LETTERS* **35**, L24303.

Wessel, P. and W. H. F. Smith, (1991). Generic Mapping Tools, *EOS*, Vol. 72, 441.

Zeng, Y.; Anderson, J. & Yu, G. (1994), 'A Composite Source Model for Computing Realistic Synthetic Strong Ground Motions', *GEOPHYSICAL RESEARCH LETTERS* **21**(21), 725-728.

Zhao D.,Tani H., Mishra O.P. (2004) Crustal heterogeneity in the 2000 western Tottori earthquake region: effect of fluids from slab dehydration. Phys. Earth Planet. Inter. 145, 161-177.